المدرسة الوطنية المتعددة التقنيات
Ecole Nationale Polytechnique

NATIONAL POLYTECHNIC SCHOOL

POLYDRILL TEAM

Drillbotics 2021 Phase I - Design Report

Prepared by:

DJAH Houssem Eddine

LATRECHE Mahdi

OUARET Fatma Manel

BOUDRAA Mohand Amokrane

DOULACHE Sid Ali

Supervisor:

LARBES Cherif

31 December 2020

Acknowledgments

We sincerely thank all the professors, students and all those who by their words, writings, advice or criticism guided our reflections and agreed answer our questions during our research.

We also want to thank all the faculty and administration of the Ecole Nationale Polytechnique and all our families and loved ones.

List of Figures

Figure 1: Well Path 9
Figure 2: different types of buckling 14
Figure 3:The torque as a function of the WOB and the internal pressure 17
Figure 4:Simulation of the drill pipe subjected to buckling 18
Figure 5: Different categories of vibrations 20
Figure 6: MSE Trending 21
Figure 7: Rig design 22
Figure 8: Table simulations for 700N applied charge 23
Figure 9: Guide rails 24
Figure 10: Hoisting system 25
Figure 11: Top Drive system 26
Figure 12: Riser alignment 26
Figure 13: PDM 27
Figure 14: Sensor Sub 28
Figure 15: Stator 28
Figure 16: Rotor 29
Figure 17: Transmission housing and double universal joint 30
Figure 18: Transmission housing and double universal joint assembly 30
Figure 19: Bent housing 31
Figure 20: Bearing section 31
Figure 21: Bit sub 32
Figure 22: BHA final design 32
Figure 23: The circulation system 34
Figure 24: Pressure loss in the swivel 37
Figure 25: Top Side Power Distribution 41
Figure 26: Downside Power Distribution 42
Figure 27: Delta ECMA-E1830S AC Servo Motor 42
Figure 28: Dual Shaft Nema 34 CNC Stepper Motor 43
Figure 29: Qingeal ZW50-10-20 Pump 43
Figure 30: ASDA-A2R-3023-U Servo Motor Drive 44
Figure 31: DM556 Stepper Motor Drive 44
Figure 32: Usfull FU9000A Pump Motor Drive 45
Figure 33: Omega TQ513 Torque Sensor 45
Figure 34: Omega Miniature Stud-Mount Load Cell 46
Figure 35: FST800-211 Piezoelectric Pressure Sensor 46
Figure 36: YF-S201 Flow Sensor 47
Figure 37: GY-521 MPU-6050 6-axis IMU 48
Figure 38: NodeMCU ESP2866 12E Wi-Fi module 48
Figure 39: Control System Overview 50
Figure 40: Siemens SIMATIC S7-1200 PLC 51
Figure 41: Top Drive Motor RPM Control Block Diagram 51
Figure 42: Hoisting Motor RPM Control Block Diagram 52
Figure 43: Pump Flow Control Block Diagram 52
Figure 44: Vertical Drilling Mode Control System Block Diagram 54
Figure 45: Steering Mode Control System Block Diagram 55
Figure 46: Directional Drilling Mode Control System Block Diagram 56
Figure 47: Control Algorithm 57

Figure 48: Drilling Algorithm 58
Figure 49: Real Time Optimization Matrixes 59
Figure 50: torque as a function of WOB 62
Figure 51: Factory I/O 64
Figure 52: Rig Specifications 1 68
Figure 53: Rig Specifications 2 69
Figure 54: Rig Specifications 3 70
Figure 55: Rig Specifications 4 71
Figure 56: Rig Specifications 5 72
Figure 57: Positive Efficiency (Rotational to Linear) 73
Figure 58: BHA Specifications 1 75
Figure 59: BHA Specifications 3 77
Figure 60: BHA Specifications 4 78
Figure 61: BHA Specifications 5 79
Figure 62: BHA Specifications 6 80
Figure 63: BHA Specifications 7 81
Figure 64: BHA Specifications 8 82
Figure 65: BHA Specifications 9 83
Figure 66: BHA Specifications 10 84
Figure 67: BHA Specifications 11 85
Figure 68: BHA Specifications 13 87
Figure 69: BHA Specifications 14 88
Figure 70: BHA Specifications 15 89
Figure 71: Top Drive Motor Specifications 1 90
Figure 72: Top Drive Motor Specifications 2 90
Figure 73: Hoisting Motor Dimensions 91
Figure 74: Top Drive Motor Drive Interface 92
Figure 75: Top Drive Motor Drive Dimensions 93
Figure 76: Hoisting Motor Drive Advantages 93
Figure 77: Hoisting Motor Drive Uses 94
Figure 78: Pump Drive Specifications 94
Figure 79: Pump Drive Interface 95
Figure 80: Torque Sensor Technical Drawing 95
Figure 81: Torque Sensor Specifications 96
Figure 82: Load Cell Technical Drawing 96
Figure 83: Load Cell Specifications 97
Figure 84: Flow Sensor Technical Drawing 101
Figure 85: Flow Sensor Specifications 101
Figure 86: Flow Sensor Flow Range 102

List of Tables

Table 1: results of pressure loss 40
Table 2: Power Consumption 49
Table 3: Different ROP criteria 60
Table 4: The correlation's coefficient R 61
Table 5: Summary of Equations 67
Table 6: Resistance of threaded shaft 74
Table 7: Hoisting Motor Specifications 91
Table 8: Hoisting Motor Step 91
Table 9: Hoisting Motor Drive Specifications 93
Table 10: Torque Sensor Specifications 95
Table 11: Load Cell Dimensions 96
Table 12: Gyroscope Specifications 98
Table 13: Accelerometer Specifications 99
Table 14: Other Specifications 100
Table 15: Wi-Fi Module Specifications 103
Table 16: Wi-Fi Module Sensitivity 104
Table 17: Wi-Fi Module Dimensions 104
Table 18: 2018-2019 Rig Cost Estimation 105
Table 19: 2019-2020 Rig Cost Estimation 106

Table des matières

List of Figures **3**

List of Tables **5**

1 Introduction **9**

2 Team Organization **10**

2.1 School 10

2.2 Team Members 10

2.3 Roles 10

3 Mechanical Calculations **12**

3.1 Drill pipe Integrity 12

3.1.1 Buckling 12

3.1.2 Burst 15

4.1.3 Bending stress 15

3.1.4 Twist off 16

3.1.5 Drill pipe simulation 17

3.2 Mechanical Specific Energy (MSE) 18

3.2.1 MSE Equation 18

3.2.2 Vibrations 19

3.2.3 MSE Trending 20

4 Mechanical Design **22**

4.1 Rig Design 22

4.2 Top Drive/Hoisting Systems Design 24

4.2.1 Hoisting System 24

4.2.2 Top Drive System 25

4.2.3 Alignment 26

4.3 BHA Design 27

4.3.1 Positive Displacement Motor 27

4.3.2 Sensor Sub 27

4.3.3 Power Section 28

4.3.4 Transmission section 29

5.3.5 Bearing section 31

4.3.6 Bit sub 31

4.3.7 Final BHA design 32

5 Hydraulic System **33**

5.1 The drilling fluid 33

5.2 The Well cleaning 34

5.3 The Mud Pump 35
5.4 Calculations 35
5.4.1 Fluid flow regime 35
5.4.2 Fluid Flow Velocity 35
5.4.3 Pressure Loss 36
5.4.4 Pump's Power 40
6 Electrical System and Instrumentation 41
6.1 System Overview 41
6.2 Rig Actuators 42
6.2.1 Top Drive Motor 42
6.2.2 Hoisting Motor 42
6.2.3 Pump Motor 43
6.3 Drives 43
6.3.1 Rotary Motor Drive 43
6.3.2 Hoisting Motor Drive 44
6.3.3 Pump Motor Drive 44
6.4 Surface Sensors 45
6.4.1 Top Drive Motor Rotary Encoder 45
6.4.2 Torque Sensor 45
6.4.3 Hoisting Motor Rotary Encoder 45
6.4.4 Load Cell 46
6.4.5 Pressure Transducer 46
6.4.6 Flow Sensor 47
6.5 Downhole Sensors 47
6.5.1 6-Axis Motion Tracking 47
6.5.2 Wireless Communication 48
6.5.3 Printed Circuit Board 48
6.6 Power Consumption 48
7 Control System 49
7.1 System Overview 49
7.2 Data Acquisition 50
7.3 Actuator Control 51
7.3.1 Top Drive Motor RPM Control 51
7.3.2 Hoisting Motor RPM Control 51
7.3.3 Pump Flow Control 52
7.3.4 Filtering 52

7.3.5 PID Tuning 52
7.4 Control Modes 52
7.4.1 Vertical Drilling Mode 52
7.4.2 Steering Mode 55
7.4.3 Directional Drilling Mode 55
7.5 Control Algorithm 57
7.6 Optimal Path 58
7.7 Optimization Algorithm 58
8 Simulation 63
9 References 65
10 Appendix 67
A Summary of Equations 67
B Rig Specifications 67
C Power Consumption 73
C.1 Top Drive Motor 73
C.2 Hoisting Motor 73
D BHA Specifications 74
E Motors Specifications 90
E.1 Top Drive Motor (Delta ECMA-E1830S Permanent Magnet AC Servo Motor) 90
E.2 Hoisting Motor (Dual Shaft Nema 34 CNC Stepper Motor) 90
F Pump Specifications (Qingeal ZW50-10-20 Pump) 92
G Drive Specifications 92
G.1 Top Drive Motor Drive (ASDA-A2R-3023-U Servo Motor Drive) 92
G.2 Hoisting Motor Drive (DM556 Stepper Motor Drive) 93
G.3 Pump Motor Drive (Usfull FU9000A Pump Motor Drive) 94
H Sensor Specifications 95
H.1 Torque Sensor (Omega TQ513 Torque Sensor) 95
H.2 Load Cell (Omega Miniature Stud-Mount Load Cell) 96
H.3 6-Axis IMU (GY-521 MPU-6050 6-axis IMU) 97
H.5 Flow Sensor (YF-S201 Flow Sensor) 100
I Wi-Fi Module Specifications (NodeMCU ESP2866 12E Wi-Fi Module) 103
J Past Rig Cost Estimations 105
J.1 2018-2019 Rig Cost Estimation 105
J.1 2019-2020 Rig Cost Estimation 105

1 Introduction

The oil and gas industry are continuously looking for innovative solutions in order to perform more with a lower cost and more safety. That's what called most drilling societies to look to automate the drilling process. The SPE and DSATS were the first to accept the challenge and proposed to make an International Competition for universities all around the world in order to design and construct an automatic rig machine with innovative ways to achieve the request.

As an answer to the SPE society, our aim of this competition is to "Design and simulate a miniature drilling rig in order to autonomously drill a directional well through a homogeneous rock sample to a given plan".

Contrary to last year, the 2021 competition's two groups have had their roles exchange, as now the main group A, is in charge of simulation, both still have the directional aspect, and must be completely autonomous from start to finish, and must contain many overlying mechanical, electric, control and hydraulic systems, as well as various safety measures, simulated in one program.

The National Polytechnic School Team, PolyDrill, with 4 of the same members and a new supervisor, is participating this year for the third time since their victory in the 2019 Drillbotics' Group B challenge, as part of Group A by simulating the 2020 rig which was intended for practical use, for the directional drill challenge and further improve it in various aspects despite the lack of time, resources and knowledge in the domain.

Competition Objective 2021

In the 2021 competition's Group A challenge the team must be able to develop a drilling system model that represents a full-scale system and corresponding control scheme to virtually drill a directional well to a given trajectory. It does not involve building a rig or drilling system. The team will design automation and control but will develop a virtual drilling system (i.e. computer models) to test and demonstrate the controls.

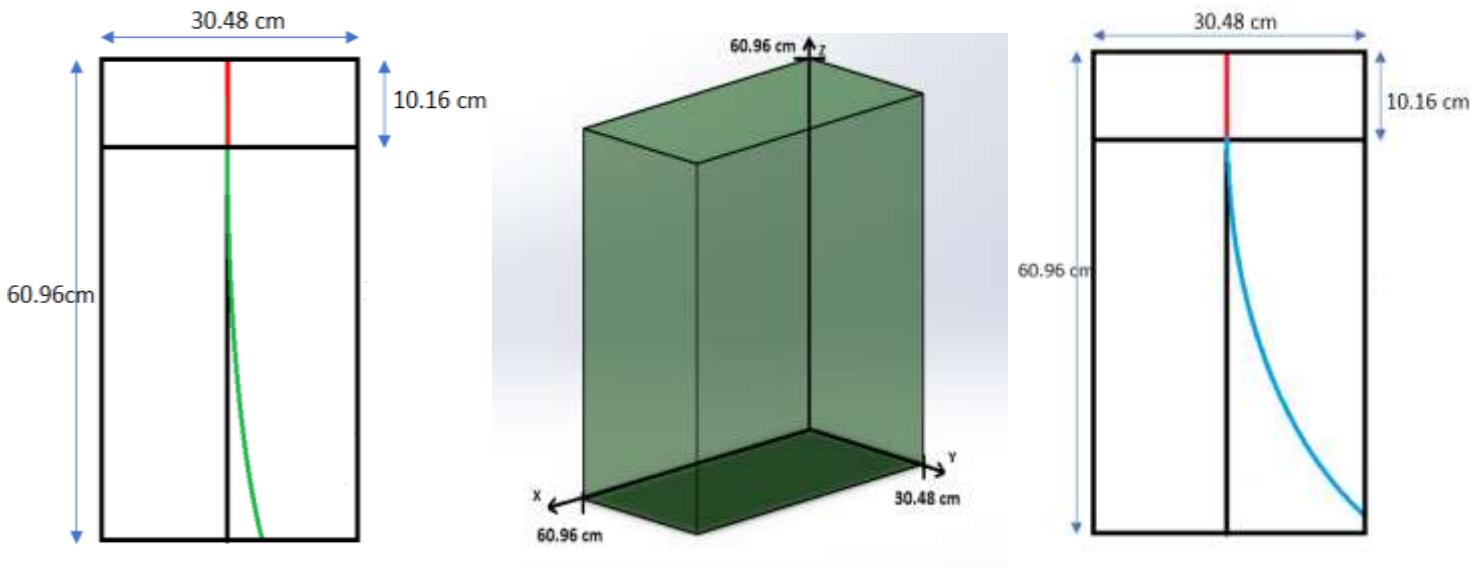

Figure 1: Well Path

2 Team Organization

2.1 School

L'École Nationale Polytechnique (ENP) or **The National Polytechnic School** is an engineering school founded in 1925. The architectural diversity of its buildings reflects the different extensions and enlargements of the areas of expertise, teachings and research.

The engineering courses offered by the **National Polytechnic School** of Algiers are provided in order to produce Engineers and Researchers able to imagine, design and develop innovative ideas, products, processes as well as building the future as well as the diversity of the Algerian economy.

The **National Polytechnic School** forms engineers in various majors/specialties, which are: **Automation**, **Chemical Engineering,** Civil Engineering**, Electrical Engineering,** Electronics**,** Industrial Engineering**,** Environmental Engineering**,** Hydraulics**, Mechanical Engineering,** QHSE - GRI (Quality, Health, Safety, Environment - Industrial Risk Management) Engineering**,** Mining Engineering, Materials Engineering, and Data Science and A.I.

The engineering courses are based on successful research centers and experienced teaching teams. The school also provides many opportunities for continuing the training by a specialization as well as a Ph.D.

2.2 Team Members

Mostly the same **PolyDrill** that participated in 2020 will be participating in 2021, **PolyDrill** is made up of engineering students from the **National Polytechnic School**, who all study different majors, our team is based on the idea of multidisciplinary and versatility, and even though we do not have any major specializing in drilling in any way, the science of our different majors and all the extra background research we've made, as well as the help of our supervisor were enough to make up this design report which we hope will be good enough for the SPE's standards.

Our members are:

- **DJAH Houssam Eddine (Team Leader):** 5th year – Mechanical Engineering.
- **LATRECHE Mahdi:** 5th year – Control & Systems Engineering (Automation).
- **OUARET Fatma Manel:** 5th year – Mechanical Engineering.
- **BOUDRAA Mokrane:** 5th year – Electrical Engineering.
- **DOULACHE Sid Ali:** 5th year – Chemical Engineering.

2.3 Roles

The team has defined various roles in order to ensure an efficient workflow, with each role having a respective group working on it with one or many members with experience in the specific field, with some versatile members in more than one group.

The roles are:

- **Finance and Coordination:**
  - DJAH Houssam Eddine

- **Design and Documentation:**
  - LATRECHE Mahdi
  - OUARET Manel

- **Safety:**
  - DJAH Houssam Eddine
  - BOUDRAA Mokrane
  - LATRECHE Mahdi

- **Mechanical Design:**
  - DJAH Houssam Eddine
  - OUARET Manel

- **Hydraulic System:**
  - DOULACHE Sid Ali
  - DJAH Houssem Eddine

- **Electric System and Instrumentation:**
  - BOUDRAA Mokrane

- **Control System:**
  - LATRECHE Mahdi

3 Mechanical Calculations

3.1 Drill pipe Integrity

The team decided to choose the aluminum pipe for the following reasons:

- Lightness: Aluminum is a very light metal with a specific gravity of 2.7 g / cm^3, about a third of that of steel (7-8 g /cm^3) or copper (8.96 g / cm^3).
- Mechanical resistance: Aluminum is used mainly in the form of alloys whose main constituent is aluminum, the additive elements can represent up to 15% of its weight. The strength of the aluminum alloy is adapted to the required application. For example, it is considered that one kilogram of aluminum can replace two kilograms of steel in automotive applications.
- Corrosion Resistance: Aluminum naturally generates an oxide layer that protects it from corrosion.
- Ductility, malleability: Aluminum can be easily worked at low temperature and deformed without breaking, which allows to give it very varied forms.

First of all, we will examine the physical limits of a thin-walled aluminum pipe with the following characteristics:

Geometric characteristics:

- Outside diameter (D_o): 3/8 in ≃ 9.53 mm
- Wall thickness (t): 0.049 in ≃ 1.24 mm
- Inside diameter (D_i): 0.277 in ≃ 7.04 mm
- Length (L_{dp}): 36 in = 914.4 mm

Mechanical characteristics: for 6061-T6 aluminum

- Ultimate tensile strength (R_{ultim}): 310 MPa
- Tensile yield strength (σ_e): 276 MPa
- Module of Elasticity (E): 68.9 GPa

3.1.1 Buckling

The critical load is the maximum load (unit: Newton, it is a force) which a column can bear while staying straight , we are doing these calculated to set a theoretical absolute upper limit for WOB.

The slenderness ratio is given by the equation: $R_S = \frac{KL}{r_g}$

Where r_g is the radius of gyration given by the equation: $r_g = \sqrt{\frac{I}{A}}$

If : $R_S > C_c$ so we have column with a high slenderness ratio, the Euler's Critical Load equation is valid and given by the formula:

$$F_{cr} = \frac{\pi^2 EI}{(KL)^2}$$

If : $R_S < C_c$ so we have column with a low slenderness ratio ,the drill pipe supports less load than calculate by the Euler equation , the Johnson equation is valid and given by the formula:

$$\sigma_{cr} = \sigma_e - (\frac{\sigma_e KL}{2\pi r_g})(\frac{1}{E})$$

Where C_c is the column constant given by equation:

$$C_c = \sqrt{\frac{2\pi^2 E}{K^2 \sigma_e}}.$$

I: area moment of inertia of the cross section of the column
A: the cross-sectional area of the column
L: unsupported length of column
K: column effective length factor
E: modulus of elasticity of column material
σ_e : yield strength

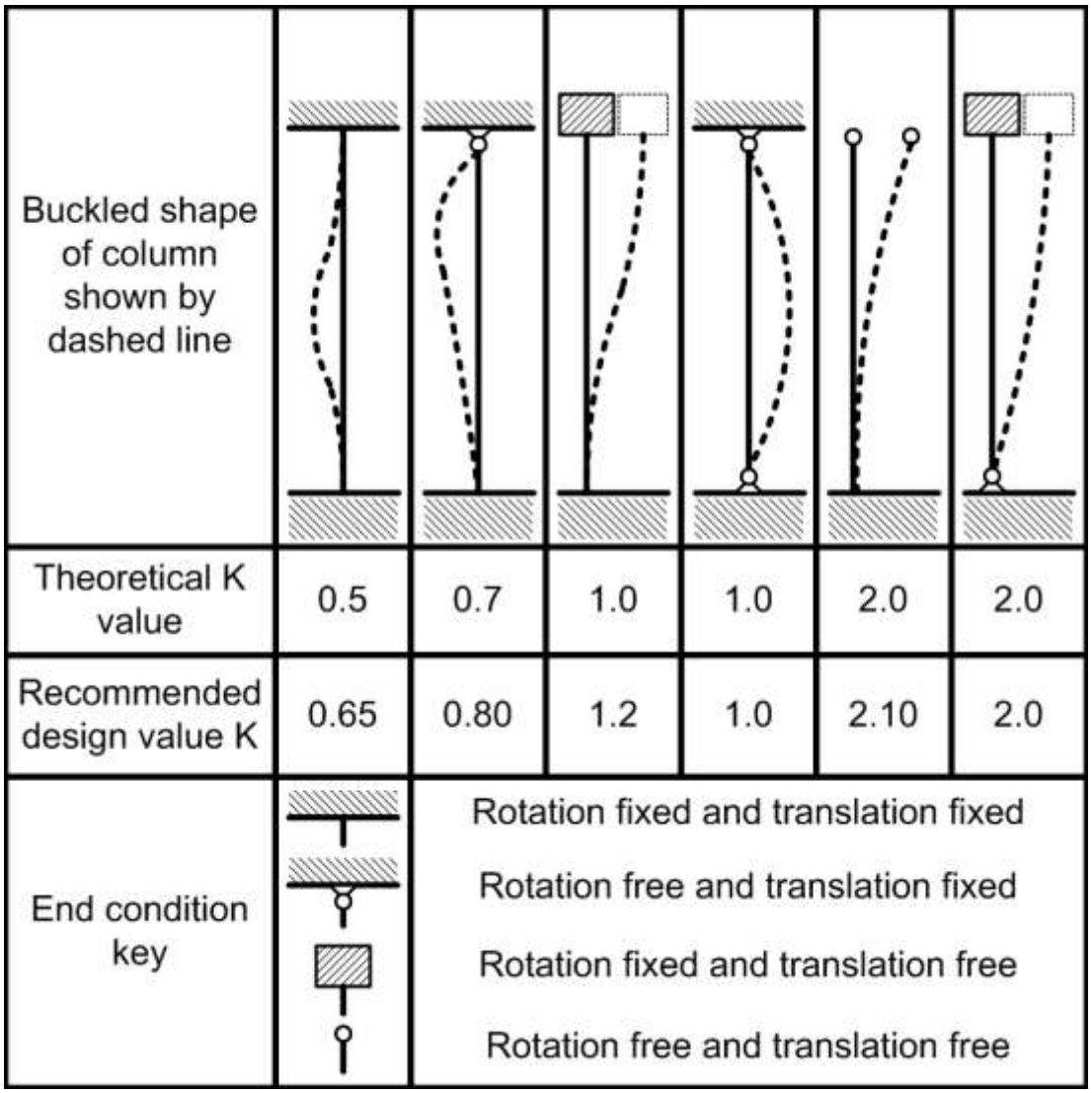

Figure 2: different types of buckling

In our case we will take the recommended length factor K=1 because both ends of the pipe have a free rotation and fixed translation

The area moment of inertia of the cross section of the drill pipe is determined :

$$I = \frac{\pi}{64}\left({D_o}^4 - {D_i}^4\right) = \frac{\pi}{64}(0.00953^4 - 0.00704^4) = 2.84 * 10^{-10}\mathrm{m}^4$$

$$A = \frac{\pi}{4}\left({D_o}^2 - {D_i}^2\right) = \frac{\pi}{4}(0.00953^2 - 0.00704^2) = 3.24 * 10^{-5}\mathrm{m}^2$$

$$R_S = \frac{1*0.9144}{\sqrt{\frac{2.84*10^{-10}}{3.24*10^{-5}}}} = 308.85$$

$$C_c = \sqrt{\frac{2\pi^2 68.9*10^9}{1*276*10^6}} = 70.2$$

Notice that $R_S > C_c$ so $F_{cr} = \frac{\pi^2 68.9*10^9*2.84*10^{-10}}{0.9144^2} = 230\ N$

or $WOB_{max} = 23.44\ kg$

3.1.2 Burst

This calculator and associated equation will determine the working pressure of a known diameter pipe. The equation used is Bellows formula which relates the internal pressure of a pipe to the dimensions and strength of material.

$$P_{burst} = \frac{2\sigma_e t}{D_o s}$$

σ_e: yield strength
t : Wall thickness of the drill pipe
D_o: Outside diameter of the drill pipe
s : safety factor

The safety factor was chosen as 3

$$P_{burst} = \frac{2*276*10^6*1.24}{9.53*3} = 239.4 * 10^5 Pa$$

4.1.3 Bending stress

The bending stress is the stress which causes the bending of the drill pipe and allows the appearance of a radius of curvature. For the drill pipe subjected to a simple bending, the bending stress is given by the equation

$$\sigma_b = \frac{My}{I}$$

Where M is the internal bending moment about the neutral axis given by the equation:

$$M = \frac{EI}{\rho}$$

y : the distance from the point of interest to the neutral axis.

E: modulus of elasticity of drill pipe material

I: area moment of inertia of the cross section of the drill pipe

ρ : radius of curvature

The combination of the two equations gives the following equation:

$$\sigma_b = Ey\frac{1}{\rho}$$

The condition that it must be satisfied for the drill pipe will be in the elastic zone is that the bending stress must remain below the yield strength ($\sigma_b < \sigma_e$) Which give:

$$\rho > \frac{Ey}{\sigma_e}$$

Generally, for the annular form the choice of y is made as follows: $y = \frac{D_o + D_i}{4}$

$$\rho > 1.034 \text{ m}$$

The drill pipe will be in the elastic zone for a radius of curvature greater than 1.034 m which means the drill pipe can be elastically bent.

3.1.4 Twist off

In this part we will calculate the maximum shear stress to know the torque that can be applied to the drill pipe, the equation below gives the maximum torque applied to the drill pipe as a function of the maximum shear stress

$$T_{max} = \tau_{max} \frac{J}{r}$$

Where:

- J : the torsion constant for the section given by the equation :

$$J = 2I = \frac{\pi}{32}\left({D_o}^4 - {D_i}^4\right)$$

- r : the perpendicular distance between the rotational axis and the farthest point in the section (at the outer surface), $r = \frac{D_o}{2}$

We can write now this formula:

$$T_{max} = \tau_{max} \frac{\pi}{16} \frac{{D_o}^4 - {D_i}^4}{D_o}$$

Now we will use the Von Mises criterion to calculate the maximum shear stress, the Von Mises criterion is given by the equation:

$$\tau_{max} = \sqrt{\frac{2(\sigma_e)^2 - (\sigma_a - \sigma_\theta)^2 - (\sigma_\theta - \sigma_r)^2 - (\sigma_r - \sigma_a)^2}{6}}$$

- ✓ If we assume that the axial stress due to internal pressure is negligible, and we consider that the axial stress is only due to the WOB, then we can express the relation of the axial stress by the following equation:

$$\sigma_a = \frac{WOB}{A}$$

A: the area of the cross section of drill pipe given by the equation: $A = \frac{\pi}{4}\left({D_o}^2 - {D_i}^2\right)$

- ✓ The radial stress is given by the equation:

$$\sigma_r = \frac{{r_i}^2}{{r_o}^2 - {r_i}^2}(1 - \frac{{r_o}^2}{r^2})P$$

- ✓ The tangential stress is given by the equation:

$$\sigma_\theta = \frac{{r_i}^2}{{r_o}^2 - {r_i}^2}(1 + \frac{{r_o}^2}{r^2})P$$

Where:
r_o: Outside radius
r_i: Inside radius
P : The internal pressure

We will draw the graph of the torque as a function of the WOB and the internal pressure by using MATLAB and we get the following graphs:

This graph can give us the maximum torque for a given internal pressure and weight, for

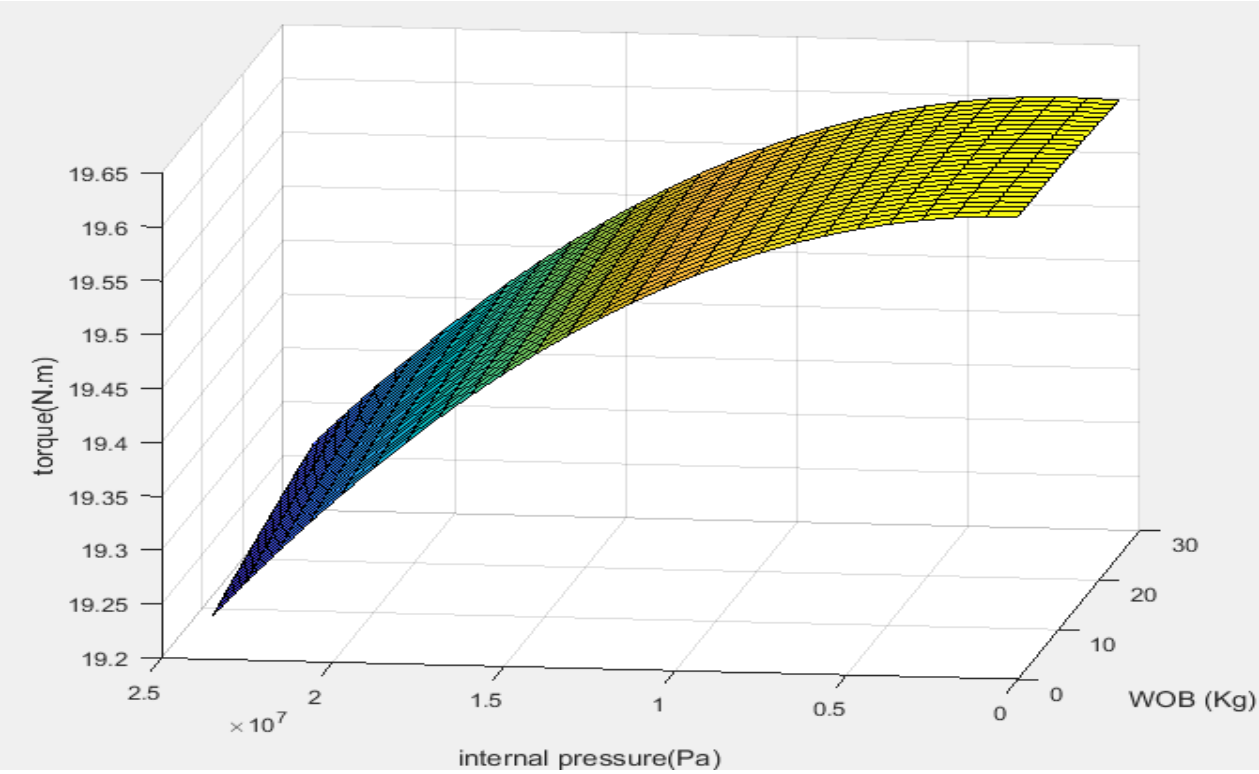

Figure 3:The torque as a function of the WOB and the internal pressure

example the maximum allowed torsion for WOB = 20 kg and P = 150.10^5 Pa is 19.49 N.m.

Note that the influence of the internal pressure on the maximum torque is more important than the influence of WOB.

3.1.5 Drill pipe simulation

We simulated the drill pipe which subjected to buckling, we note that the maximum displacement is at the center of the drill pipe

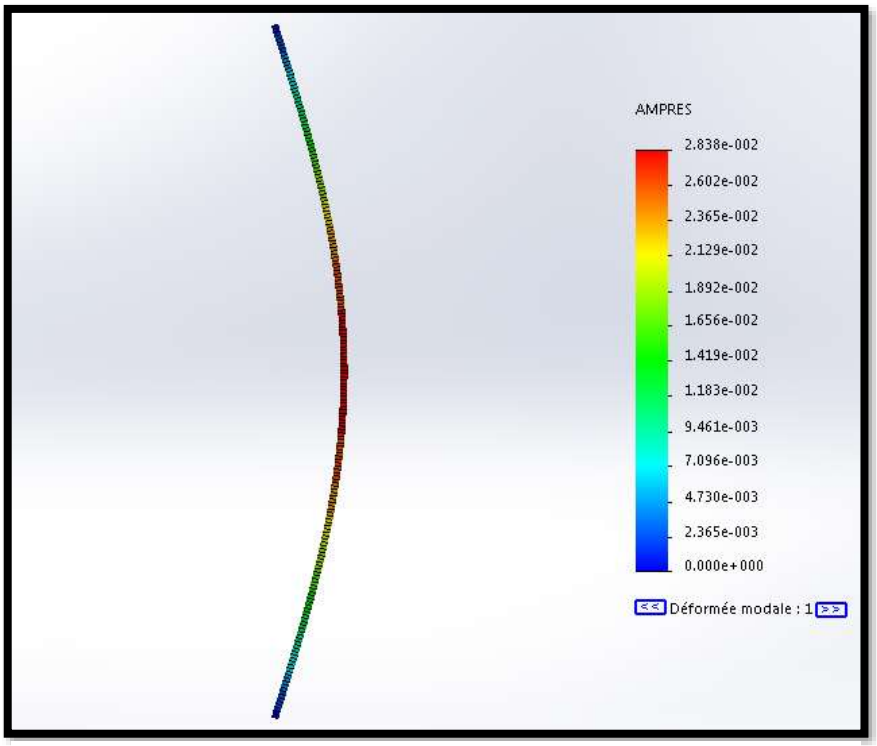

Figure 4:Simulation of the drill pipe subjected to buckling

3.2 Mechanical Specific Energy (MSE)

3.2.1 MSE Equation

In drilling there are two forces acting on the bit; weight on bit (axial force) and torque (rotational force). These are additive to MSE, so there are two terms in the MSE equation.

The MSE equation can be expressed when drill rotation mode and when drill with Down Hole Motor in terms of drilling parameters as:

$$\mathrm{MSE} = \frac{\mathrm{WOB}}{\mathrm{A_b}} + \frac{120 * \pi * \mathrm{RPM} * \mathrm{Torque}}{\mathrm{ROP}}$$

Where:

MSE: Mechanical Specific Energy

WOB: Weight on bit

$\mathrm{A_b}$: ross sectional area of bit or borehole area

RPM: Rotations per minute

Torque: Rotations torque

ROP: Rate of penetration

Teale equation is composed of two parts:

1. Thrust force or weight on bit component

2. Rotary speed component.

We can use Miguel's equation (2008) who added a bit hydraulic and defined Drilling Specific Energy (**DSE**) as the work done to excavate and remove, underneath the bit, a unit volume of rock. See Miguel equation below:

$$\mathrm{DSE} = \frac{\mathrm{WOB}}{\mathrm{A_B}} + \frac{120 * \pi * \mathrm{RPM} * \mathrm{Torque}}{\mathrm{ROP} * \mathrm{A_B}} - \frac{1980000 * \lambda * \mathrm{HP_B}}{\mathrm{ROP} * \mathrm{A_B}}$$

Where:

λ: Dimensionless bit-hydraulic factor depending on the bit diameter

$\mathrm{HP_B}$: bit hydraulic power

3.2.2 Vibrations

Vibrations in the drillstring is a common cause for drilling inefficiency. MSE trending could be used to identify different types if drillstring vibrations.
Vibrations usually occur when one or more of the following factors are present; lithological transitions, use of under-reamer, poor BHA design and/or poor drilling parameter management, usually in combination with high WOB and relatively high RPM. The most common problems associated with vibrations are complications causing additional stress to both the wellbore and the drillstring. This type of stress could cause severe fatigue and damage to the drillstring over time, resulting in tool failure and an additional re-trip. This is expensive for the operation in terms of both time and cost.

Vibrations could be detected by reduced ROP, but are also some times measured by sensors tracking in real-time. Vibrations can be divided in to three different categories as illustrated in graph below:

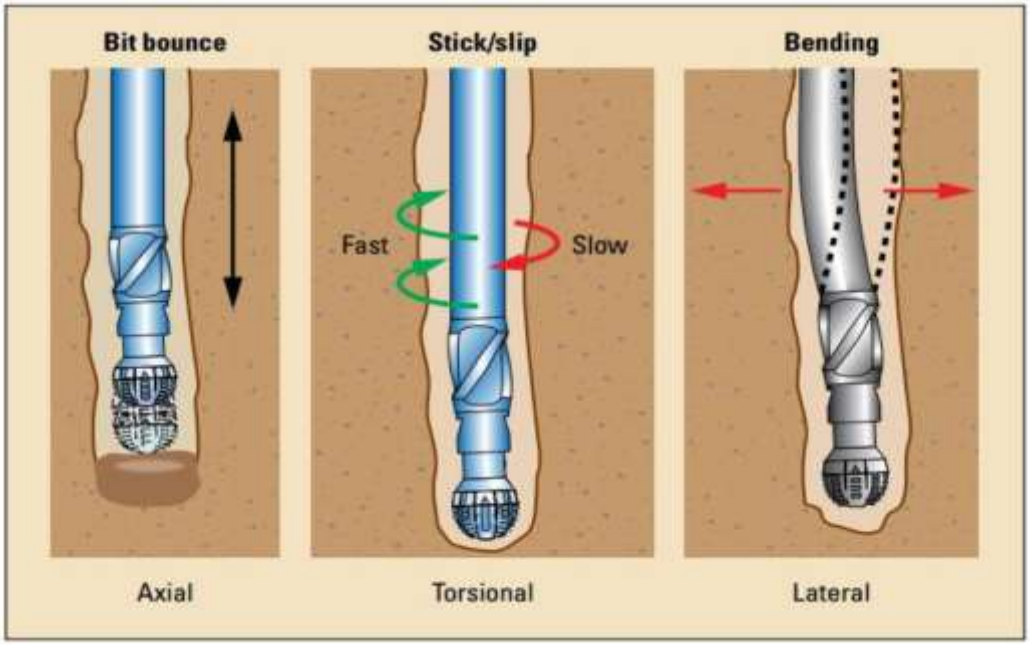

Figure 5: Different categories of vibrations

- ✓ **Axial vibrations**, also known as bit bounce, are vibrations along the trajectory of the wellbore. This type of vibration mostly affects the bit cutters and the bearings, but also prevent energy from being efficiently transferred to the formation.

- ✓ **Stick and Slip vibrations** happen when a part of the drillstring intermittent gets stuck at high frequency, while the part of the drillstring above the stuck section keeps rotating. The drillstring then gather potential energy as the string itself gets twirled. At one point the torque becomes too high for the wellbore to hold, and the formation lets go of the drillstring. The drillstring will then rotate rapidly as the torsional energy is released. If the problem is not solved the drillstring will once again go stuck until enough energy onceagain is worked up. This type of vibrations cause fatigue to drill collar connections, and may also damage the bit.

- ✓ **Lateral vibrations** are the most harmful type of vibrations. Here the drillstring move in a circular motion around the larger diameter of the wellbore. This type of behavior damages the surface of the wellbore, but can also cause severe fatigue to the drillstring components. Lateral vibrations may come as backward whirl and forward synchronous, differencing at what direction the rotary motion against the wellbore occurs.

3.2.3 MSE Trending

MSE is primarily used as a trending tool. This means that the specific value of the MSE curve is of less importance than the trend. Each hole section often starts with a drill-off test to identify the optimal parameters for this formation in combination with this drillstring setup.

From this information, the driller can calculate the new-bit-MSE. The new-bit-MSE is the optimal MSE available for this system, and should be identified at the start of the section. This is because, at this point, the bit is still sharp, and should be able to achieve optimal performance.

The new-bit-MSE will then be the lowest possible MSE for this system, and all future drilling should be evaluated against this value.
When new-bit-MSE is identified, a trend-line should be established. The trend-line is assumed to increase linearly with elapsed time, as illustrated in below figure, due to the need of higher mechanical input energy which is mainly caused by three factors; bit dullness, formation compaction and additional drag due to increased well depth.

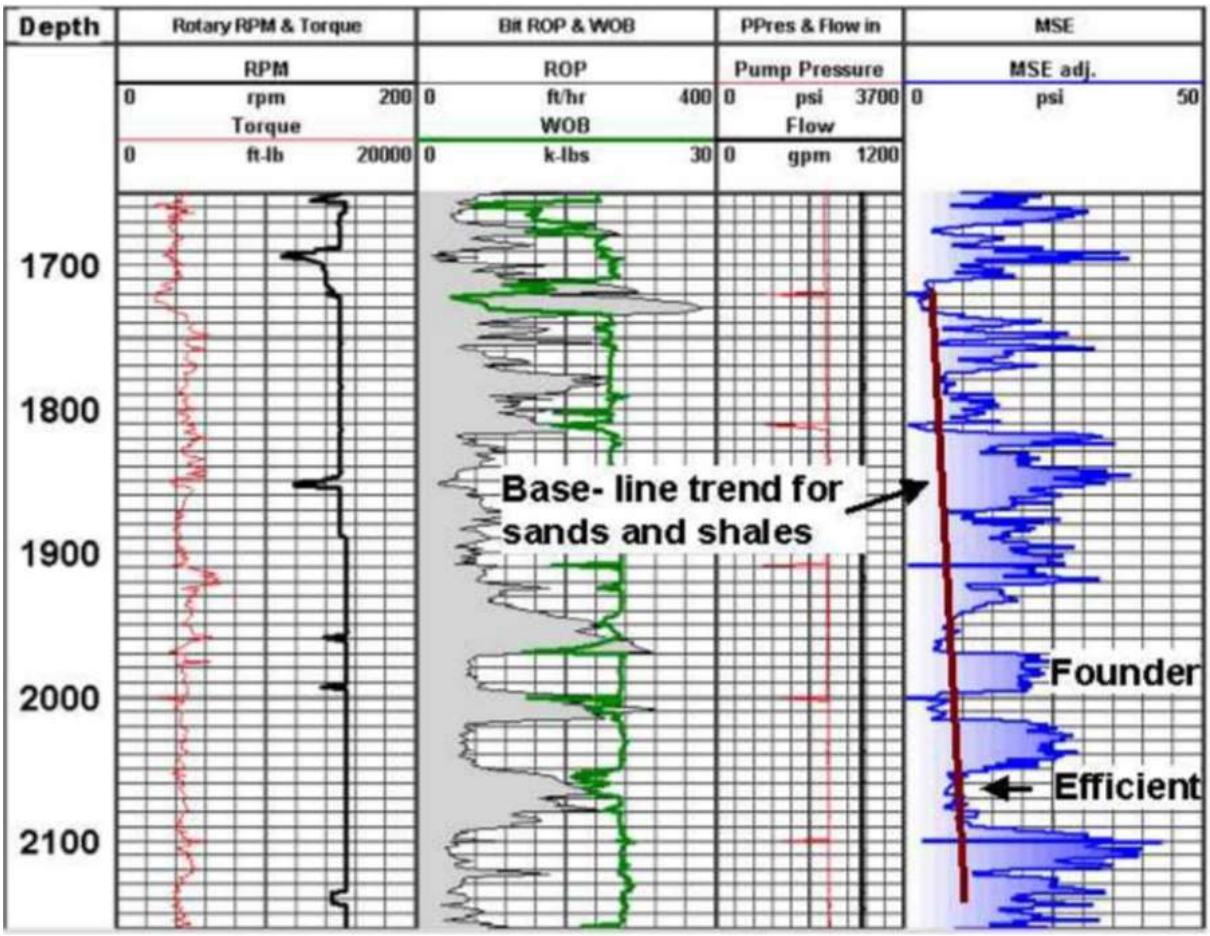

Figure 6: MSE Trending

4 Mechanical Design

4.1 Rig Design

The rig design is based on the design criteria given in the competition guidelines and industry norms. Mobility, functionality, versatility, stability, and safety have been the main concerns while designing the rig. the already available drilling rig will be used in this year's competition with some modifications.

For the material of construction of the drill rig, we have opted for the Stainless Steel to ensure stability and because of the rigidity that we can gain, Moreover, his cost is efficient and easily accessible.

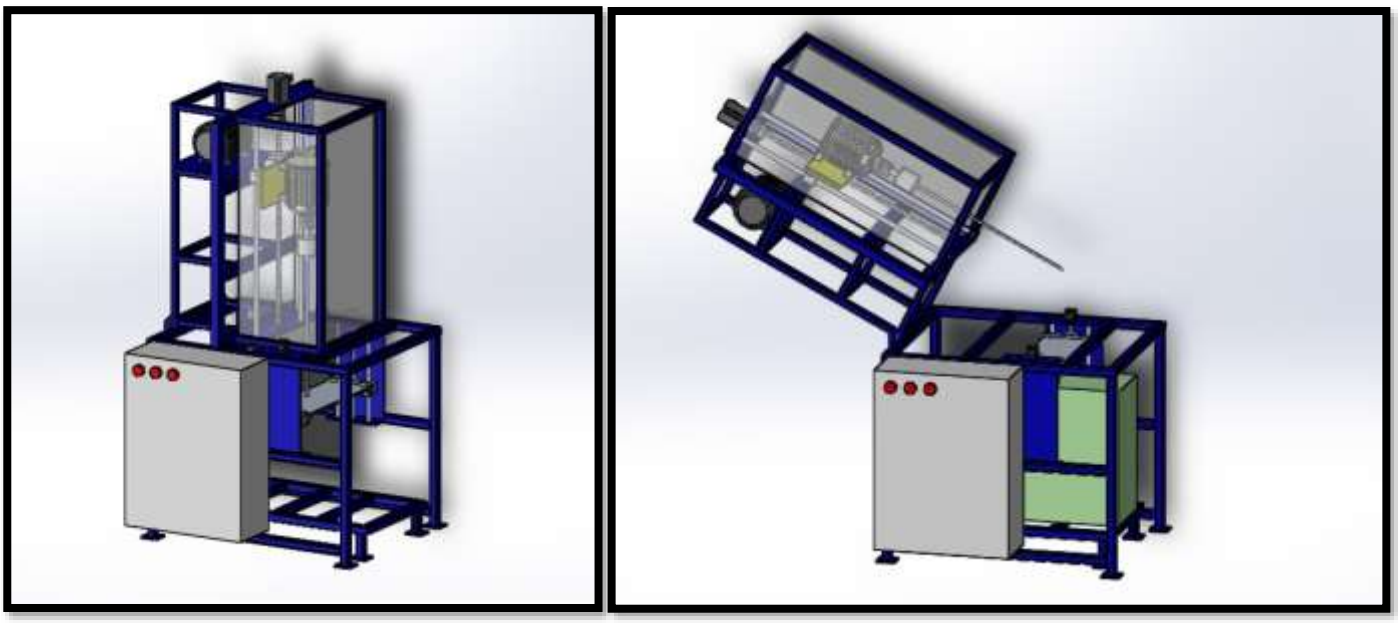

Figure 7: Rig design

The rig is made of 40×40 mm steel, the vertical height is 2200 mm from the floor surface and 840 mm wide, that make the weight of the rig estimated to be 162 Kg. The height was estimated based on the rock sample height (60 cm) and the total length of assembled drill string, and of course the availability of the slide rails.

The rig is designed to be easily moved around, as well as to ensure quick rig up and rig down. Jack up casters are used on each leg so that the rig can effortlessly be operated by one person. The casters will also make it possible to put the structure down on its steel legs to ensure stability when operating. The derrick is mounted to the rest of the structure by hinges and bolts, and can be folded down for a steady and safe transport. The structure is designed to be able to pass through a standard doorway.
For more mobility, we have chosen to divide the structure in two parts to be more transportable.

Mechanical Simulation

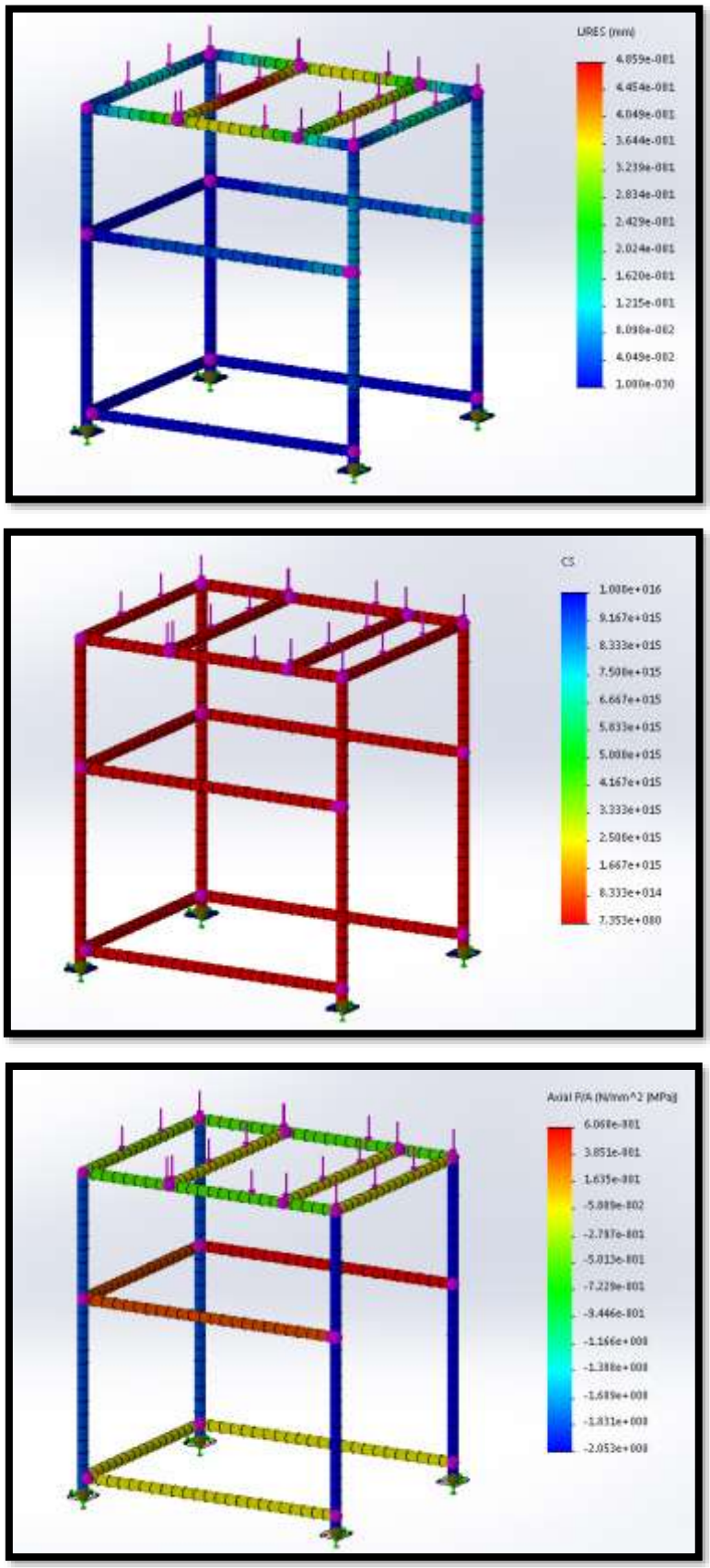

Figure 8: Table simulations for 700N applied charge

Maximal displacement: 0.5 mm
Maximal stress: 0.6 MPa
Minimal security factor: 7.4

The table is stable for an applied charge of 700N.

4.2 Top Drive/Hoisting Systems Design

4.2.1 Hoisting System

The Hoisting System is the system used on a drilling rig to perform all lifting activities. These activities basically include the lowering and lifting of necessary equipment in or out of the hole. This system is the main component that performs the drilling operation by either lifting or lowering the casing or drill pipes to drill and finally complete the well.

This system is one of the important systems to achieve the objective of this competition.
In our hoisting system, we will be using:

- The slides (rails) of 1200 mm.

- guides (containing a linear bearing) that direct the movement in linear vertical direction

Figure 9: Guide rails

The reasons that made us take this choice are:

- Availability and low cost in the market.
- Practical use and simple functioning (without lubrification).
- They are made with specific materials so they can resist to dirt, dust and moisture.

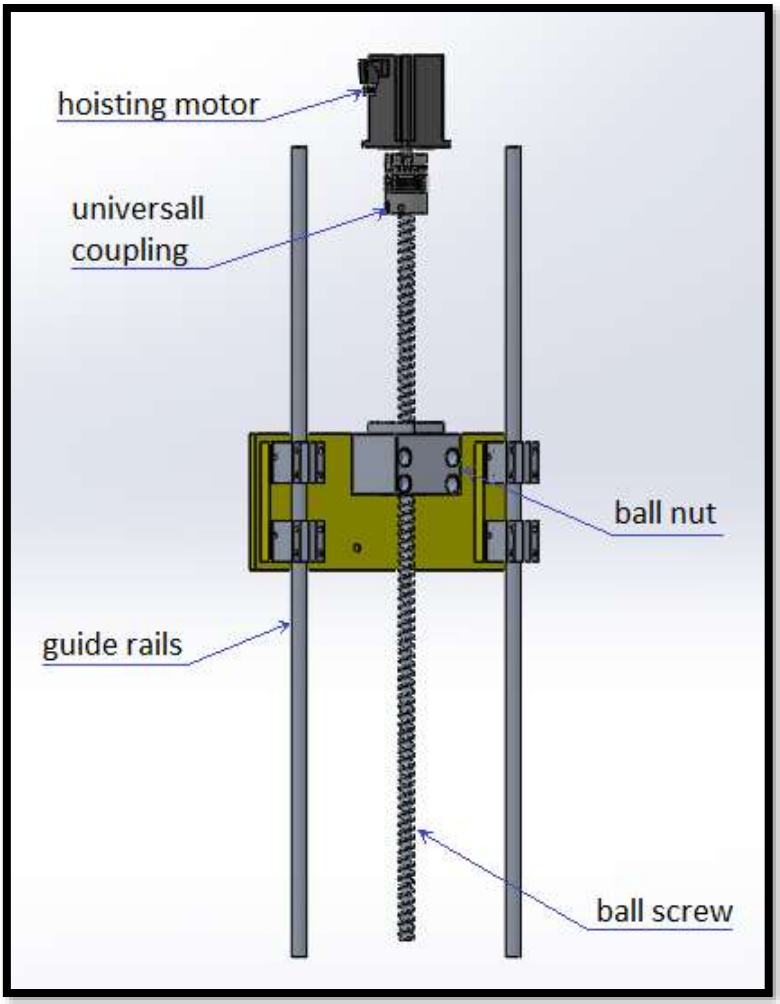

Figure 10: Hoisting system

4.2.2 Top Drive System

The rotary system includes all of the equipment used to achieve bit rotation. The main driver in the system is the top drive motor; he is connected to the swivel by a universal coupling. The swivel is connected directly to the drill pipe.

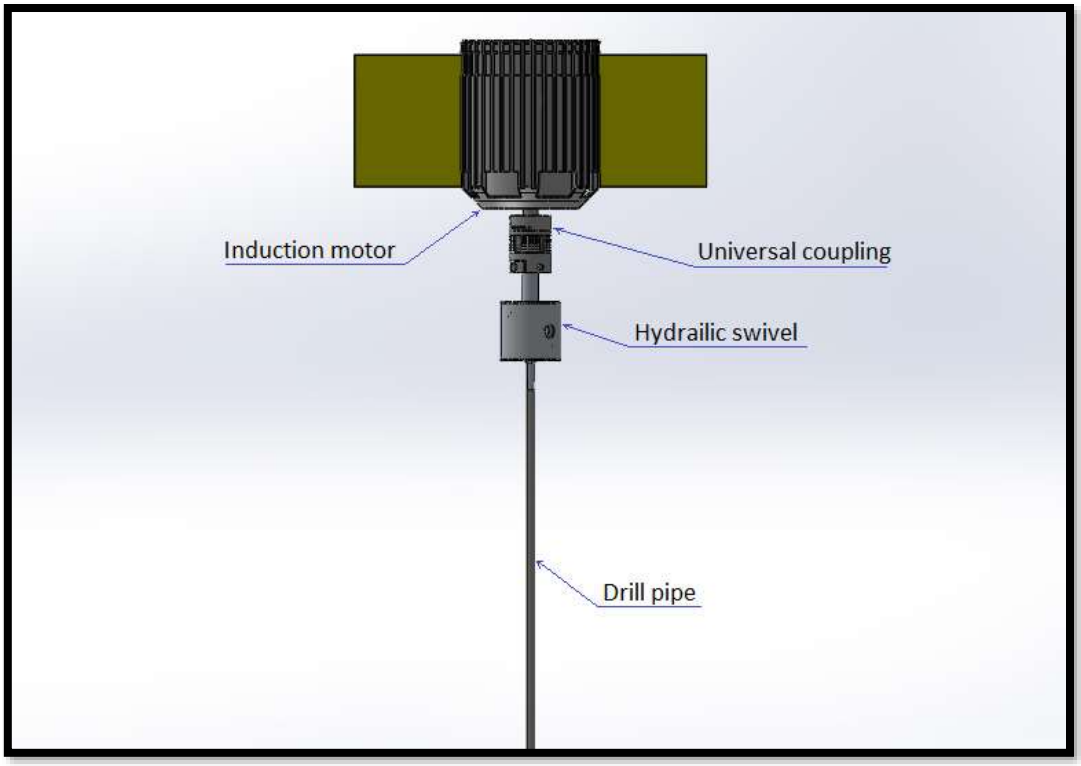

Figure 11: Top Drive system

4.2.3 Alignment

To eliminate the alignment problem, we proposed a design for riser alignment shown in the figure below.

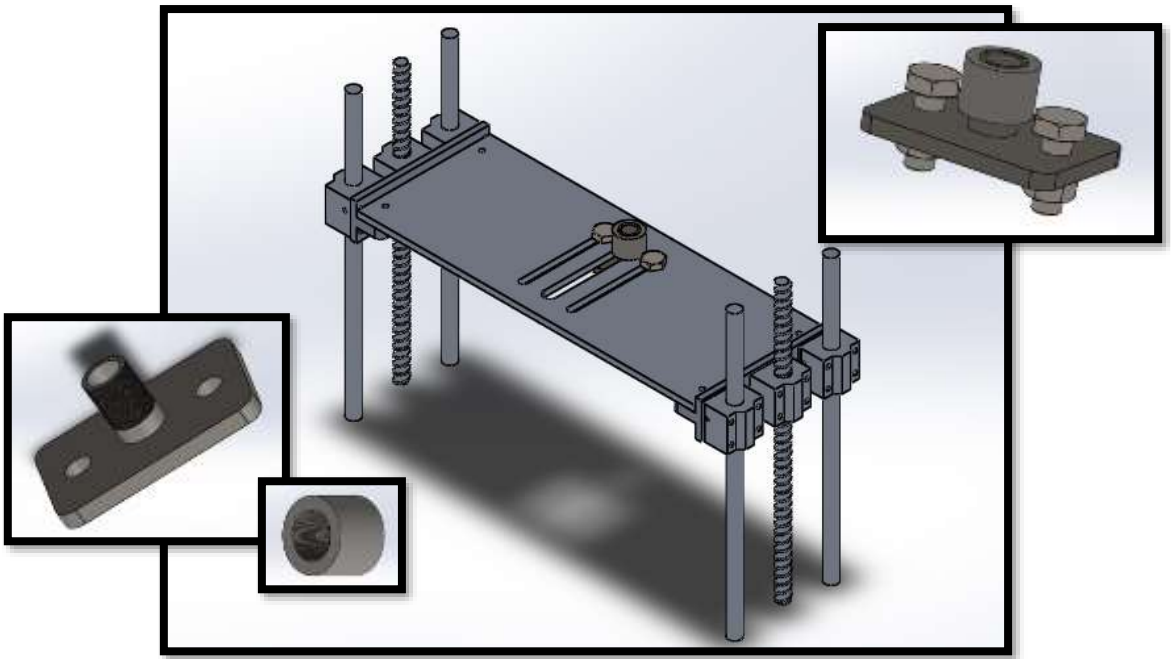

Figure 12: Riser alignment

4.3 BHA Design

4.3.1 Positive Displacement Motor

The Mud motor is a positive displacement motor. It is based on the geometrical fit between the rotating element (rotor), and the stationary element (stator). The rotor typically has a single helix shape and is normally made of a metallic material. The stator is formed as a double helix. The interference fit between the rotor and the stator creates a series of sealed chambers called cavities.

Pumping action is achieved by the rotor turning eccentrically within the stator. Fluid enters the cavity formed at the inlet and progresses within that cavity to the outlet. The result is a true positive displacement, non-pulsating flow that is directly proportional to the pump's speed. This allows the pump to deliver material at a wide range of flow rates from small shots to continuous flow. The motor usually operates at higher pressures, temperatures and high speeds.

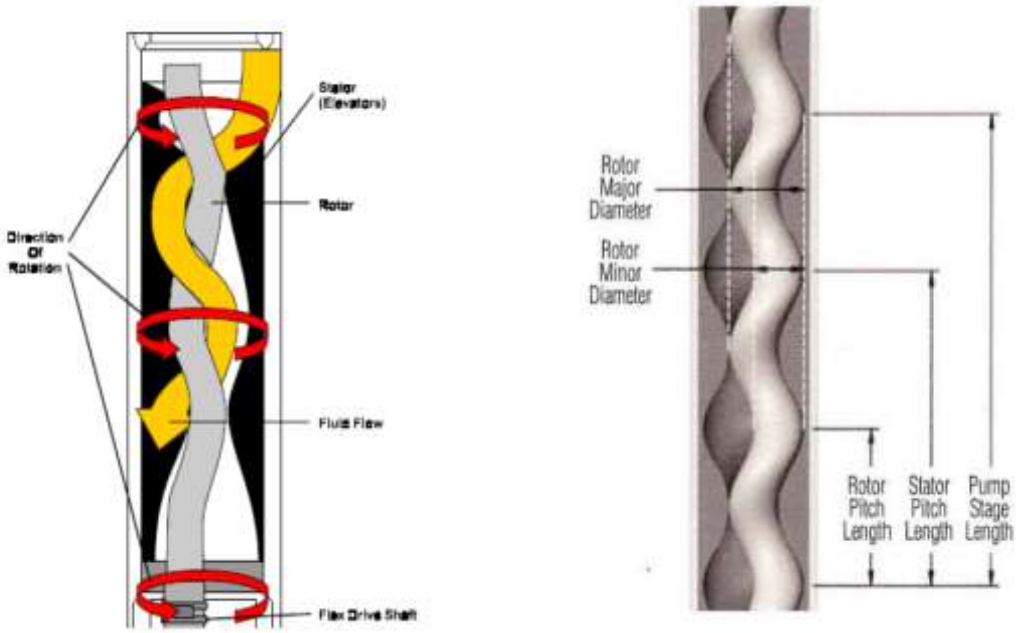

Figure 13: PDM

4.3.2 Sensor Sub

The proposed sensor sub is directly connected to the drill pipe, it contains an emplacement for the sensor card; it can work as a stabilizer to reduce vibrations.

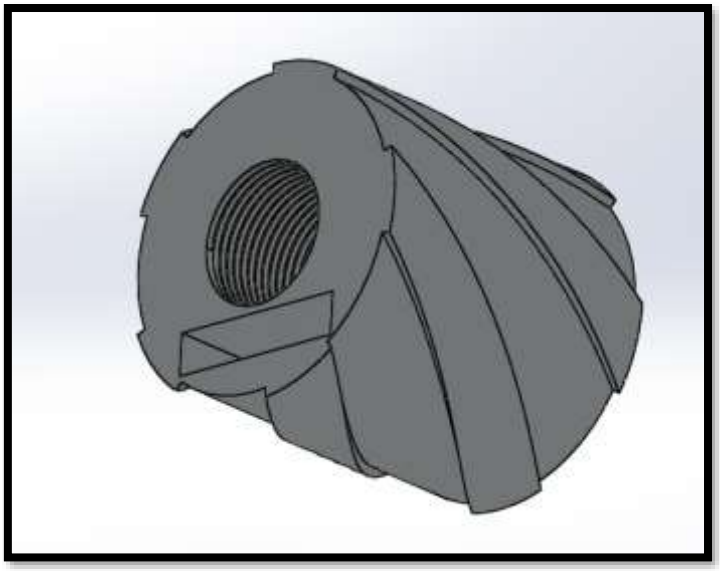

Figure 14: Sensor Sub

4.3.3 Power Section

Generally, as the number of lobes increases so does the torque (reducing the speed).

The 1 to 2 lobe configuration, used in high-speed motors, has a helical shaped rotor with a circular cross section (1 lobe). The elastomeric liner opening of the stator is oblong in cross section (2 lobes), and is molded in a helical shape with a pitch length twice that of the rotor pitch length. The multi-lobe configuration, employed in low speed, high torque motors, uses a rotor with a multiple-lobed cross section that also forms a helix. Its pitch length is longer than the rotor's pitch length by the ratio of the number of stator lobes divided by the number of rotor lobes.

We choose for our design the 1 to 2 lobe configuration for its simplicity.

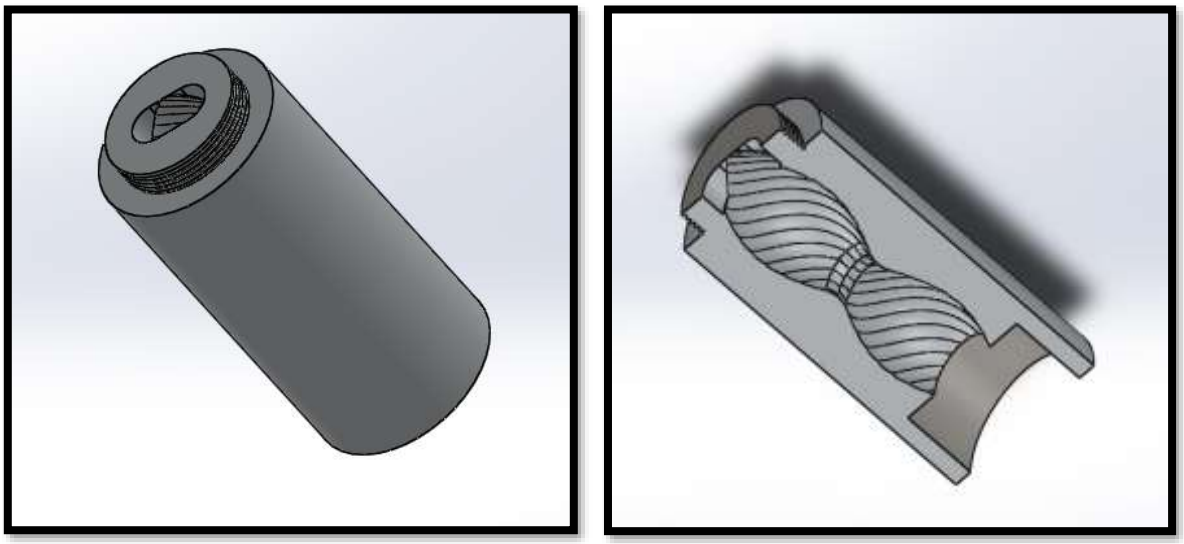

Figure 15: Stator

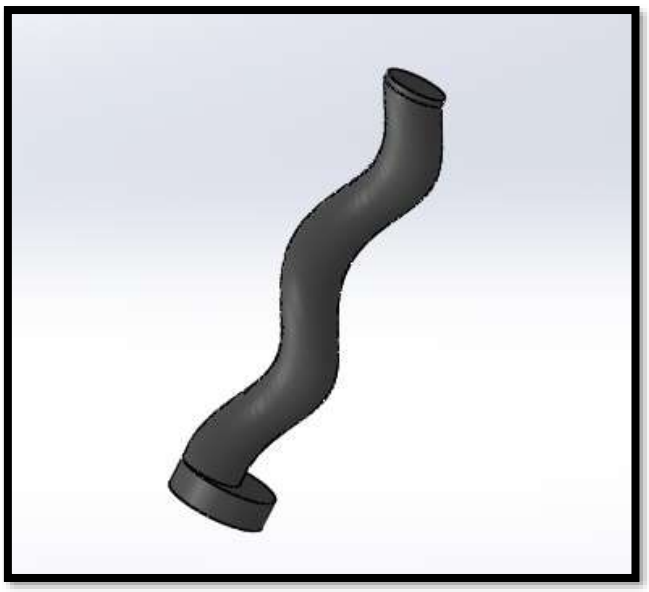

Figure 16: Rotor

The rotor forms a continuous seal lengthwise with the stator at their contact points creating wedge-shaped cavities containing drilling fluid in it. During drill ling operations, high pressure fluid is pumped into the top end of the Power section where it fills the first set of open cavities.

When drilling fluid pressure is applied to these cavities, the rotor is forced to rotate within the stator in a motion known as nutation. Nutation is defined as the oscillatory movement of the rotor's axis.

4.3.4 Transmission section

A double universal joint has been used; connected directly to the lower part of the rotor.

The fluid passes through holes in the bottom of the transmission housing.

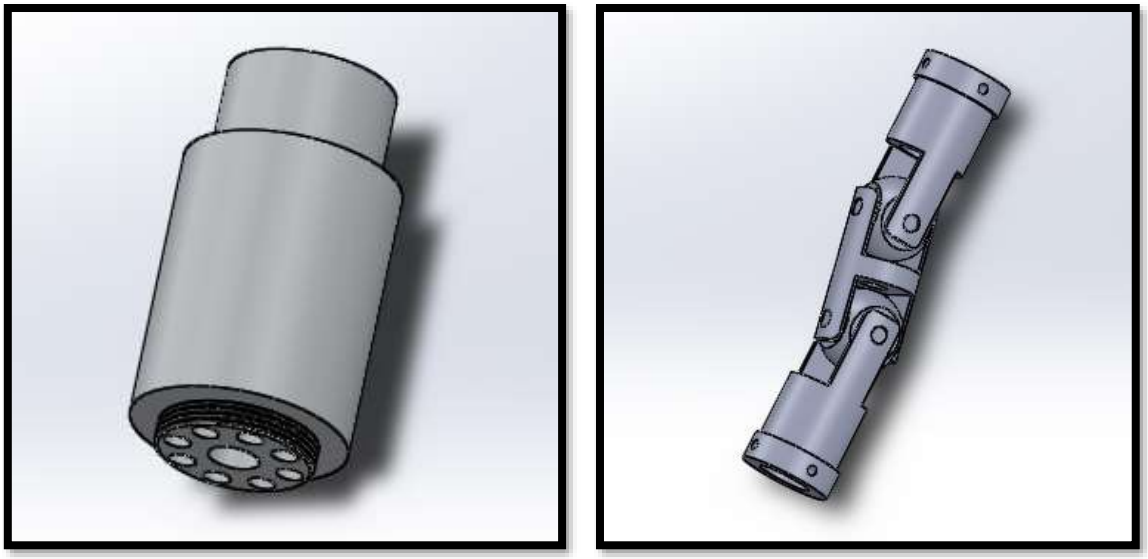

Figure 17: Transmission housing and double universal joint

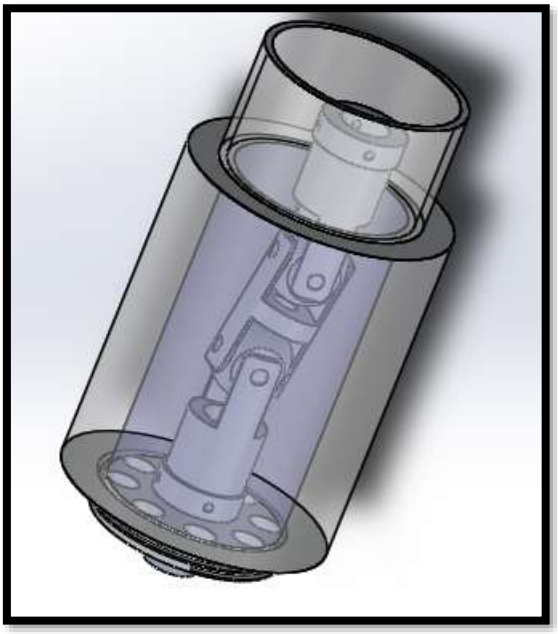

Figure 18: Transmission housing and double universal joint assembly

The bent housing is the part that allows the directional drilling, the inclination in reality is variable, and we fixed it just to simplify the conception.

A universal single joint has been used inside the bent housing, it will be coupled to the double joint with the drive shaft.

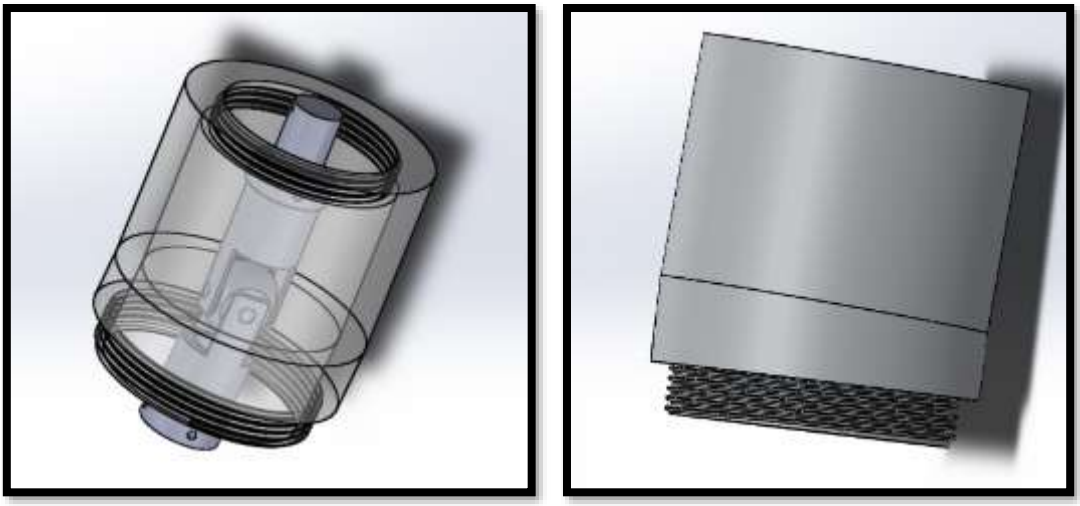

Figure 19: Bent housing

5.3.5 Bearing section

The bearing section contains the drive shaft that will make the drill bit rotate and the bearing assembly.

A simple ball bearing is used at the bottom for making the output concentric and to hold the rotor. We used a radial ball bearing_68_SKF with outer diameter of 19 mm and inner diameter 6 mm.

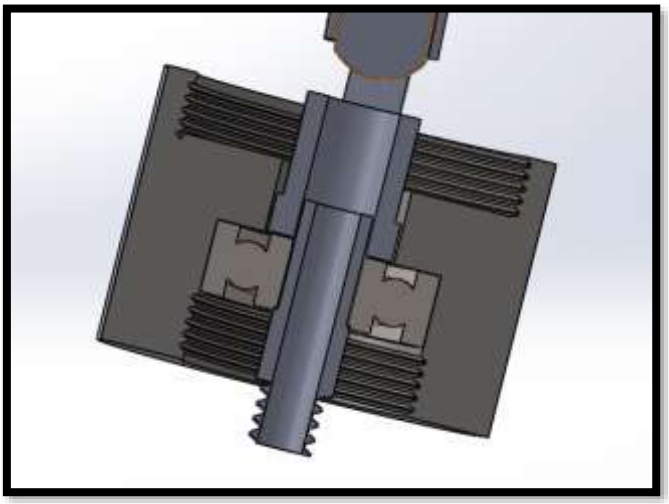

Figure 20: Bearing section

4.3.6 Bit sub

The bit sub is connected to the drive shaft on one end and to the bit on the other end.

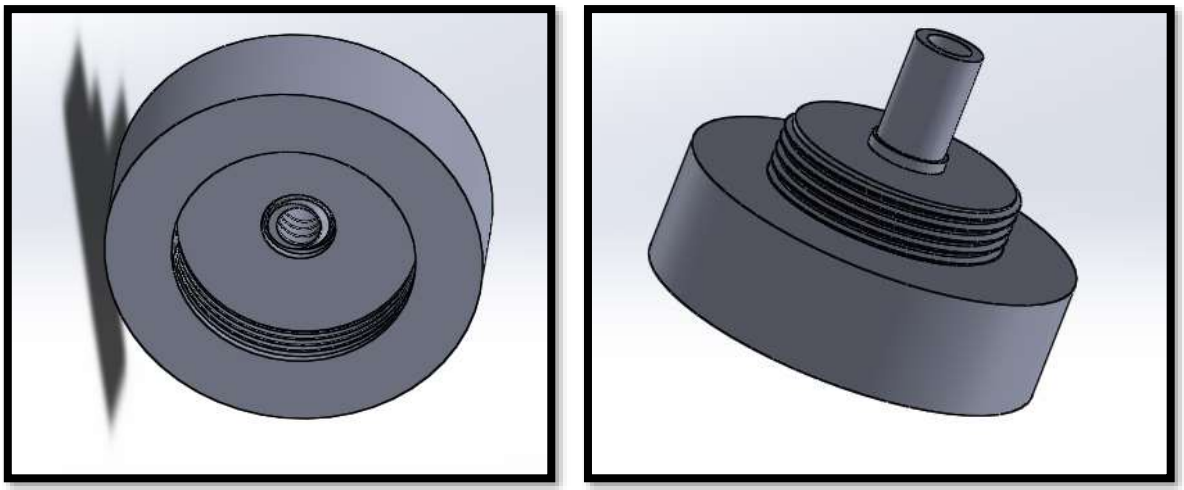

Figure 21: Bit sub

4.3.7 Final BHA design

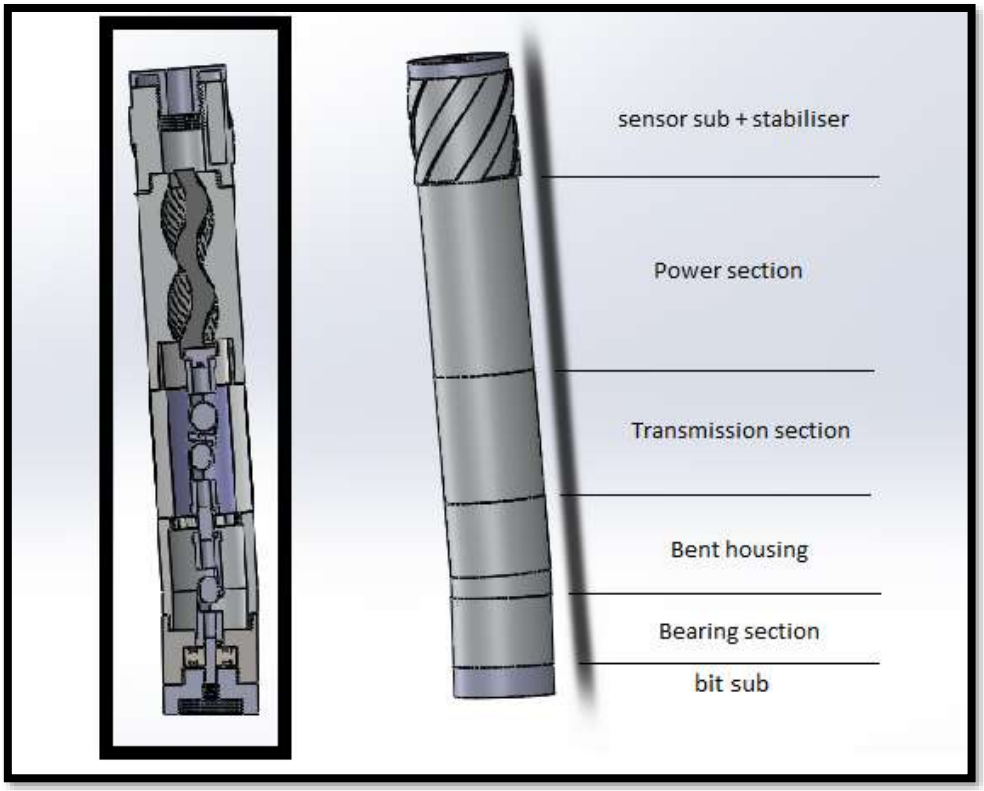

Figure 22: BHA final design

5 Hydraulic System

In the field of drilling, the drilling fluid has a significant role in carrying out drilling operations, such as the transfer of sludge from the green surface to the drill bit. Causes a pressure drop at the level of the drilling tool that increases the penetration rate. Part of the fluid energy issued in the face of the drill bit and prevent clogging of the drill bit by the cuttings so that the drilling fluid can perform its functions (transporting cuttings to the surface of the well of the hole), it is necessary that the sludge pumps be able to prevail the pressure of the channel and, consequently, to transport the cuttings out of the hole. Load in the annulus depends on the pressure exerted at the bottom of the well. Our system must provide adequate fluid pressures and flows.

The automated machine will be equipped with a circulation system to lubricate and cool the drill and machinery, to remove cuttings from the borehole and to provide additional pressure in the pipe to prevent buckling.

As cuttings are produced, the bit can grind the trenches repeatedly (grinding or cutting particles causes high friction and heat that can degrade machine performance), resulting in a low RDP as well as a loss of energy and time. Both problems can be solved by installing a circulation system.

Because the platform design does not have a closed loop fluid circulation system, a separate tank is included to collect circulating fluid and guide it to a drainage area or to storage to prevent slips and problems of electrical circuits due to wet ground. We will then see in the phase II if the cost threshold will not be exceeded, the possibility of making a closed circulation system.

We decided to keep the flow rate maintained constant during the drilling operation.

5.1 The drilling fluid

For reasons of cost, availability and efficiency we chose water as a mud fluid. His density is taken at 25 C (ambient temperature) and it is equal to 997.13 (kg/m3) and its dynamic

viscosity is equal to 0.000891 (kg/m.s).

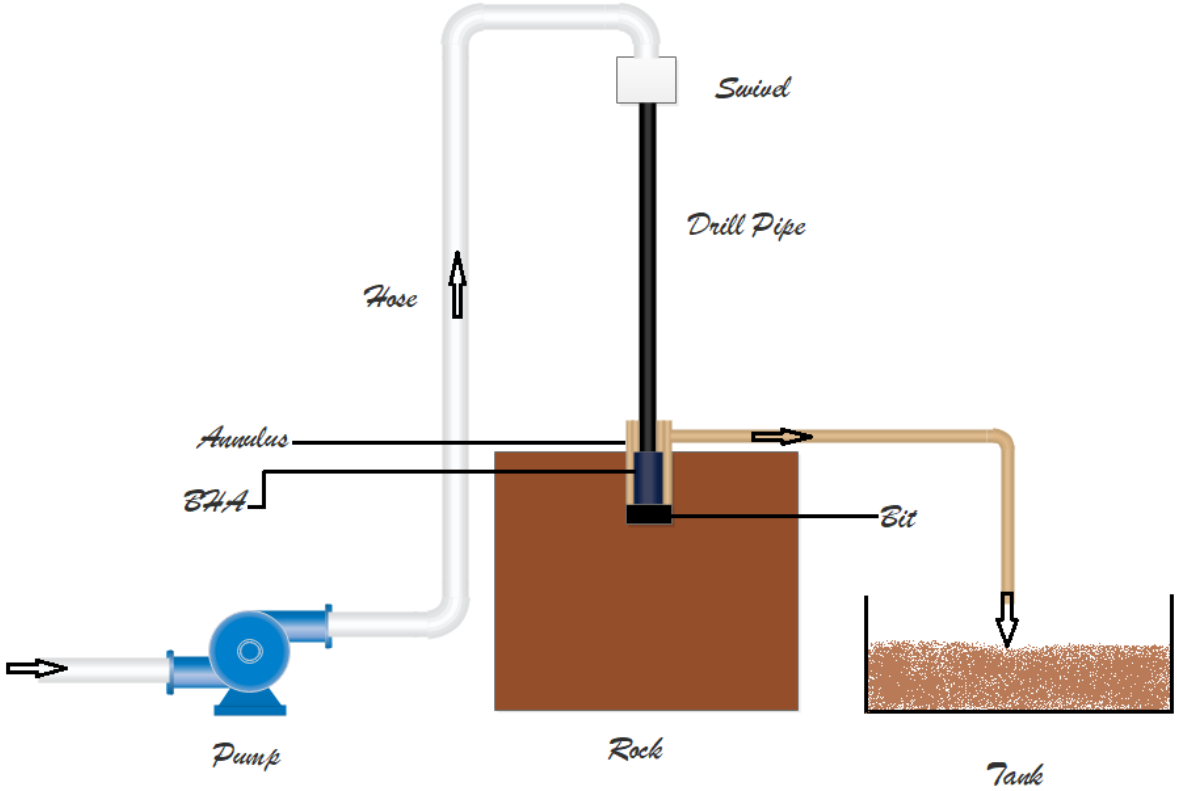

Figure 23: The circulation system

5.2 The Well cleaning

Well cleaning depends primarily on the nature of the drilling fluid, the size of the hole, the size of the cuttings and the circulation parameters.

As the drilled cuttings are generated by the drill bit, it is necessary to remove them from the well; to do this, then, the drilling mud is circulated in the well inside the pipe, then through the drilling tool, causing the cuttings at the top of the ring and then to the surface. The cleaning efficiency is according to different parameters such as:
- the size, shape, and density of cuttings.
- the speed of rotation.
-the viscosity and the annular velocity of the drilling mud.

The speed of the mud must be adapted to the nature of the drilled rock and the waste to rise to the surface. The viscosity of the mud is also an important property; if it is too weak, the fragments of rock will tend to settle at the bottom of the well, and if it is too high, the mud will circulate badly.
During the ascent, an annular top speed improves the transport of the cuttings; the ascent rate should be at least 50% faster.
Poor movement or upset of drill cuttings can cause narrowing and variation in fluid density, which can lead to loss of circulation.

5.3 The Mud Pump

The mud pump must provide a flow rate that is compatible with the optimum performance of the bit used. It is a diverse volume of mud by the drilling pumps through the stand pipe and the drill string inside the borehole.

The team decide to use Hypro 6500C Roller Pump w/ 1321-0006 (300 PSI, 22 GPM, CI, CW). It is a good choice as a drilling pump, with its higher flow rates, it allows higher usage peaks and less wear in normal use.

5.4 Calculations

5.4.1 Fluid flow regime

The type of flow regime will be determined by the liquid velocity, the diameters annular and mud characteristics and the rheological type of fluid.
It is necessary to know the type of the flow regime, not only for their physical effect but also to calculate the pressure losses, this is a very important part of the analysis hydraulic.
The transition from one regime to another is a function of the characteristics of the fluid and the flow, and to determine the flow regime, a numerical and dimensionless number called the Reynolds number (Re) is calculated using the relation:

$$Re=\rho v di$$

Re: The Reynolds number (dimensionless).
: density of the fluid [kg / m3].
ν : kinematic viscosity of the fluid [m2 / s].
di : characteristic dimension [m]
: dynamic viscosity of the fluid [Pa·s or kg / (m·s) or Pl peacle, or a tenth of PO poise]
Laminar flow is when Re<2500, transitional flow when 2,500<Re<4000 and turbulent flow when Re>4000.

5.4.2 Fluid Flow Velocity

To remove cuttings from the wellbore, the annular velocity must be greater than the cutting slip velocity. The cutting slip velocity for a turbulent flow is estimated to be 0.0992 m²/2.
it is given by the law for setting velocity in Newtonian fluid in the turbulent flow:

$$Vsl=1,54\ ds(s-f)f$$

Where,
Vsl : slip velocity, m/s
s: density of solid particle, kg/m³
f : density of fluid, kg/m³
ds : diameter of particle, m
We made several assumptions:

- the maximum particle diameter was assumed equal to the distance between the hole wall and the outer diameter of the BHA
- the density of the solid was 2400 kg/m3
- The equivalent diameter of the grains is spherical and the sphericity factor is equal to 1 (non-hollow grains)

Generally, a large annular velocity of the drilling mud improves the transport of the cuttings, moreover, with the fluidizing fluids, these high speeds can cause a turbulent regime, which increases the cleaning efficiency of the well. It is usually desirable to have a transport efficiency; the aim will therefore be to have an annulus fluid velocity (Va) of 0.35 m/s.

transport efficiency=Va -Vsl Va =71.66%

Assuming the flow rate is constant throughout the system, the minimum flow rate delivered by the pump will be then determined by multiplying the annulus velocity by the annulus cross-sectional area.

The diameter of the bore hole is estimated to be close to the diameter of the bit (38,1 mm) and the outside diameter of the pipe is 9,53mm, which gives a cross sectional area of 1068,76 mm^2. The minimum flow in the system is therefore 3,74 10^{-4} m^3/s

- **The velocity in the nozzle:**

we assume that the bit has two nozzles with a diameter of 3.10 mm (like last year) we have:
The total area of nozzles is 15.09 mm^2, so the velocity in nozzles is estimated to be 24.78 m/s using the equation:

$$Vn=QAn$$

Where:
Q: Volume flow rate
A: Cross section

5.4.3 Pressure Loss

- **Pressure Loss in Hose**

first, we calculate the velocity of fluid in hose Vh using the equation:

$$Vh=QAh$$

so, the velocity in the hose is estimated to be 9.61 m/s.
We determine the type of flow regime. This can be done by estimating the Reynold‘s number given by the equation:

$$Re=\rho vdi$$

Where:
Re is Reynold's number (dimensionless) calculated 75712.94> 4000 => turbulent flow
The Darcy friction factor is a dimensionless number; the pipe roughness and the pipe diameter which are used to determine the friction factor should be dimensionally consistent (e.g. we use roughness and diameter both measured in mm, or both measured in inches).
The flow is turbulent. In this case, the friction factor must be determined using an empirical correlation. The Colebrook Equation, which is widely used in the field of fluid dynamics, was

chosen as a good approximation and is given by the equation (this equation will be solved numerically using Excel):

$$1f=-2(\varepsilon 3,7D+2,51Ref)$$

where:
ε: the roughness of the hose is estimated to be 0,0001(m)
f: the Darcy friction factor (dimensionless) calculated 0.019.
Then we use the equation:

$$\Delta P_1=\rho g h_F$$

Where:
g: the gravity and its value is 9,81 (m/s2)
: the density of the fluid (Kg/m3)
ΔP1 : the pressure loss (Pa)
h_F: calculated using the equation:

$$h_F=4\lambda LV^2 2gd$$

where: 4ʎ = f
L: the length of the hose (m)
V: the velocity in the hose (m/s)

The pressure drop through the hose is estimated to be 0.575 bar (ΔP1).

- **Pressure Loss in Swivel**

We found the guide of the swivels cited in the references the following chart which helped us to make a first estimate of the pressure loss in the swivel:

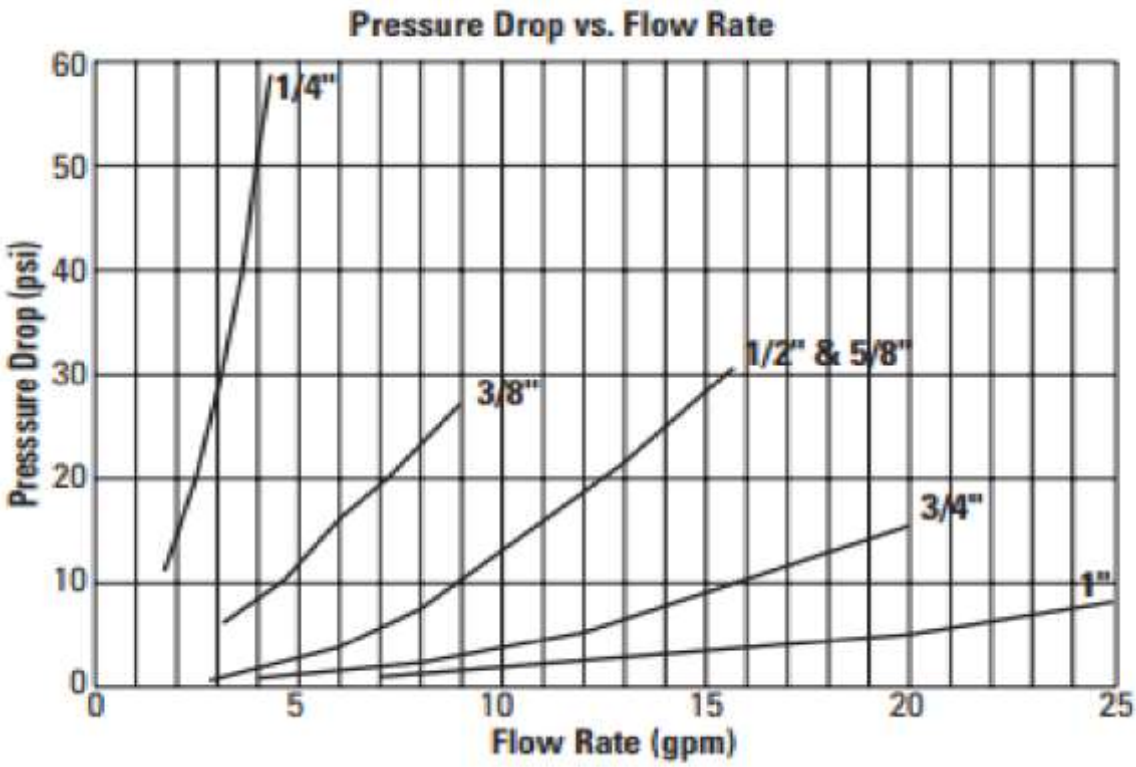

Figure 24: Pressure loss in the swivel

For the flow rate of 3,74 10^{-4} m3/s (5.93gpm) and the dimension of 1‘‘ we have the estimate of around 0.2 bar (ΔP2).
A more accurate estimate of the pressure loss in the swivel will be provided by the manufacturer of the swivel in the phase II.

- **Pressure Loss in Pipe**

first, we calculate the velocity of fluid in the pipe Vp using the equation:

$$Vp=QAp$$

so, the velocity in the pipe is estimated to be 9.61 m/s.
We determine the type of flow regime. This can be done by estimating the Reynold‘s number given by the equation:

$$Re=\rho vdi$$

Where:
Re is Reynold's number (dimensionless) calculated 75712.94> 4000 => turbulent flow
We use these equations with the same procedure:

$$1f=-2(\varepsilon 3,7D+2,51Ref)$$

$$\Delta P3=\rho g h_F$$

$$h_F=4\lambda LV^2 2gd$$

The pressure drop through the pipe is estimated to be 1.136 bar (ΔP3).

- **Pressure Loss in Bottom Hole Assembly (BHA)**

The pressure drops caused by flow resistance through the bottom hole assembly (BHA) must be calculated separately with the equation:

$$\Delta P_4=0.5V2ev$$

With: $ev=(1-1)^2$ and $\beta=A_2^2/A^2_1$
V is the velocity in the BHA, calculate with this equation: $V=QA_2$

A_1: the pipe section
A_2: BHA section
We consider the pressure drop in BHA is negligible because it is very small, then it is not important to calculate it

- **Pressure Loss in Bit**

first, we calculate the velocity of fluid in the bit Vb using the equation:

$$Vb=QAb$$

so, the velocity in the pipe is estimated to be 0.328 m/s.
We determine the type of flow regime. This can be done by estimating the Reynold‘s number given by the equation:

$$Re=\rho vdi$$

Where:
Re is Reynold's number (dimensionless) calculated 12460.93> 4000 => turbulent flow
We use these equations with the same procedure:

$$1f=-2(\varepsilon 3,7D+2,51Ref)$$

$$\Delta P4=\rho gh_F$$

$$h_F=4\lambda LV^2 2gd$$

The pressure drop through the pipe is estimated to be 0.0095 bar (ΔP4).

- **Pressure Loss in Nozzles**

We use the equation:

$$\Delta P5=\rho f.Q^2 12032Cd^2An^2$$

Where
Cd: the nozzle coefficient was determined to be 1.03 instead of 0.96 used by most bit companies
P5: Nozzle pressure loss (psi)
Q: flow rate (gpm)
f: mud weight (ppg)
An: the total area of nozzles($inch^2$)

The pressure loss in the two nozzles is estimated to be 2,884 bars.

- **Pressure Loss in Annulus**

The value of the diameter used in these equations is an equivalent diameter calculated using the equation:

$$deq=da^2-dp^2$$

where:
da is the diameter of the annulus and dp is the outer diameter of the pipe (9.53mm).

- deq=35.64mm

first, we calculate the velocity of fluid in annulus Va using the equation:

$$Va=QAa$$

so the velocity in the annulus is estimated to be 0.37 m/s.
The pressure loss through the annulus was based on previous equations as for as the hose. The flow rate is estimated to be turbulent through the annulus as well and resulted in a pressure drop, the loss pressure in annulus is estimated to be 0,0073 bar (ΔP6).

Summary of pressure loss
The total pressure loss is:

Table 1: results of pressure loss

Component	Pressure loss (bar)
Hose P1	0.5750
Swivel P2	0.2000
Drill pipe P3	1.1360
Bit P4	0.0095
Nozzles P5	2.8840
Annulus P6	0.0073
Total Pt	4.8118

5.4.4 Pump's Power

It's given by :

$$Ppump=\Delta PtQ\eta$$

Where:
ΔPt : is the total pressure loss in the drilling machine
Q : is the volumetric flow giving by m^3/s
η : is the efficacity of the pump = 0.8
Hence:

$$Ppump = 4.81183,74\ 10^{-4}0.8*100=0.225Kw$$

6 Electrical System and Instrumentation

In this section, the electrical system's actuators (motors) and the various drives that control their speed and torque will be described, as well as the sensors both top side and downhole, that serve as the control system's senses, most are the same as last year's except for a few improvements and changes so this section will be describing each part and mentioning why it was kept and why it was chosen in the first place or why it was changed for another one.

6.1 System Overview

The electrical system of the miniature drilling rig consists of a combination of motors, motor drives and sensors, top side and downside that make automatizing the drilling process possible, and are wired in such a way, optimizing the power distribution and meticulously choosing the different parts so as to make the rig provide the best possible communication flow between its various components.

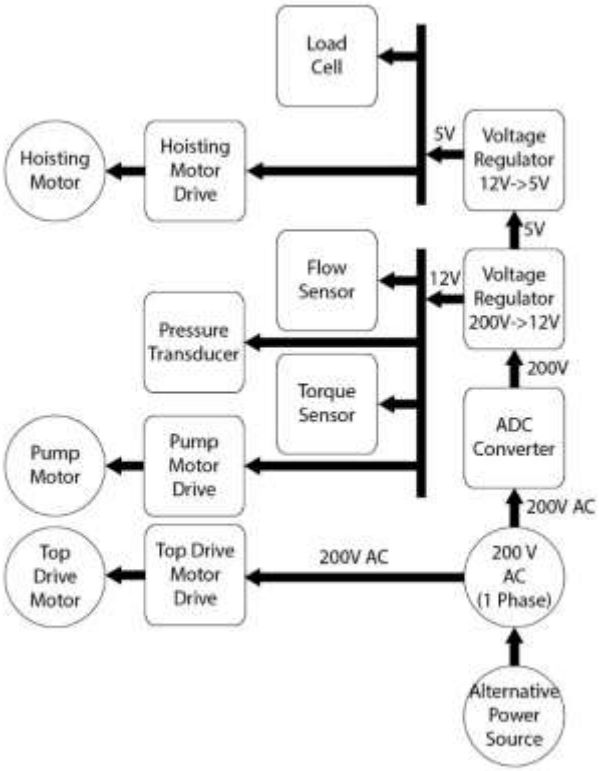

Figure 25: Top Side Power Distribution

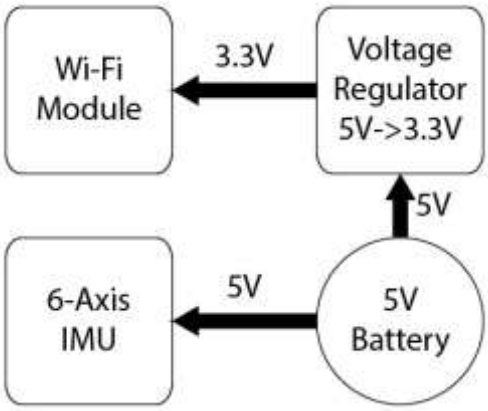

Figure 26: Downside Power Distribution

6.2 Rig Actuators

6.2.1 Top Drive Motor

This year's rig has as a top drive the **Delta ECMA-E1830S Permanent Magnet AC Servo Motor**, instead of last year's , **ATO-SERVO-150S3000 Brushless AC Servo Motor** chosen mainly for the aiming aspect of directional drilling, its power rating of 3 kW, its precision speed control, and the enhanced durability it features in harsh industrial environments, it has a rated speed of 3000 rpm (max speed up to 4500 rpm), a rated torque of 14.32 N.m (max torque up to 42.97 N.m), with a 180x180 mm design frame that's 200 mm in length.

Figure 27: Delta ECMA-E1830S AC Servo Motor

6.2.2 Hoisting Motor

Last year's choice works perfectly for this year's competition, which was a **"Dual Shaft Nema 34 CNC Stepper Motor"**, initially chosen for its high torque-density rating, high torque-to-inertia ratio, and small but effective, cool running design, it has a calculated maximum power output of 1800 rpm, a step angle of 1.8° which allows for more precision, a maximum output torque of 8.5 Nm, and an overall 86x86 mm design frame and 114 mm of length.

Figure 28: Dual Shaft Nema 34 CNC Stepper Motor

6.2.3 Pump Motor

The pump used is **Qingeal ZW50-10-20 Pump**, made from Cast Iron and able to flow 10m3/h, while consuming 2.2kW and either 220v or 380v.

Figure 29: Qingeal ZW50-10-20 Pump

6.3 Drives

6.3.1 Rotary Motor Drive

ATOMG-1000 AC Servo Motor Drive was used in 2020 for the ATO-SERVO-150S3000 Brushless AC Servo Motor. This year, since the top drive motor was changed to the **Delta ECMA-E1830S Permanent Magnet AC Servo Motor**, the drive had to be changed to **ASDA-A2R-3023-U Servo Motor Drive**, its matched drive model.

The first, the power drive unit is rectified by the three-phase full bridge rectifier circuit to input the three-phase electric or municipal power, and the corresponding DC power is obtained. The three-phase power or electric supply after rectifying can drive the AC servo motor through three-phase sine PWM voltage source inverter frequency conversion. The whole process of the power drive unit can be simply described as the process of AC-DC-AC. The main topology of the rectifier unit (AC-DC) is the three-phase full bridge uncontrolled rectifier circuit.

The Drive will be programmed using its corresponding software, the **ASDA-Soft Configuration Software**, which is user-friendly, allowing for fast configuration of the drive

Figure 30: ASDA-A2R-3023-U Servo Motor Drive

6.3.2 Hoisting Motor Drive

DM556 is used to control the hoisting motor's Torque and RPM according to the varying values of ROP which need to be controlled, the position and force calculated by the Position Sensor and Load Cell respectively, are used to calculate ROP and then to feed back into the PLC, and it would, in turn, following an optimization algorithm proposed but not used in the 2019 rig, control the hoisting motor's Torque and RPM using a varying output signal (in voltage).

Figure 31: DM556 Stepper Motor Drive

6.3.3 Pump Motor Drive

Usfull FU9000A Pump Motor Drive is used to control the speed of the pump's motor, whose role is even more important in 2020 due the use of the Hydraulic Mud Motor, the fluid's flow rate is proportional to the pump's motor's RPM which can be controlled using this drive, this controlling the fluid's flow rate.

Figure 32: Usfull FU9000A Pump Motor Drive

6.4 Surface Sensors

6.4.1 Top Drive Motor Rotary Encoder

The top drive motor's rotary encoder (**Delta ECMA-E1830S Permanent Magnet AC Servo Motor**) is used to measure the RPM within the drillpipe, which is the top drive RPM, eliminating the need for an RPM sensor, it sends back a signal indicating the motor's position which can be used to calculate the RPM.

6.4.2 Torque Sensor

Inorder to measure the top drive Torque, the 2019 rig was supposed to have a current sensor installed, because initially it had a BLDC Motor, now that the rig has an AC Servo Motor as a top drive motor, the **Omega TQ513 Torque Sensor**, is used to measure torque applied on the drill pipe, it has silver slip rings for a secure connextion, operates with a speed of up to 5000 RPM, and can measure RPM, it has a torque range of 0 to 0.35 N.m, an accuracy of ±0.1%, a weight capacity of 50 in-oz.

Figure 33: Omega TQ513 Torque Sensor

6.4.3 Hoisting Motor Rotary Encoder

The hoisting motor's rotary encoder (**Dual Shaft Nema 34 CNC Stepper Motor**) is used to measure the drill pipe's linear displacement in order to calculate and control ROP (Rate of Penetration), the incremental rotary encoder sends back a signal indicating the motor's position which can be converted into millimeters.

6.4.4 Load Cell

One of the most vital measured parameters for drilling is Weight-on-Bit (WOB), will be measured by the **Omega Miniature Stud-Mount Load Cell** used last year, a force transducer that converts force applied to the drill line into an electrical signal, because it's directly related to the force/weight applied on the bit, it's perfect for calculating WOB, and it needs to be both precise and efficient because of its importance in the control procedure, the Load Cell has an input voltage of 5-10 V (DC), an accuracy of ±(0.15-0.20)% FSO, and an ultimate overload equal to 300% of capacity.

Figure 34: Omega Miniature Stud-Mount Load Cell

6.4.5 Pressure Transducer

Pressure applied on the hydraulic pipes by the fluid has to be controlled and thus a **FST800-211 Silicon Strain Gauge Piezoelectric Pressure Sensor**, just like last year's will be used and mounted behind the pump, it has an input voltage of 12-24 V (DC), is made of stainless steel and has a pressure range of 1-300 Bar.

Figure 35: FST800-211 Piezoelectric Pressure Sensor

6.4.6 Flow Sensor

The **YF-S201 Flow Sensor** (used in 2019) is a Hall Effect based flow sensor that was mounted in line with the circulating system fluid, that contains a Pinwheel Sensor to measure how much liquid has moved through it, in addition to an integrated magnetic Hall Effect Sensor that outputs an electrical pulse with every revolution, the Hall Effect Sensor is sealed from the water pipe and allows the sensor to stay safe, the Flow Sensor has an input voltage of 5-18 V (DC), draws a maximum current of 15mA (at 5 V), has an accuracy of ±10%, and can detect a maximum water pressure of 2.0 MPa.

Figure 36: YF-S201 Flow Sensor

6.5 Downhole Sensors

6.5.1 6-Axis Motion Tracking

Since vibrations are an important limiter of ROP optimization, they must be measured and controlled for an optimal drilling process, the 3-Axial Accelerometer in the Measurement Unit uses the principle of the piezoelectric effect to measure and monitor the amplitude of vibrations in the BHA, so they can be used to control ROP and to check for any abnormal downhole activity.

And since this is a directional drilling challenge, the use of a 3-Axial Gyroscope is more pivotal than ever, so it measure at all times, the position of the bit and its inclination and azimuth, in order to effectively minimize the angle of defection from the calculated trajectory, and to know when the bit has taken an abnormal trajectory, so the rig can correct it, in the both the vertical and directional drilling phases, and to calculate the new trajectory in case a correction is needed.

The 6-Axis Inertial Measurement Unit being used is a **GY-521 MPU-6050 6-axis IMU**, it has, in one sensor, both a 3-Axis Accelerometer for measuring the BHA's vibrations and a 3-Axis Gyroscope mainly for measuring the bit's coordinates as well as its inclination and azimuth.

The IMU is 21.2x16.4x3.3 mm, has an input voltage of 5 V (DC), can detect acceleration of up to 16 g, its gyroscope has a range of up to 2000 °/s (dps), and includes a 3.3 V voltage regulator.

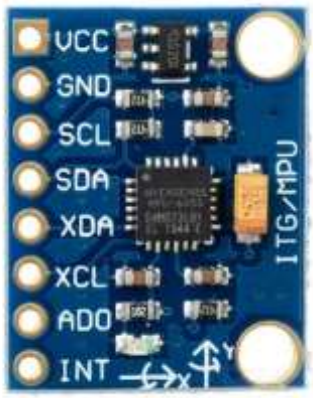

Figure 37: GY-521 MPU-6050 6-axis IMU

6.5.2 Wireless Communication

To enable data transfer from the BHA a small size **NodeMCU ESP2866 12E Wi-Fi Module** is perfect for connecting with the **GY-521 MPU-6050 6-axis IMU, its** external size is small which allows for placement inside the BHA, it has an operating voltage of 3-3.6 V (DC), an operating current of around 80 mA, and it is 16x24x3mm in dimensions.

Figure 38: NodeMCU ESP2866 12E Wi-Fi module

6.5.3 Printed Circuit Board

A Printed Circuit Board (or PCB for short) will be inserted inside the BHA, which contains the Motion Tracking IMU and the Wireless Communication device, with a 5v power supply powering both of them in order to have real time communication with the computer and the PLC running the drilling.

6.6 Power Consumption

Table 2: Power Consumption

Rig actuators	Power (KW)
Top drive motor	3 Kw
Hoisting motor	1.5 Kw
Pump	2.2 Kw
Total	≈6.7 Kw

7 Control System

In this section, the control system is going to be described, it is a centralized control system using a Programmable Logic Controller for I/O Control, and using a computer for data collection and acquisition, which uses LabVIEW as the interfacing software, PC based control systems have the advantages of being durable and reliable, as well as the ability to add extra I/O to acquire or control extra areas in order to perfect the system, Data logging can be triggered by an event within the process or scheduled to occur at regular intervals. Also, once the data is collected, it will be transferred to the PC for acquisition and monitoring.

The control system uses the electrical parts and actuators mentioned in the last part, and uses three different drilling modes, to allow the drilling operation to reach its target point with the most precision and least vibrations possible.

7.1 System Overview

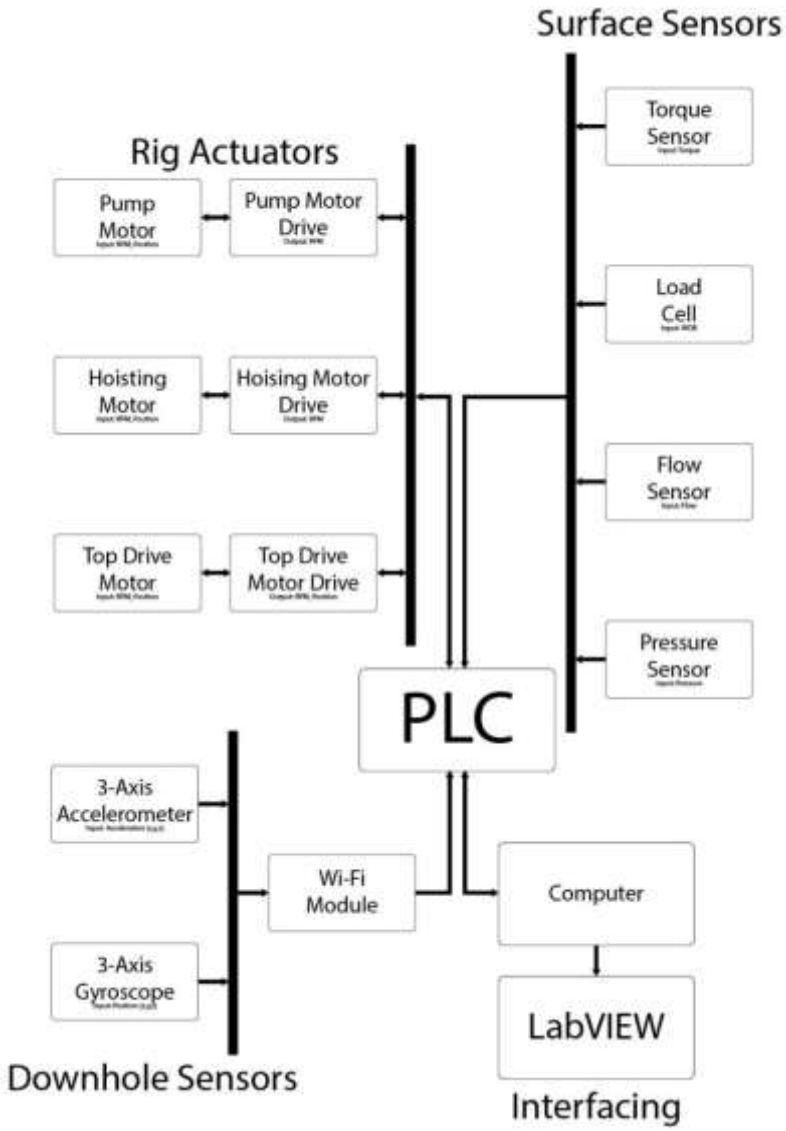

Figure 39: Control System Overview

7.2 Data Acquisition

In order to make use of all the rig's sensors' and drives' signals and command the whole electric system, a main I/O control unit is necessary in order to form a centralized system, and for that, last year's **Siemens SIMATIC S7-1200 PLC** was kept, all the parameters from the sensors and drives are converted into measurable electric signals (voltage) which are next transferred in this central unit, then they'd be transported to the computer via Ethernet to be exploited for different uses, mainly interfacing and simulation, the advantage of this centralized system is that it can realize synchronous data acquisition, as well as real-time display and preservation.

Considering the PLC is a SIEMENS, SIMATIC STEP7 serves as a perfect programming software for it, which is user-friendly, intuitive and efficiency offer a transparent, intelligent and straightforward experience.

Factory I/O, the simulation software, will be used for interfacing. It is known to not only effectively play the performance of an ordinary data acquisition system.

Figure 40: Siemens SIMATIC S7-1200 PLC

7.3 Actuator Control

This sub-section will be covering the basic and elemental control systems, of the different actuators which are the rig's performing parts, and which are, the Top Drive Motor, the Hoisting Motor and the Pump

7.3.1 Top Drive Motor RPM Control

The Top Drive System, has a control system which regulates its RPM, so that it can easily follow its defined RPM Set Point, which is set to the maximum RPM possible for the Top Drive Motor (before the start of the vibrations), using a PID controller, a limiter before the motor, and Low-Pass Filter for the feedback brought from its rotary encoder.

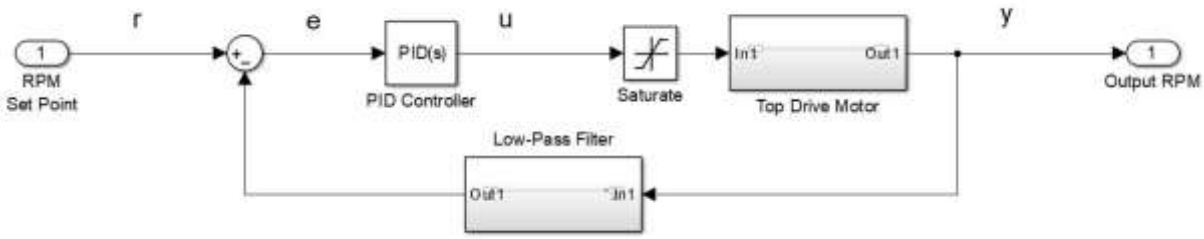

Figure 41: Top Drive Motor RPM Control Block Diagram

7.3.2 Hoisting Motor RPM Control

The Hoisting System, just like the Top Drive System, has an internal controller regulating its RPM, which has as a Set Point, being constantly fed into the Hoisting System by the other PID controllers which will be mentioned, the system also filters the feedback using the Low-Pass Filter filter.

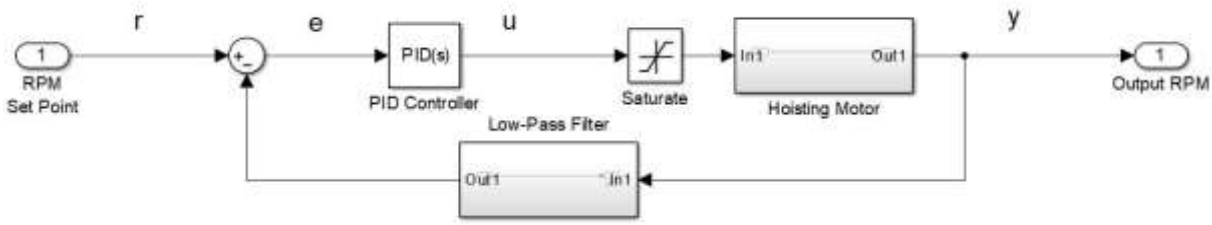

Figure 42: Hoisting Motor RPM Control Block Diagram

7.3.3 Pump Flow Control

The Pumping System has an internal control system regulating the Flow passing through the fluid pipes, using the same techniques as the previously mentions RPM controllers.

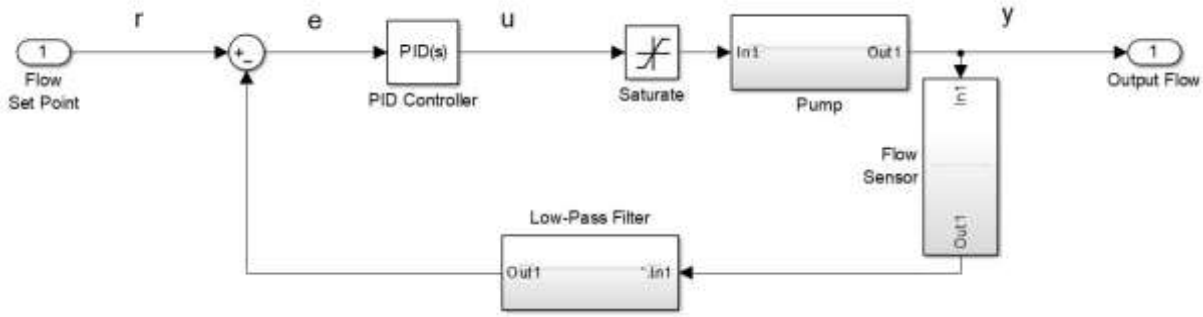

Figure 43: Pump Flow Control Block Diagram

7.3.4 Filtering

The feedback from the various Systems will be run through both a Low-Pass Filter in order to remove noise and have a clear signal that does not disturb the correction process in any way.

7.3.5 PID Tuning

The Cohen-Coon and Ziegler Nichols methods will be used to tune the PID controllers for the various Systems

7.4 Control Modes

This sub-section will cover the three essential modes that will operate the rig, which will be doing different tasks depending on the situation and the BHA's position, which are in order, the Vertical Drilling Mode, the Steering Mode, and the Directional Drilling Mode, each of which will be explained in detail in the following sub-section parts.

7.4.1 Vertical Drilling Mode

The first mode, the Vertical Drilling Mode, controls the Hoisting Motor's RPM using both the drill pipe torque resulting from the Top Drive Motor's RPM whose feedback signal is sent back by the Torque Sensor installed with the drill pipe, and the WOB sensed by the Load Cell with two different PID controllers, these two modes can either alternate or be active at the same time to guarantee the best Hoisting RPM and an optimal lowering speed that doesn't disturb the Torque or the WOB, all the while the system is controlling the position of the drill

bit using another PID controller, which is very important so the drilling can switch to the steering mode when at the kickoff point.

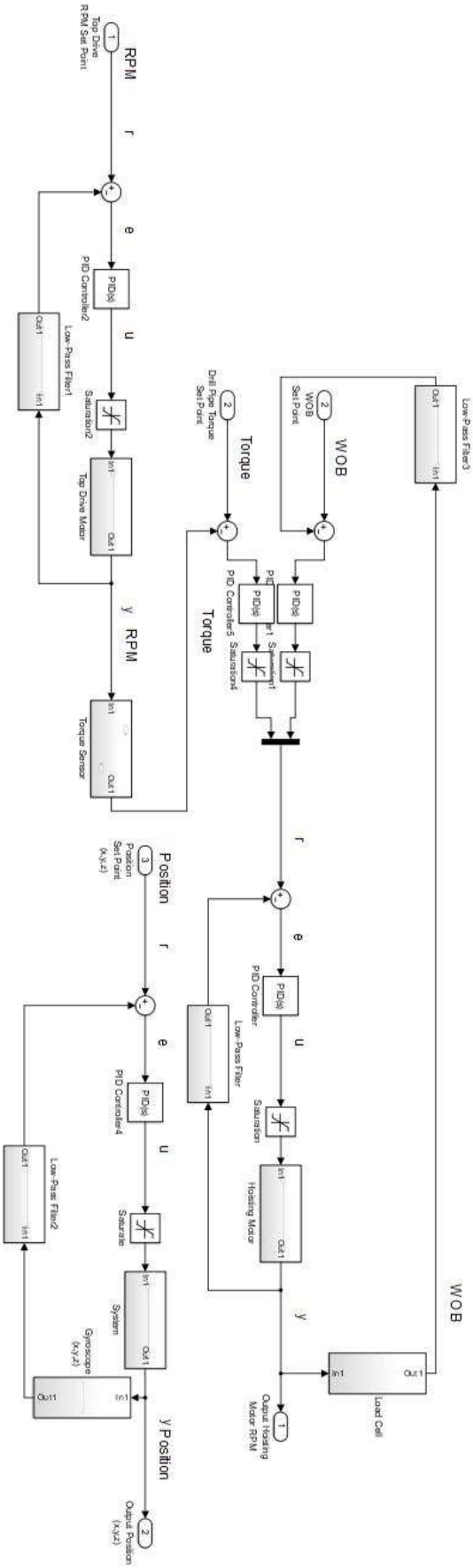

Figure 44: Vertical Drilling Mode Control System Block Diagram

7.4.2 Steering Mode

The Steering Mode rotates the drill pipe horizontally, so the drill bit can be pointed at the target point, using the azimuth (which is calculated using the coordinates of the target point entered into the system before the drilling operation begins), as a set point, the feedback is brought back by the gyroscope, and the control is provided by a PID controller.

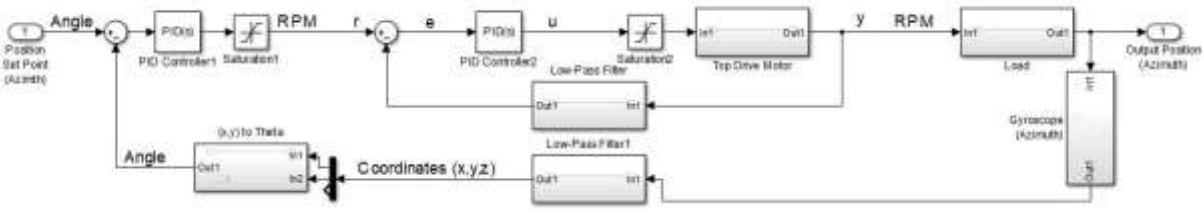

Figure 45: Steering Mode Control System Block Diagram

7.4.3 Directional Drilling Mode

The Directional Drilling Mode, the drilling operation's most important part, controls the Hoisting Motor's RPM with the same method used in the Vertical Drilling Mode, and also controlling the position, to accurately identify the distance to the target point and allow the operation to stop when it is reached, the three PID controllers used in these two operations are the same as the ones used in the vertical drilling, the Pumping System will also be pumping the fluid, which is being regulated by another PID controller, so it can power the hydraulic Mud Motor (Positive Displacement Motor), which allows the drill bit to push down and to the side, sliding with its fixed angle til it reaches the target point.

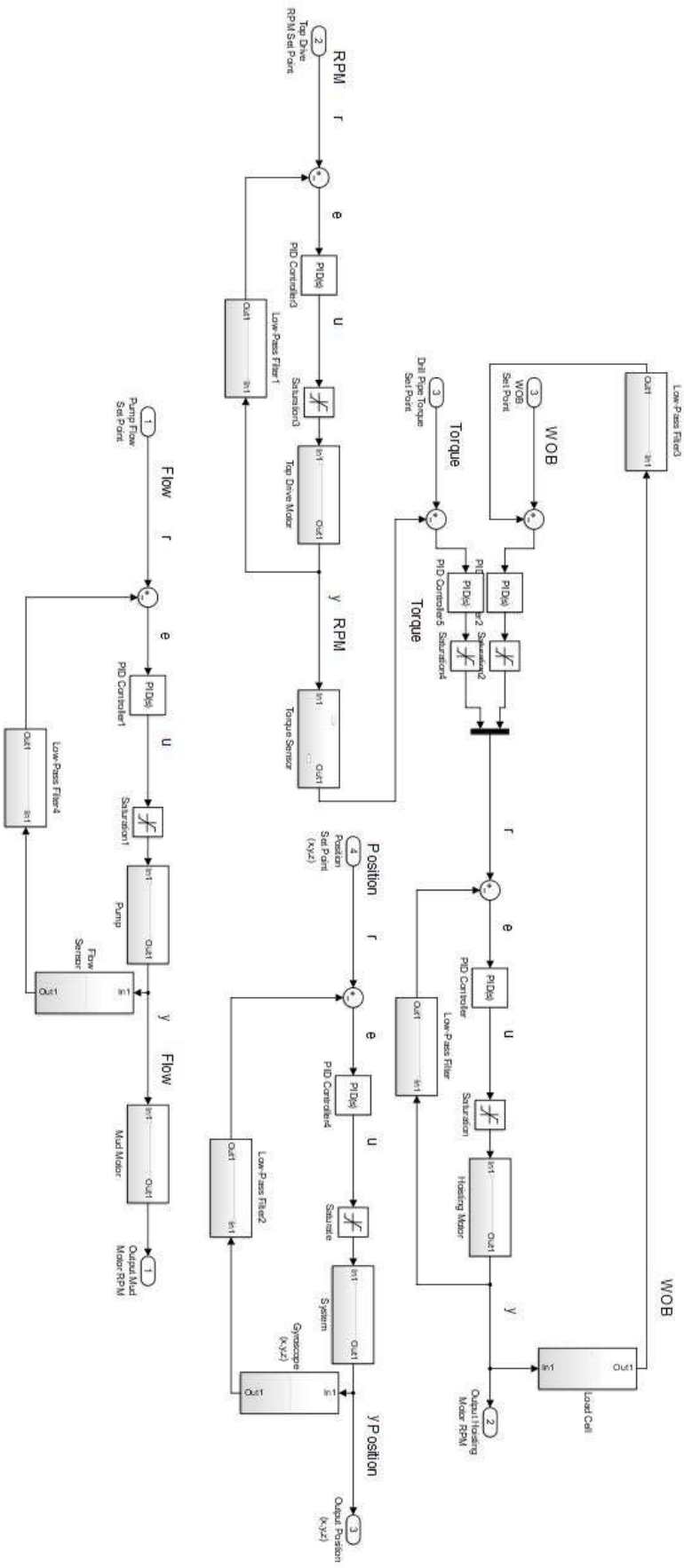

Figure 46: Directional Drilling Mode Control System Block Diagram

7.5 Control Algorithm

The control algorithm consists of a combination of the three modes already mentioned, that will be alternating when the drilling operation begins, when the x, y and z coordinates are entered into the system, the optimal drilling path will be calculated, and the vertical drilling mode will be initiated and the rig will keep on drilling vertically until it reaches the kickoff point from which the optimal path begins (which depends on the BHA's bending angle), it will then initiate the steering mode, to turn the BHA so as to be facing the target point, after that, the final mode, the directional drilling mode will start and will the rig will drill and start deviating from the vertical well, with a fixed angle until it reaches the target point, with maximum precision, all the while deploying the optimization algorithm which will be optimizing ROP based on MSE.

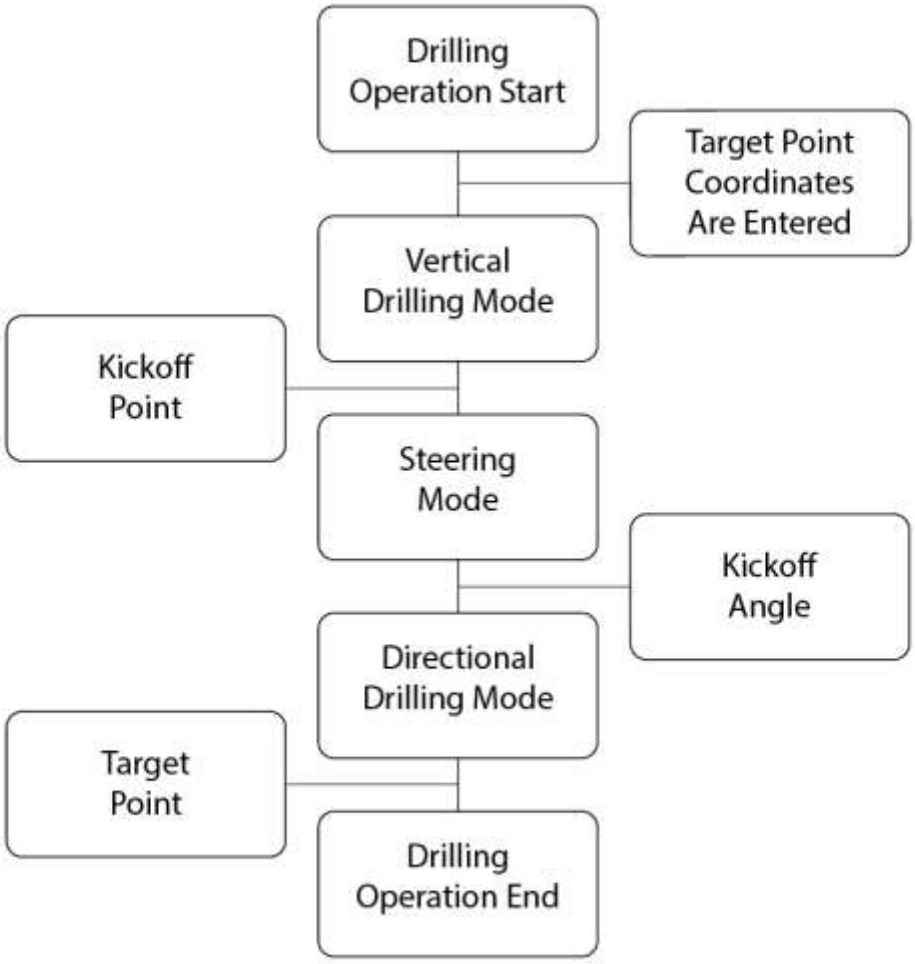

Figure 47: Control Algorithm

7.6 Optimal Path

The optimal path will be calculated using an algorithm based on the drill pipe's limit of elasticity and the time it would take for the drill bit to reach its destination, its trajectory is initially vertical for a few centimeters and then it bends over with an angle that is narrow enough to respect the drill pipe's limit of elasticity, but wide enough to reach the point with the required depth (z).

7.7 Optimization Algorithm

The same Optimization Algorithm theorized in 2019 will be implemented into the Control System, that will change the parameters on the basis of the vibrations measured from the sensors attached to the drill string. An initial set of parameters can be fed into the system. If the system is stable and the vibrations are negligible, we can program the system to change the drilling parameters in order to increase ROP. If the system is unstable with large vibrations, drilling parameters will be gradually decreased until the vibrations are mitigated. For the implementation of such systems, measurements of rotational speed, ROP, WOB, and torque along with feedback control system for rotational speed and WOB, are crucial. Algorithm-1, seen in the figure, will be used to implement the system.

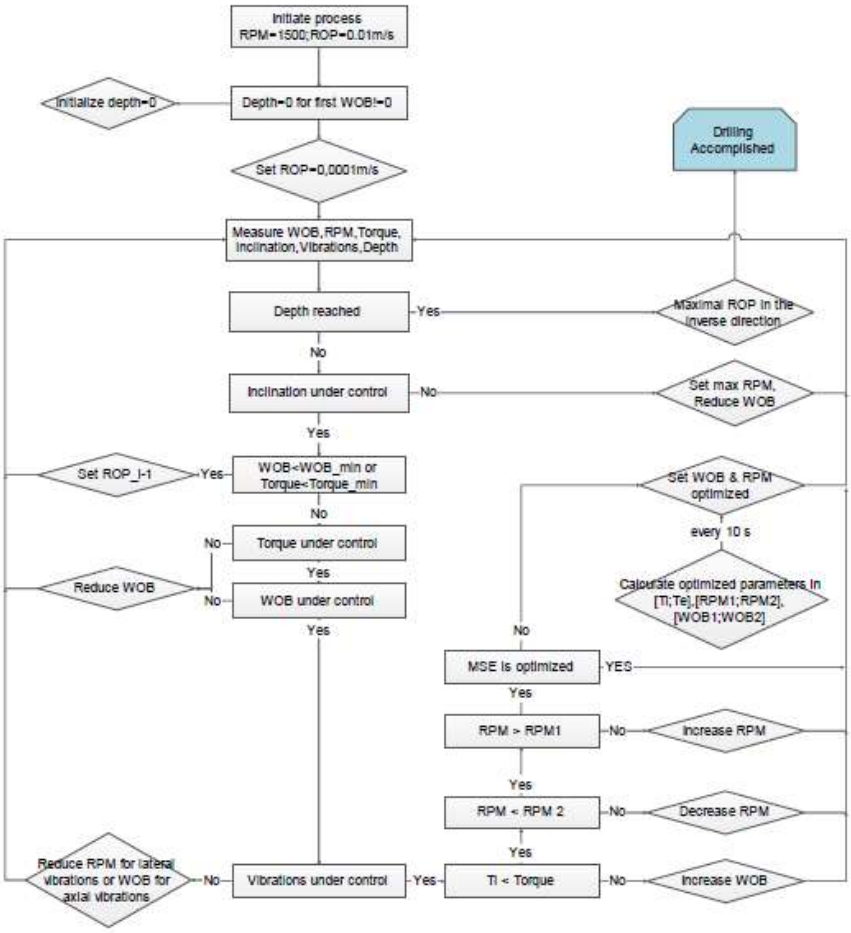

Figure 48: Drilling Algorithm

Before starting the drilling operation, we have no idea about the formation, so we start drilling the first layer with random parameters and saving drilling parameters in the same time in order to construct a database. When we obtain sufficient data for optimization, then we will be able to evaluate the optimal parameters.

We suppose that the next layer has the same nature of the formation, so the same optimal parameters; we apply these parameters and save the new data in order to use them in the next layer.

So, we are going to work with two matrixes, the first one to save parameters in real time and the second one contains the parameters of the last layer.

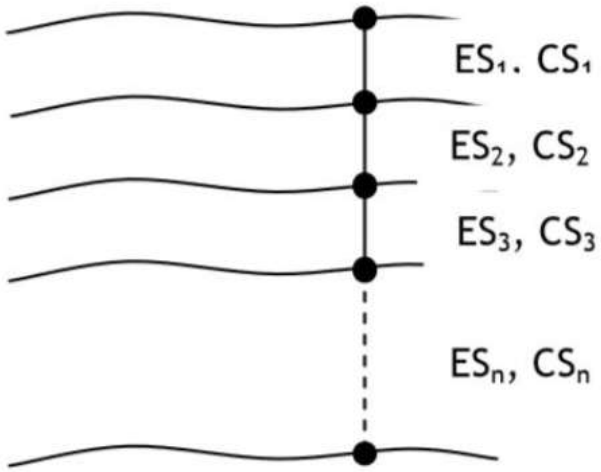

Figure 49: Real Time Optimization Matrixes

The Rate of Penetration (ROP)

While we were searching on the expression of ROP in function of the WOB and RPM for a PDC bit, we found that many criteria exist. We report them in the table below:

Table 3: Different ROP criteria

Criteria	Model
Moore	$ROP = a\,WOB\,RPM$
Maurer	$ROP = a\,(WOB + b)^2\,RPM$
Bingham	$ROP = a\,WOB^b\,RPM$
Cumigham	$ROP = a\,WOB\,RPM^c$
Eckel	$ROP = a\,WOB^b\,RPM^c$
Gall	$ROP = a\,(WOB - b)RPM^c$

In order to choose the adequate and suitable criteria of modeling the ROP in function of WOB and RPM, we need to analyze each one of these criteria and the nearest one to the reality should be taken.

To make the decision, we looked for in the documentation and we found a sub-program that already conceived in advance and called MODSTAT and it is based on the "*Statistic Modeling"*

The program gives the value of the correlation's coefficient R that compares between the theoretical results and the experimental ones.

R is given by the equation: $$R = \sqrt{1 - \frac{\Sigma(Y_{mod_i} - Y_{exp_i})2}{\Sigma(Y_{mod_i} - Y_{moy})}}$$

More the coefficient R is near to 1, the model is more adequate, and the results of an PDC bit are shown in the figure.

Table 4: The correlation's coefficient R

Eckel	Maurer	Gall	Moore	Bingham	Cumigham
The correlation's coefficient R (mean value)					
0.6323	0.5950	0.5476	0.4678	0.5381	0.5389
0.6753	0.6705	0.6807	0.5056	0.6668	0.5177
0.7363	-	0.1193	-	0.6385	-
0.8026	0.8926	0.9275	-	0.5390	-
0.5247	0.5258	-	0.4447	0.4541	0.4756
0.6716	0.6573	0.5321	-	0.6264	0.2994
0.8646	0.8889	0.1634	-	0.7855	-
0.9663	0.9756	0.9830	-	0.9323	0.5045
0.3679	0.4296	-	-	0.3957	-
0.6996	0.7364	0.8282	-	0.5143	-
0.6482	0.6593	0.6863	0.2412	0.6270	0.4204
0.6480	0.6538	-	-	0.6455	-
0.9047	0.7957	0.9132	0.3481	0.7605	0.8814
0.3559	0.3275	-	0.3035	0.1545	0.3748
0.8032	0.7070	0.8143	0.3225	0.6382	0.6699
0.5412	0.3107	0.5206	0.2952	0.2656	0.4237
0.4129	0.3246	-	0.3184	0.2006	0.3964

Therefore, using the results of MODSTAT we conclude that the suitable criteria modeling the ROP in function of WOB and RPM is **Eckel's Criteria.**

So now we have, the relation between the ROP and (WOB, RPM):

$$\boldsymbol{ROP = a\, WOB^{b}\, RPM^{c}} \ \ldots \ (\mathbf{1})$$

Identification of the coefficients a, b and c:

Since we found the correlation of ROP, we have just to identify the coefficients a, b and c from previous data (the previous layer), For that we will use the Least Squared sense:

$$\begin{bmatrix} \sum \ln(WOB)^2 & \sum \ln(WOB)\ln(RPM) & \sum \ln(WOB) \\ \sum \ln(WOB)\ln(RPM) & \sum \ln(RPM)^2 & \sum \ln(\mathrm{RPM}) \\ \sum \ln(WOB) & \sum \ln(\mathrm{RPM}) & \sum 1 \end{bmatrix} \begin{pmatrix} b \\ c \\ \ln(a) \end{pmatrix} = \begin{pmatrix} \sum \ln(WOB)\ln(ROP) \\ \sum \ln(RPM)\ln(ROP) \\ \sum \ln(ROP) \end{pmatrix}$$

Torque :

The torque is a linear function of the WOB, it can be written as following:

$$Torque = \alpha WOB + \beta$$

In the ideal case, β=0 but in reality, is not the case.

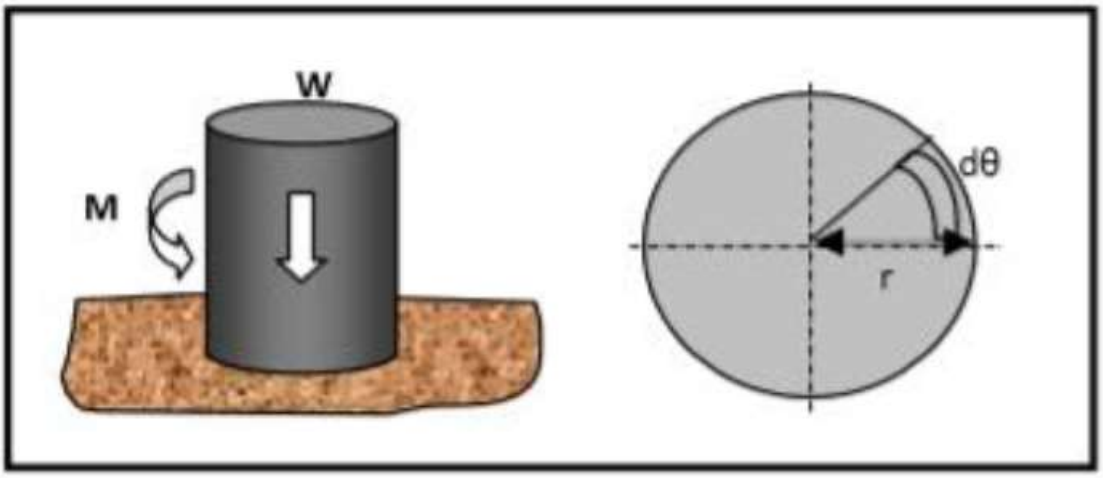

Figure 50: torque as a function of WOB

Identification of α and β:

We will be using the Least Squares method based of the previous data of Torque and WOB and therefore we can get the α and β coefficients.

Mechanical specific energy in function of WOB and RPM:

Since we already have the expressions of ROP and Torque, we just have to inject them in the MSE previous expression, Hence, we find that:

$$\mathrm{MSE} = \frac{\mathrm{WOB}}{\mathrm{A_b}} + \frac{120*\pi*\alpha*\mathrm{RPM}^{1-c}*\mathrm{WOB}^{1-b}}{\mathrm{A_b}*a} + \frac{120*\pi*\beta*\mathrm{RPM}^{1-c}*\mathrm{WOB}^{-b}}{\mathrm{A_b}*a}$$

In order to make it clearer, we note that:

$\mathrm{C_1} = \frac{1}{\mathrm{A_b}}$ $\qquad$ $\mathrm{C_2} = \frac{120*\pi*\alpha}{\mathrm{A_b}*a}$ $\qquad$ $\mathrm{C_3} = \frac{120*\pi*\beta}{\mathrm{A_b}*a}$

$$\mathrm{MSE} = \mathrm{C_1WOB} + \mathrm{C_2RPM}^{1-c}\mathrm{WOB}^{1-b} + \mathrm{C_3RPM}^{1-c}\mathrm{WOB}^{-b}$$

constraints

The constraints are subdivided in two categories:

1. Linear constraints imposed by the resistance of the drill pipe:

$$\mathrm{WOB_{min}} < WOB < \mathrm{WOB_{max}}$$

$$\mathrm{RPM_{min}} < RPM < \mathrm{RPM_{max}}$$

$$\mathrm{Torque_{min}} < Torque < \mathrm{Torque_{max}}$$

The last constraint can be written as:

$$\mathrm{Torque_{min}} < \alpha WOB + \beta < \mathrm{Torque_{max}}$$

So finally,

$$\frac{(\mathrm{Torque_{min}} - \beta)}{\alpha} < WOB < min(\frac{(\mathrm{Torque_{max}} - \beta)}{\alpha}, \mathrm{WOB_{max}})$$

2. Nonlinear constraints imposed by the cutter's usury:

$$0 < 1 - \frac{1}{8}\sum w_{ci}\, WOB_i ROP_i A_{abri} Cs_i \leq 1$$

Where:

w_c: Usury Coefficient
A_{abr}: Coefficient of Abrasiveness
Cs: Compressive Strength
i: Number of the layer

That can be written as:

$$(1 - \frac{depth_i}{2*total\ depth} - \frac{1}{8} w_{ci} WOB_i ROP_i A_{abri} Cs_i)^2 \leq (\frac{depth_i}{2*total\ depth})^2$$

WOB_i and ROP_i represent the average values on the layer "i"

The problem obtained is a nonlinear programming problem (PNL), with linear and nonlinear constraints. Which requires a previous WOB and ROP's data.

Final mathematical problem:
We have:

$$W_f = 1 - \frac{1}{8}\sum w_{ci}\, WOB_i ROP_i A_{abri} Cs_i$$

In real time optimization, the following considerations should be taken:

$$\begin{cases} W_f = 0\,, for\ the\ first\ time \\ W_f = 1 - \frac{1}{8}\sum w_{ci}\, WOB_i ROP_i A_{abri} Cs_i\,, otherwise \end{cases}$$

Final mathematical problem is:

$$\begin{cases} \boldsymbol{Min}\ (\mathbf{C_1 WOB + C_2 RPM^{1-c} WOB^{1-b} + C_3 RPM^{1-c} WOB^{-b}}) \\ \frac{(\mathbf{Torque_{min} - \beta})}{\boldsymbol{\alpha}} < \mathbf{WOB} < \mathbf{min}\left(\frac{(\mathbf{Torque_{max} - \beta})}{\boldsymbol{\alpha}}, \mathbf{WOB_{max}}\right) \\ \mathbf{RPM_{min}} < \mathbf{RPM} < \mathbf{RPM_{max}} \\ (\mathbf{1} - \frac{\boldsymbol{depth_i}}{\mathbf{2} * \boldsymbol{total\ depth}} - \frac{\mathbf{1}}{\mathbf{8}} \boldsymbol{w_{ci} WOB_i ROP_i A_{abri} Cs_i})^{\mathbf{2}} \leq (\frac{\boldsymbol{depth_i}}{\mathbf{2} * \boldsymbol{total\ depth}})^{\mathbf{2}} \end{cases}$$

8 Simulation

The simulation software used is Factory I/O, it is a 3D factory simulation. Being veery easy to use, it allows us to quickly build a virtual factory using a selection of common industrial parts, as well as add ours. Factory I/O also includes many scenes inspired by typical industrial applications, ranging from beginner to advanced difficulty levels.

Factory I/O provides a collection of parts based on the most common industrial equipment. Including sensors, operators, and stations. As well as a list of ready-to-use scenes inspired by

typical industrial applications, which can be seen as ranging from beginner to advanced difficulty levels. It also includes many I/O Drivers, each one intended to be used with a specific technology, our PLC for example. All of which will significantly help in the simulation process.

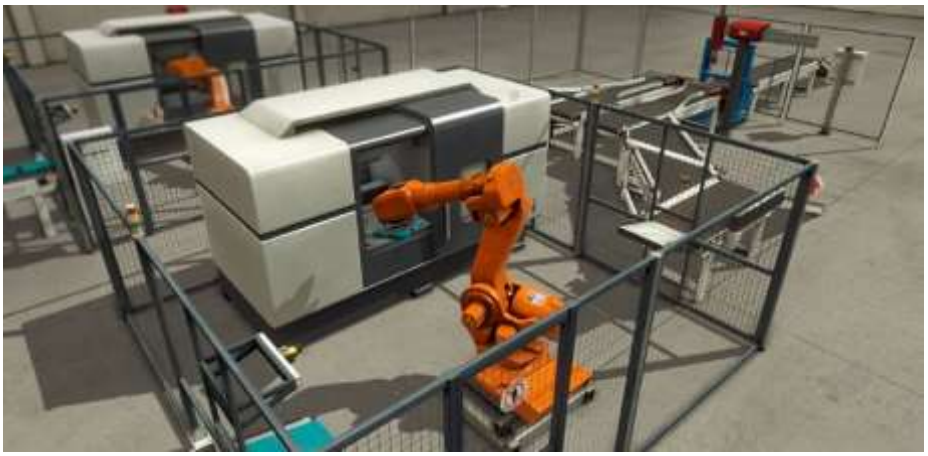

Figure 51: Factory I/O

9 References

1. Model for evaluating drilling efficiency based on the concept of Mechanical Specific Energy, Paal Vegar Berg, Øyvind Sæther Tveit, Norwegian University of Science and Technology.

2. Optimizing Rate of Penetration Using Weight and Torque Controllers, Casey Hubbell.

3. Linear Moving Horizon Estimation With Pre-estimating Observer, Dan Sui, Tor Arne Johansen and Le Feng, IEEE TRANSACTIONS ON AUTOMATIC CONTROL.

4. Robust output-feedback control to eliminate stick-slip oscillations in drill-string systems, Thijs Vromen, Cam-Hing Dai, Nathan van de Wouw, Tom Oomen, Patricia Astrid, Henk Nijmeijer, 2nd IFAC Workshop on Automatic Control in Offshore Oil and Gas Production, May 27-29, 2015, Florianópolis, Brazil.

5. Real-time Rate of Penetration Optimization of an Autonomous Lab-Scale Rig using a Scheduled-Gain PID Controller and Mechanical Specific Energy, Enrique Z. Losoya, Eduardo Gildin, Samuel F. Noynaert, Proceedings of the 3rd IFAC Workshop on Automatic Control in Offshore Oil and Gas Production, Esbjerg, Denmark, May 30 - June 1, 2018.

6. Rate of Penetration Optimization using Moving Horizon Estimation, Dan Sui, Bernt Sigve Aadnoy, Modeling, Identification and Control, Vol. 37, No. 3, 2016.

7. Implementation of Active Control Design for Crown Mounted Compensator to Improve Drilling Performance, Atle Aalerud, Tomas Klevmo, University of Agder.

8. Estimation and Control for Efficient Autonomous Drilling through Layered Materials, Steven J. Spencer, Anirban Mazumdar, Jiann-Cherng Su, Adam Foris, and Stephen P. Buerger, SAND2017-2106C.

9. Application of Real-Time Field Data to Optimize Drilling Hydraulics Using Neural Network Approach, Saeed Salehi, University of Oklahoma.

10. AC Servo Motor Speed and Position Control Using Particle Swarm Optimization (PSO), Mehmet Fatih Isik, Halil Aykul, Erhan Çetin, Hitit University.

11. AC Position Control System, ELP225.

12. ARMOIRE AUTOMATE, RÈGLES GÉNÉRALES ET SCHEMAS DE CÂBLAGE: LIAISONS AUTOMATE / BORNIER / EQUIPEMENT.

13. MULTIVARIABLE FEEDBACK CONTROL, Analysis and Design, Sigurd Skogestad, Norwegian University of Science and Technology, Ian Postlethwaite, University of Leicester.

14. Development of a PLC Controlled Drilling Machine, Ruhul Amin, Dhaka University of Engineering & Technology, Himangshu Bhowmik, Dhofar University.

15. Automated Drilling Machine Based on PLC, Yousef M. Abueejela, Abdulgani Albagul, College of Electronic Technology-Bani Walid, Libya.

16. The impact of Soft Torque Technology on Drilling Performance, Fares Attar, Qatar Shell; Odion Ikhajiagbe, Gulf Drilling International; Rob Grauwmans, Shell Global Solutions.

17. The Drilling Process: A Plantwide Control Approach, Dag-Erik Helgestad, Norwegian University of Science and Technology, Department of Chemical Engineering.

18. Identification and control of stick-slip vibrations using Kalman estimator in oil-well drill strings, L. Hong, Irving Paul Girsang, Jaspreet Singh Dhupia.

19. Real-Time Prediction and Optimization of Drilling Performance Based on a New Mechanical Specific Energy Model, Xuyue Chen, Honghai Fan, Boyun Guo.

20. Mechanics of Materials, 7th Edition, James M. Gere.

21. DIRECTIONAL WELL DESIGN, TRAJECTORY AND SURVEY CALCULATIONS, WITH A CASE STUDY IN FIALE, ASAL RIFT, DJIBOUTI, Farah Omar Farah.

22. Drill Bit Nozzle Pressure Loss [EXPLOITATION OF FINAGLE FACTOR TECHNOLOGY] Leon Robinson, American Association of Drilling Engineers.

23. Schlumberger Drilling and Measurements. (2010). Drillstring Vibrations and Vibration Modelling. Retrieved December 9, 2016, from https://www.slb.com/~/media/Files/drilling/brochures/drilling_opt/drillstring_vib_br.pdf

24. G. Han, B. M and L. K, "Percussion Drilling in Oil Industry: Review and Rock Failure Modelling," in AADE 2005 National Technical Conference and Exhibition, Houston, Texas, 2005.

25. Resistance of materials courses, Dr. Belkacemi, National Polytechnic School

26. Applied thermal courses, Ph.D. Smaili, National Polytechnic School

27. https://www.alibaba.com/product-detail/Usfull-high-performance-ac-drive-frequency_1756183605.html?spm=a2700.7735675.topad_classic.d_image.442c3d14uu67ZD

Delta ECMA-E1830S Permanent Magnet AC Servo Motor official datasheet, http://www.deltronics.ru/images/catalogue/ASDA-A2_C_EN_20180302.pdf

10 Appendix

A Summary of Equations

Table 5: Summary of Equations

Calculations	Formula	Results
Euler's Critical Load	$F_{cr} = \frac{\pi^2 EI}{(KL)^2}$	230 N
The area moment of inertia of the cross section of the drill pipe	$I = \frac{\pi}{64}(D_o{}^4 - D_i{}^4)$	$2.84 * 10^{-10} m^4$
the cross-sectional are	$A = \frac{\pi}{4}(D_o{}^2 - D_i{}^2)$	$3.24 * 10^{-5} m^2$
The slenderness ratio	$R_S = \frac{KL}{r_g}$	308.85
column constant	$C_c = \sqrt{\frac{2\pi^2 E}{K^2 \sigma_e}}$	70.2
Barlow burst equation	$P_{burst} = \frac{2\sigma_e t}{D_o s}$	$239.4 * 10^5 Pa$
Minimum radius of curvature	$\rho = \frac{Ey}{\sigma_e}$	1.034 m
radial stress	$\sigma_r = \frac{r_i{}^2}{r_o{}^2 - r_i{}^2}(1 - \frac{r_o{}^2}{r^2})P$	depends on internal pressure
tangential stress	$\sigma_\theta = \frac{r_i{}^2}{r_o{}^2 - r_i{}^2}(1 + \frac{r_o{}^2}{r^2})P$	depends on internal pressure
axial stress	$\sigma_a = \frac{WOB}{A}$	depends on WOB
Maximum shear stress	$\tau_{max} = \sqrt{\frac{2(\sigma_e)^2 - (\sigma_a - \sigma_\theta)^2 - (\sigma_\theta - \sigma_r)^2 - (\sigma_r - \sigma_a)^2}{6}}$	depends on internal pressure and WOB
Maximum torque	$T_{max} = \tau_{max} \frac{\pi}{16} \frac{D_o{}^4 - D_i{}^4}{D_o}$	depends on internal pressure and WOB, see Figure 4
Pressure Loss	$\Delta P = \rho g h_f$	See Table 6
Pump's Power	$P_{pump} = \Delta P_t \frac{Q}{\eta}$	0.225Kw

B Rig Specifications

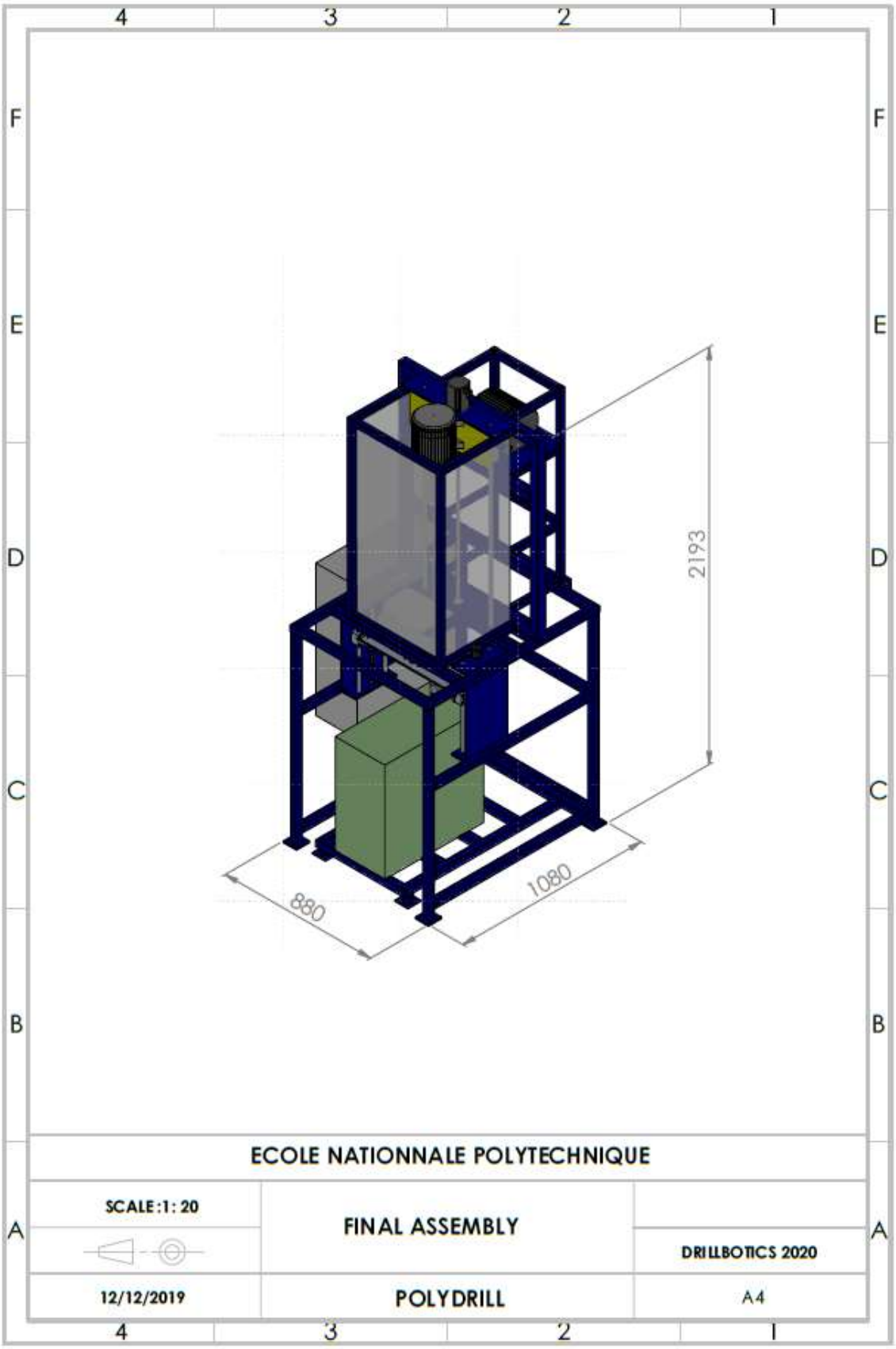

Figure 52: Rig Specifications 1

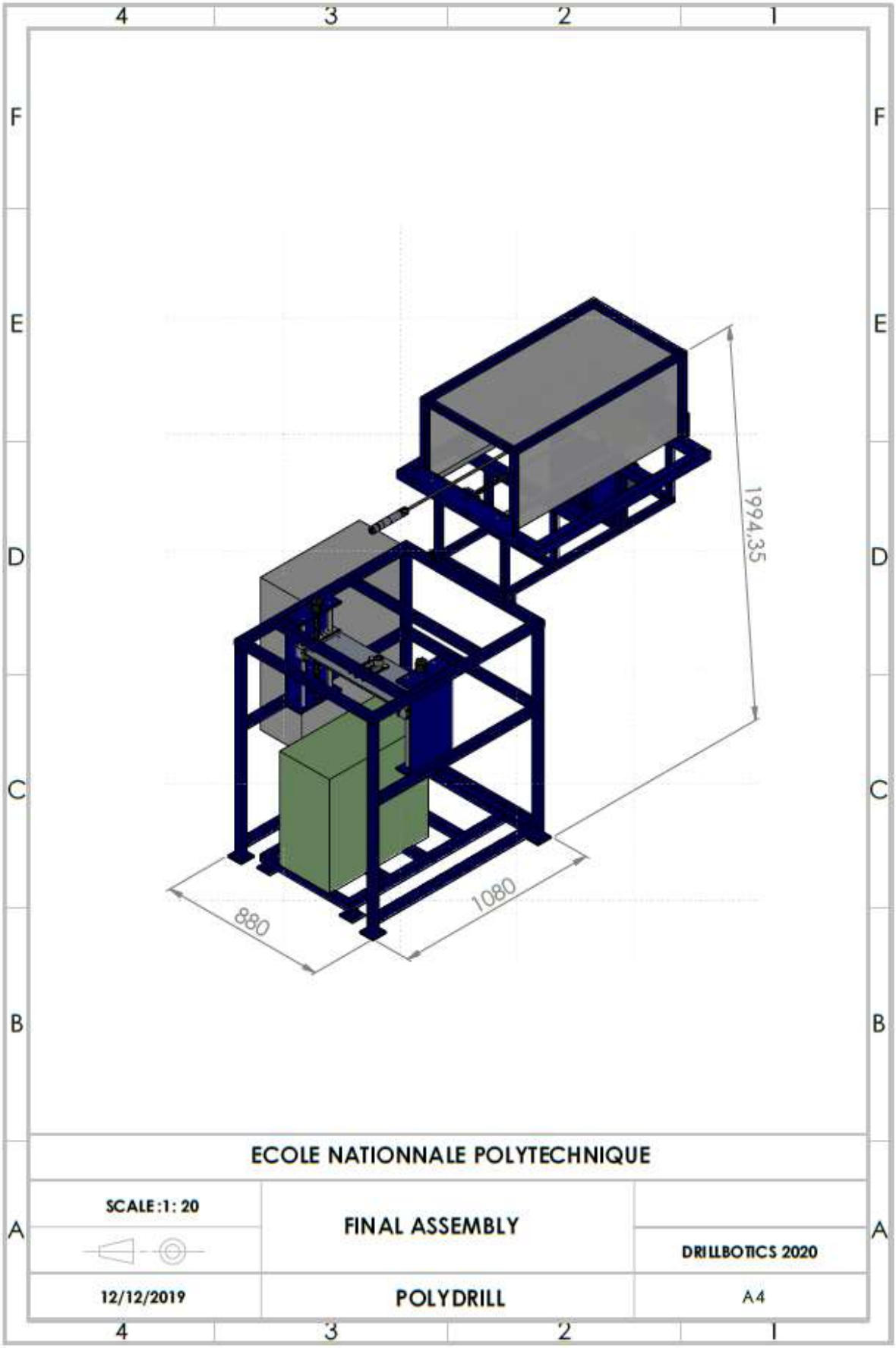

Figure 53: Rig Specifications 2

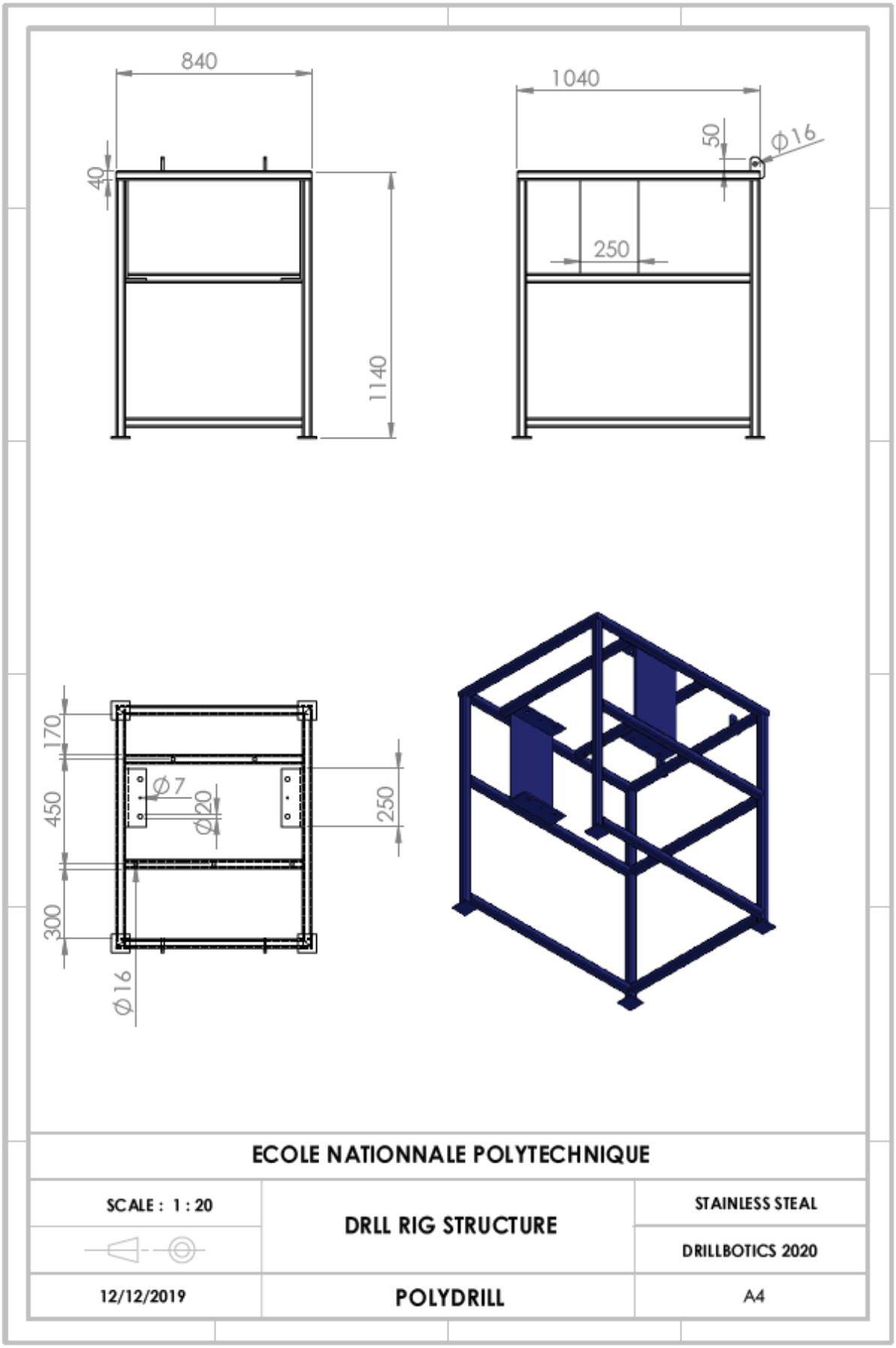

Figure 54: Rig Specifications 3

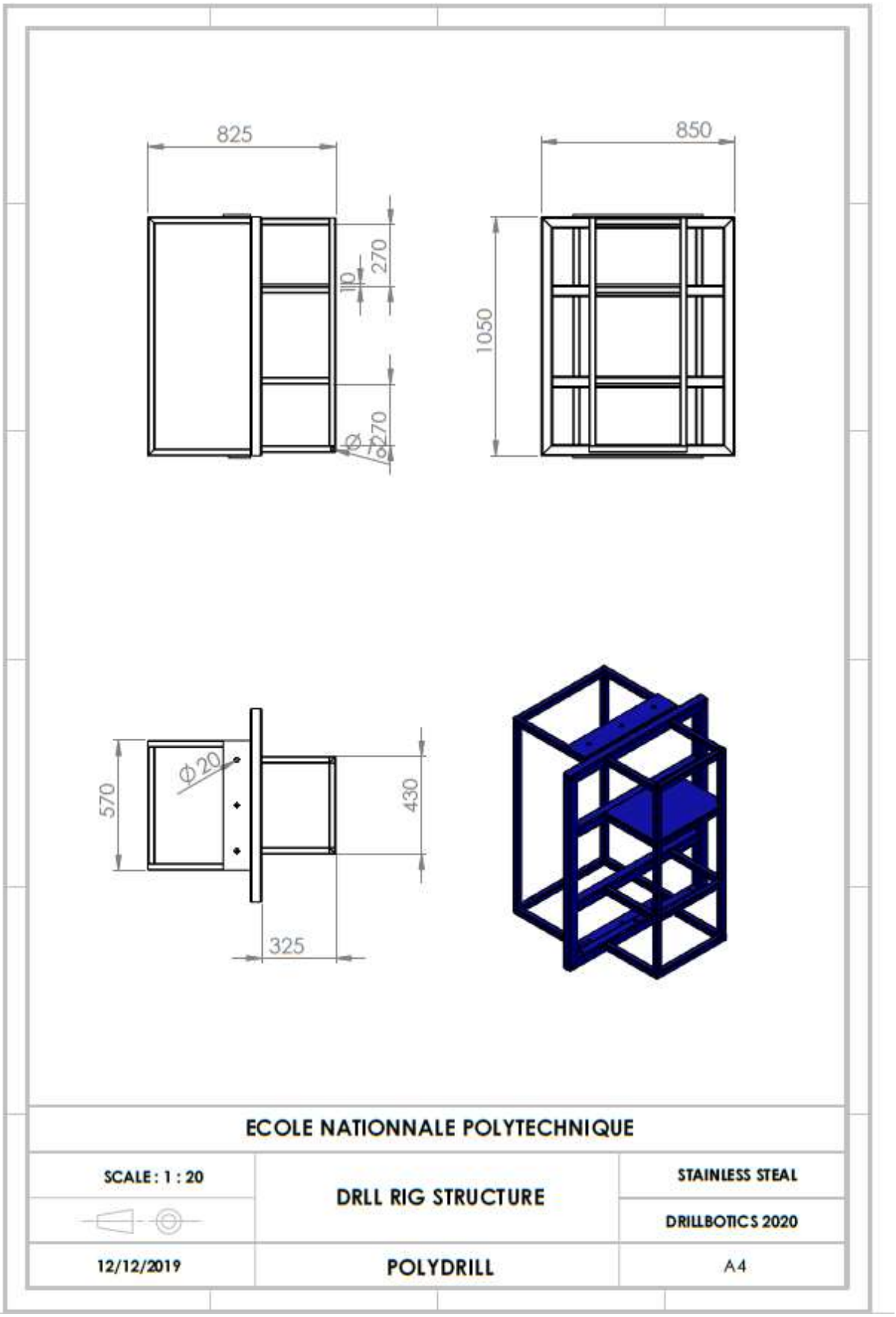

Figure 55: Rig Specifications 4

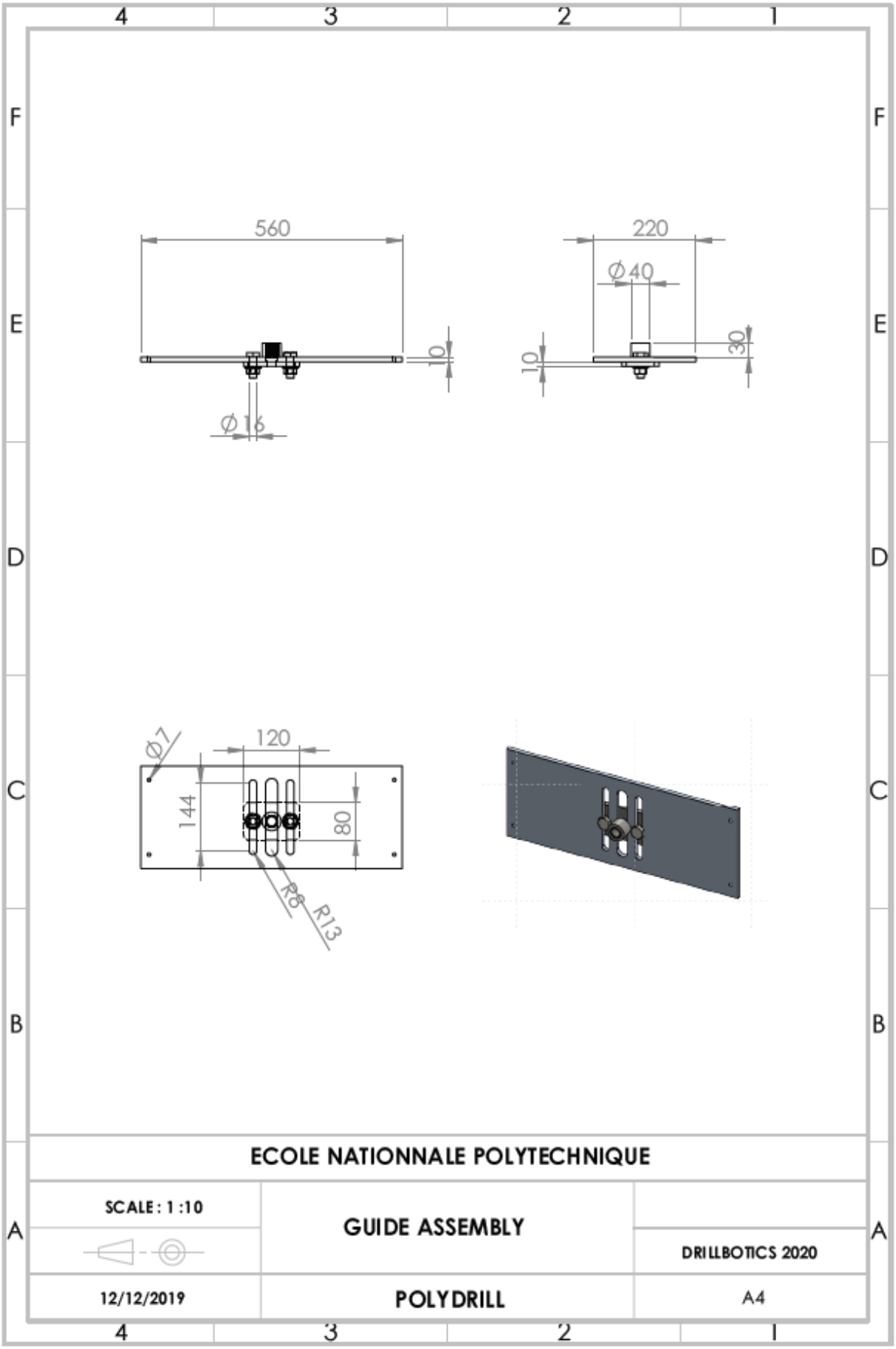

Figure 56: Rig Specifications 5

C Power Consumption

C.1 Top Drive Motor

The planned Top Drive Motor (**ATO-SERVO-150S3000 Brushless AC Servo Motor**), has a rated speed of 3000 rpm (max speed up to 4500 rpm), and a rated torque of 14.32 N.m (max torque up to 42.97 N.m), if these parameters (3000 rpm/14.32 N.m) were used, the power consumed would be of 3kW

C.2 Hoisting Motor

The same power consumption calculations as the 2019 ones can be used since the hoisting motor is the same one.

The torque is estimated using the equation bellow:

$$T = \frac{F.p}{2\pi.\eta}$$

Where:

F: force acting on the ball screw.
P: The lead of the ball screw.
η: Efficiency factor for the ball screw

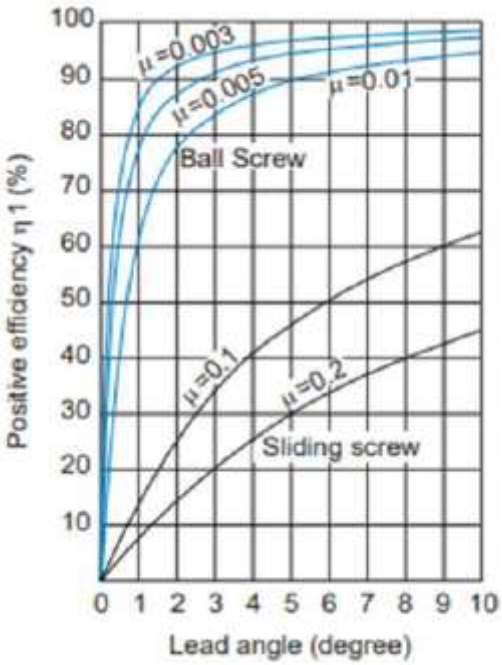

Figure 57: Positive Efficiency (Rotational to Linear)

The total force acting in the ball screw was estimated to be at most 500 N, from weight of drill string, top drive motor and carriage.

For the lead, we have chosen M14 ball screw, to ensure precision in WOB and to get a large domain of variation for the ROP, Safix has been chosen as supplier and their smallest available lead for M14 ball screw is 2 mm.

The efficiency factor for the ball screw was set as 0.32

Finally, we find: T=0.5 N.m

Table 6: Resistance of threaded shaft

Ø	PAS	section	section d'épreuve	limite élastique	Rupture mini	Couple serrage	Tension Fo mini	Tension Fo maxi
mm		mm²	daN	daN	daN	daN	daN	daN
3	0,50	5,03	292	322	402	0,12	170	208
4	0,70	8,78	510	562	702	0,27	294	359
5	0,80	14,20	823	909	1135	0,52	482	589
6	1,00	20,10	1160	1286	1610	0,91	679	830
8	1,25	36,60	2120	2342	2920	2,20	1247	1524
10	1,50	58,00	3370	3712	4640	4,40	1986	2428
12	1,75	84,30	4890	5395	6740	7,60	2896	3540
14	2,00	115,00	6670	7360	9200	12,10	3978	4862
16	2,00	157,00	9100	10048	12500	18,90	5478	6696
18	2,50	192,00	11500	12288	15900	26,10	6654	8133
20	2,50	245,00	14700	15680	20300	37,00	8560	10462
22	2,50	303,00	18200	19392	25200	50,90	10704	13083
24	3,00	353,00	21200	22592	29300	63,70	12326	15065
27	3,00	459,00	27500	29376	38100	94,40	16240	19849
30	3,50	581,00	33700	37184	46600	12,80	19732	24116
33	3,50	694,00	41600	44416	57600	17,39	24612	30082
36	4,00	817,00	4900	52288	67800	22,32	28871	35287
39	4,00	976,00	58600	62464	81000	29,00	34719	42434

To provide a rough estimate of the power consumption of the hoisting motor, the carriage is estimated to be able to move from bottom to top of the rock within 10 seconds, which results in ω=188.5 Rad/s, the efficiency factor for the hoisting motor was set as 0.9, and the motor power required was calculated to be: P=105 W

D BHA Specifications

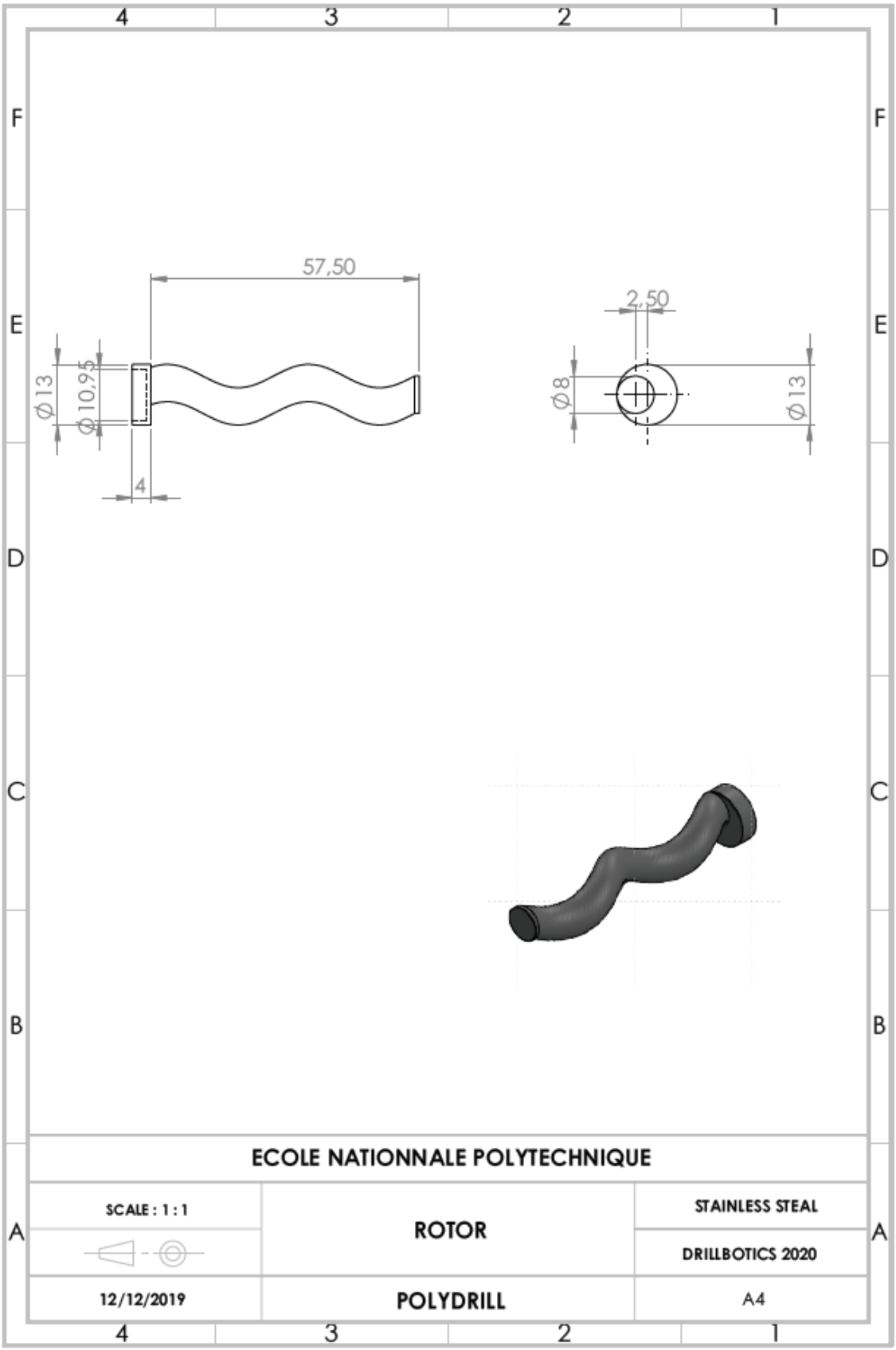

Figure 58: BHA Specifications 1

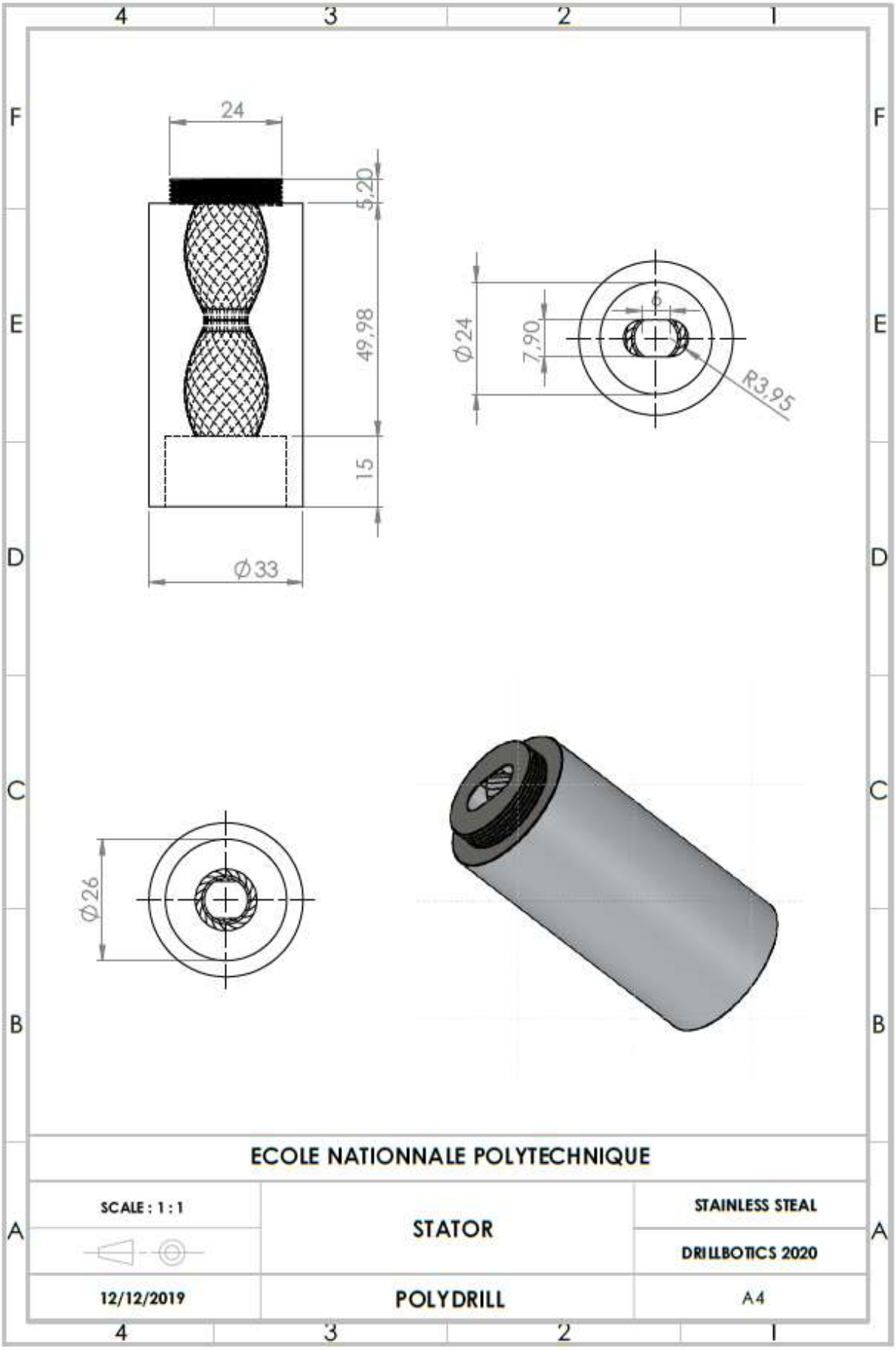

Figure 59: BHA Specifications 2

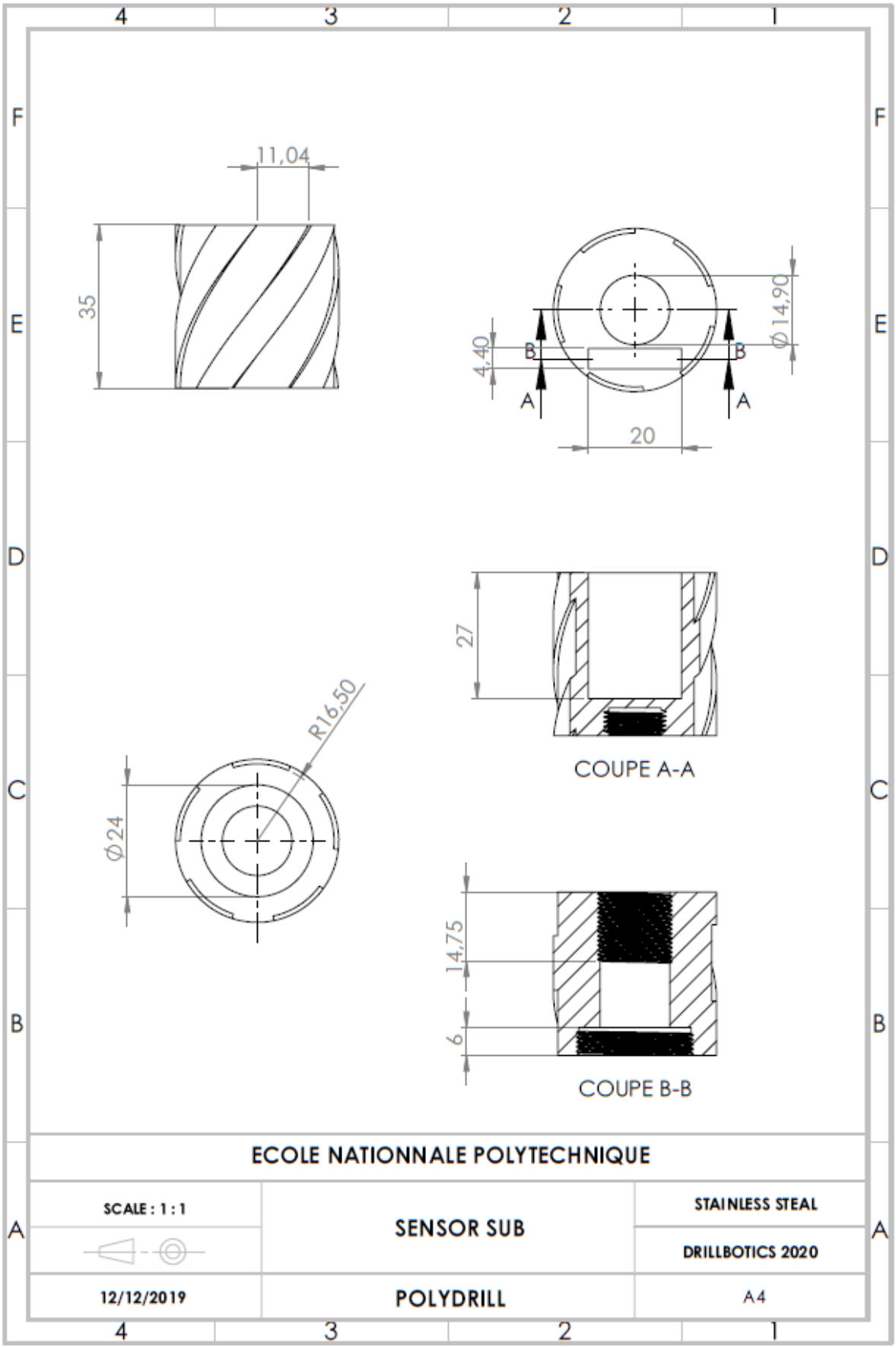

Figure 59: BHA Specifications 3

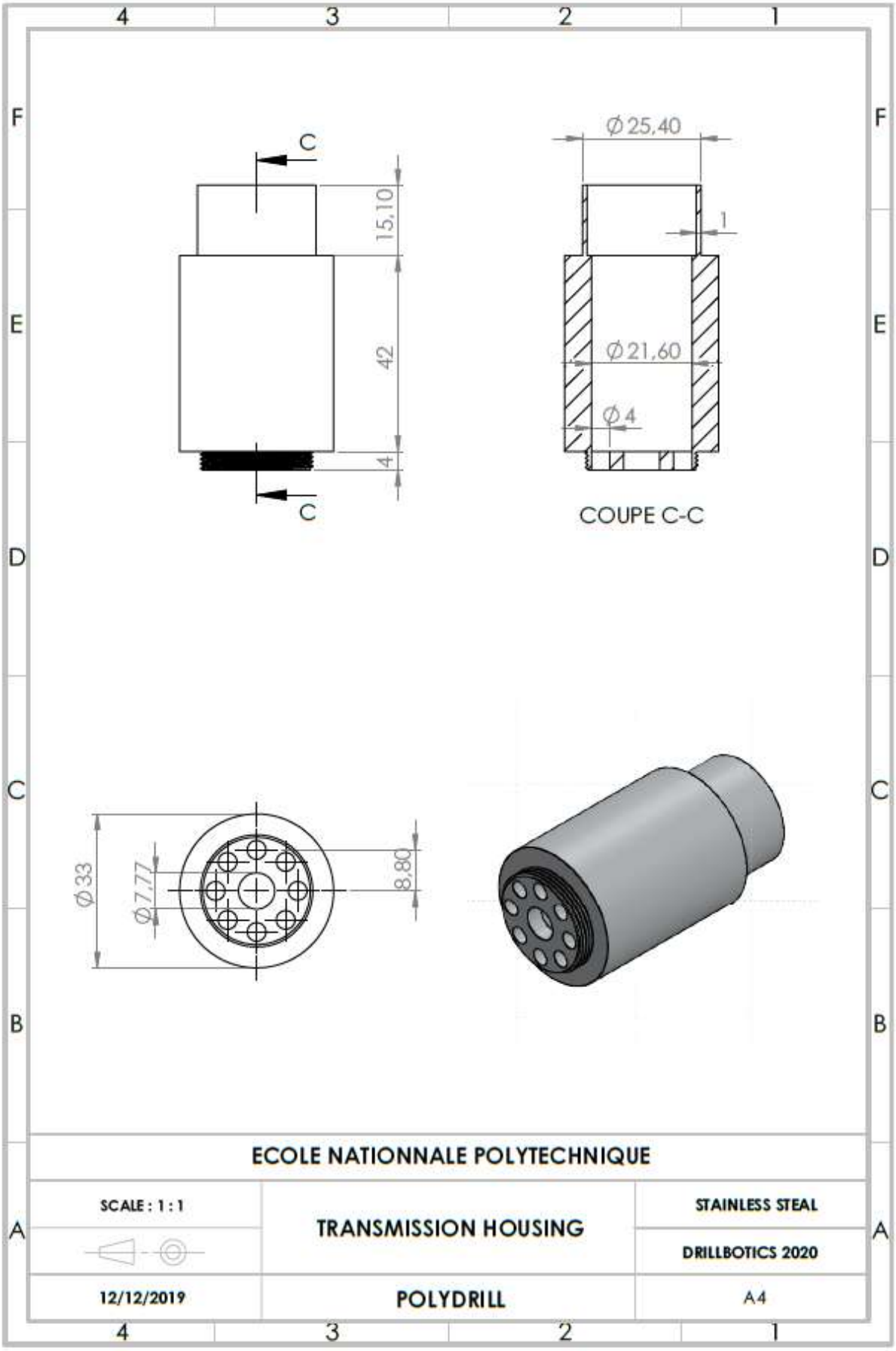

Figure 60: BHA Specifications 4

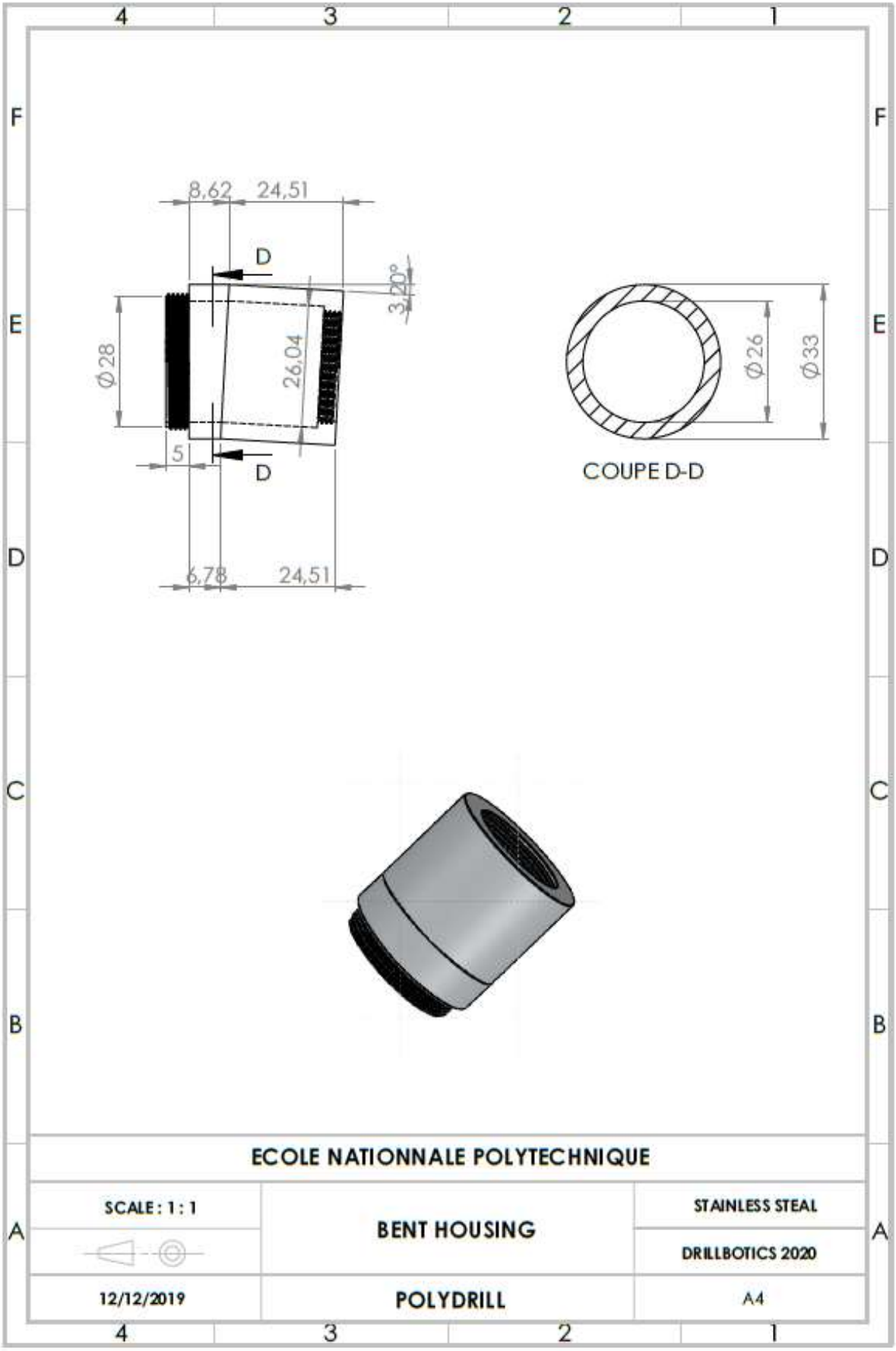

Figure 61: BHA Specifications 5

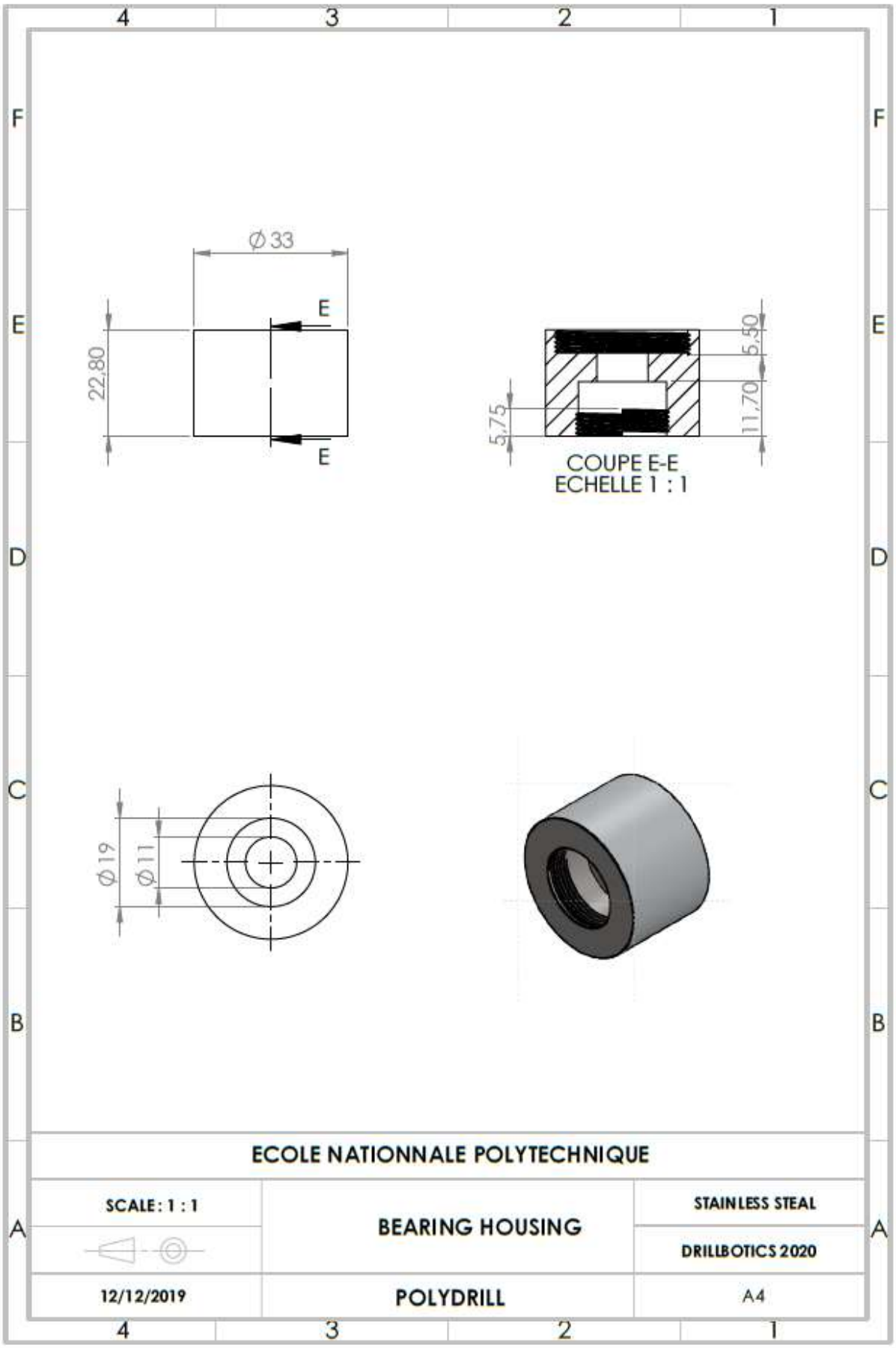

Figure 62: BHA Specifications 6

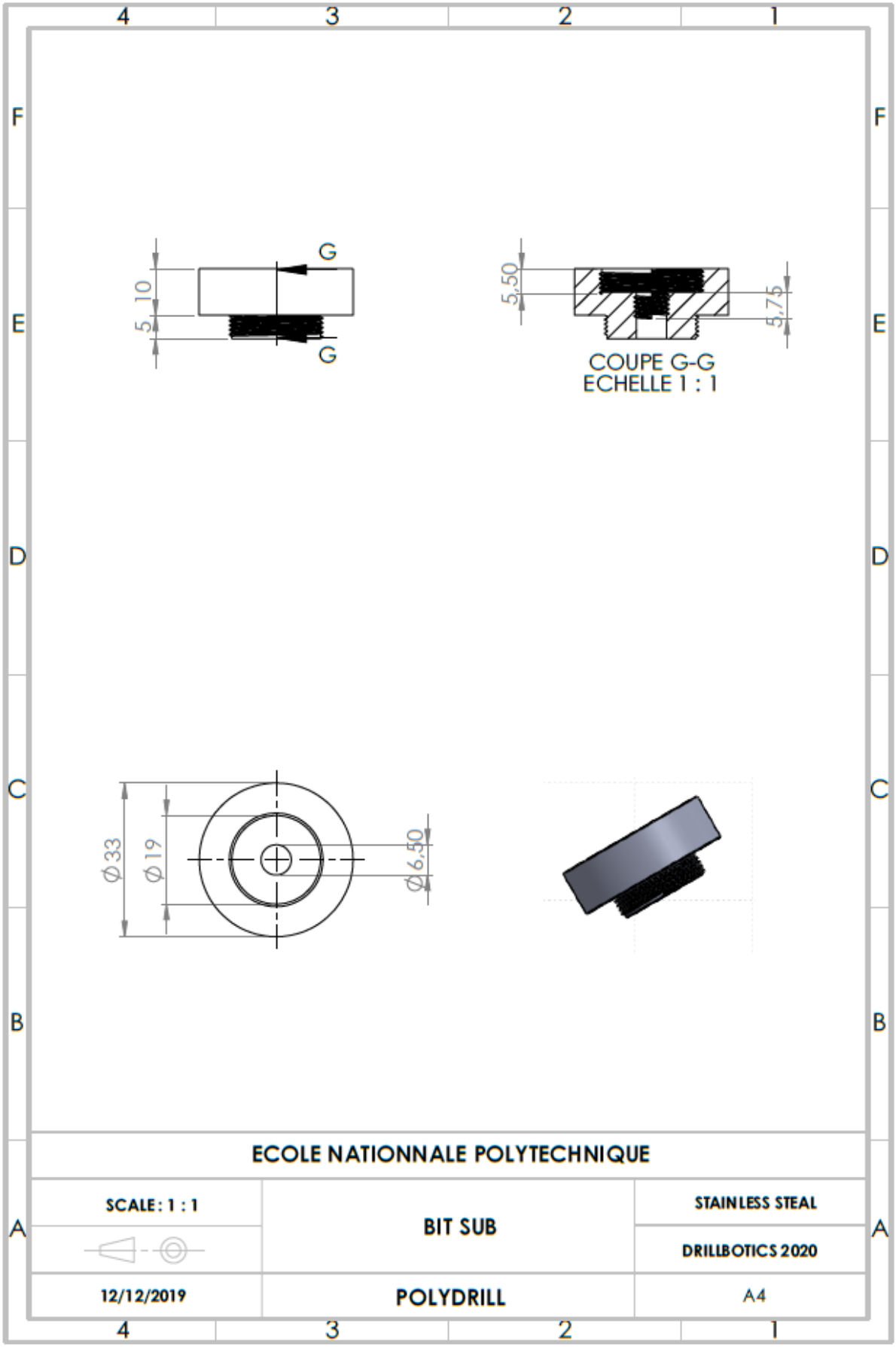

Figure 63: BHA Specifications 7

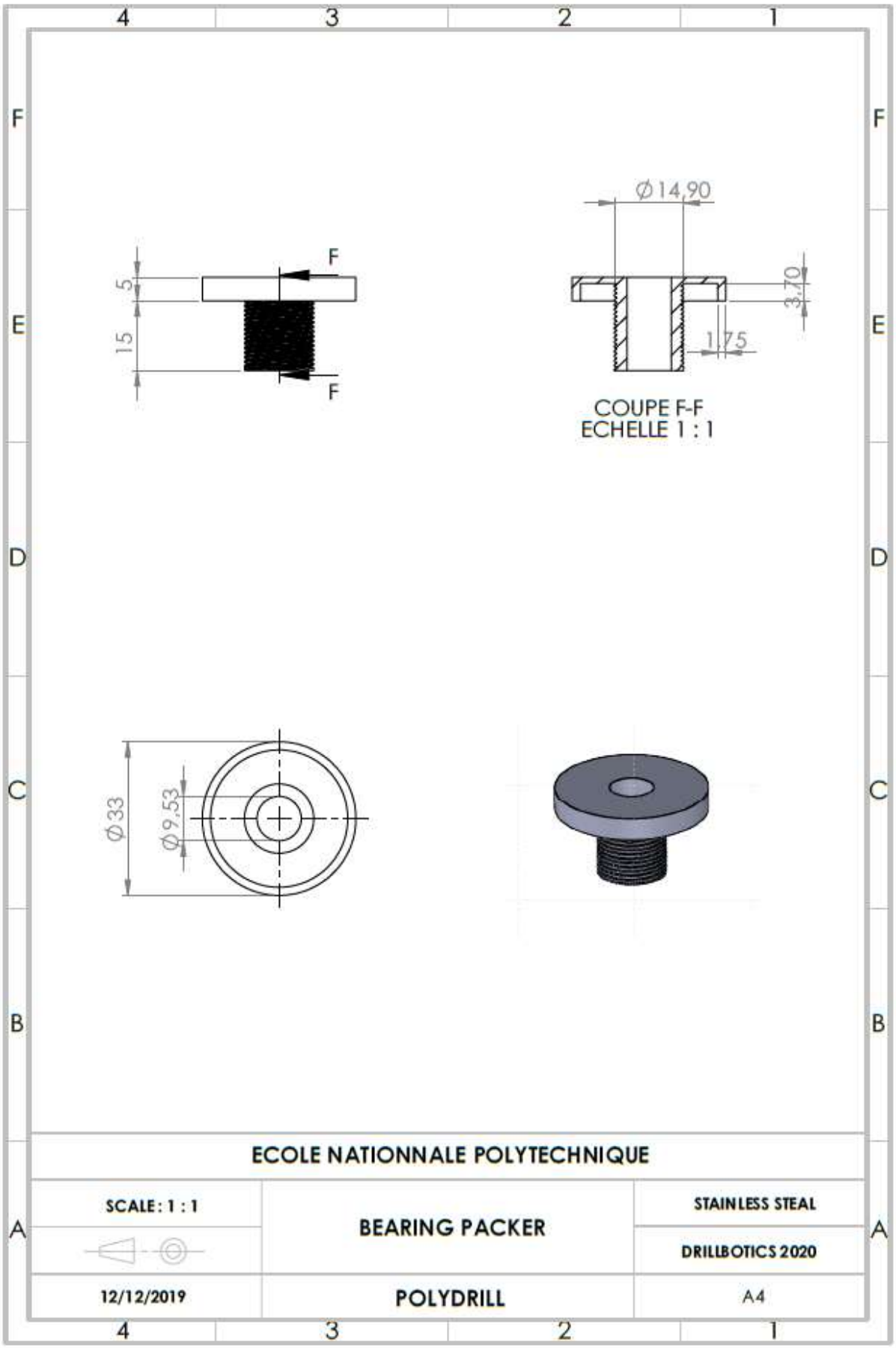

Figure 64: BHA Specifications 8

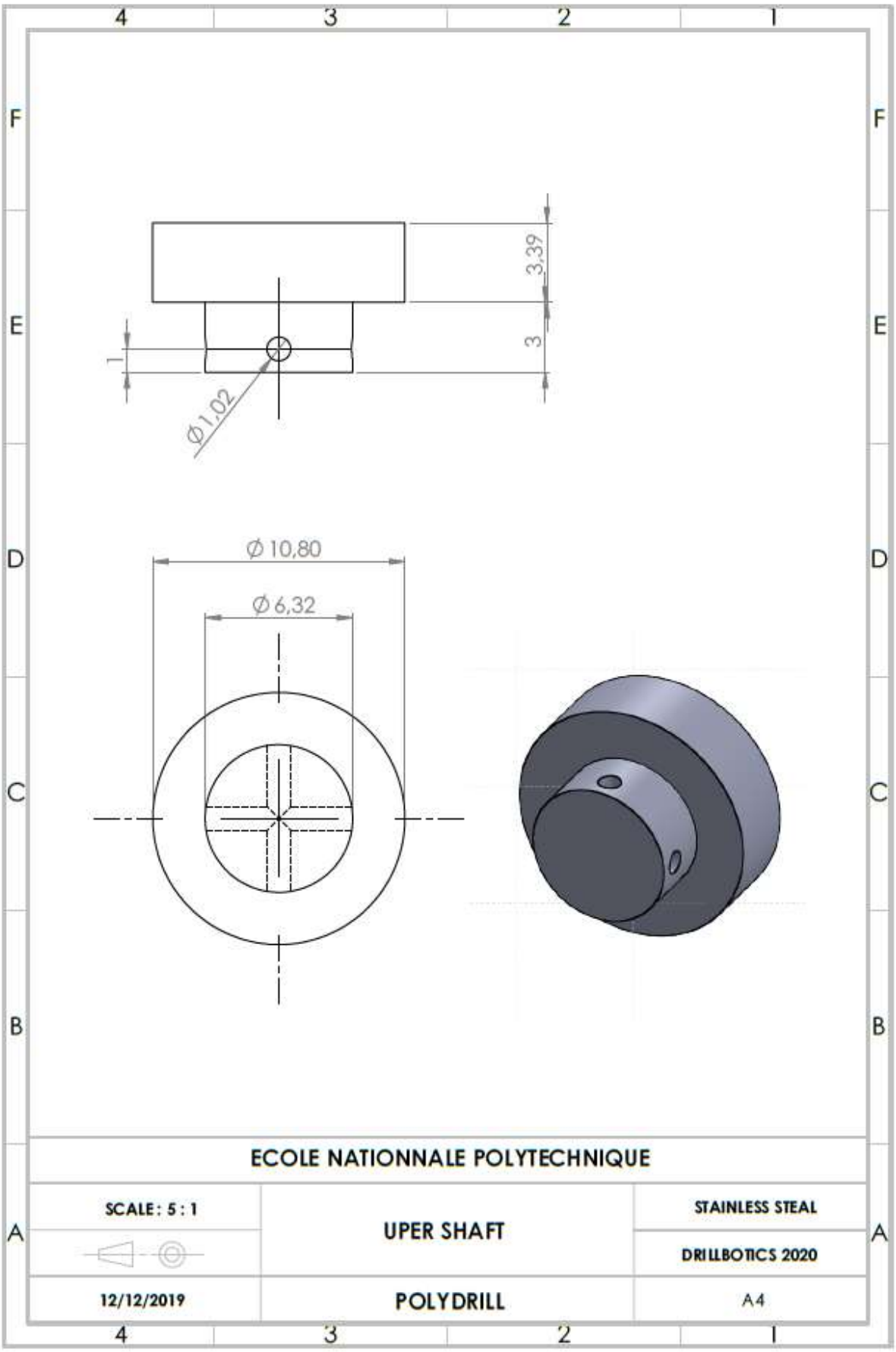

Figure 65: BHA Specifications 9

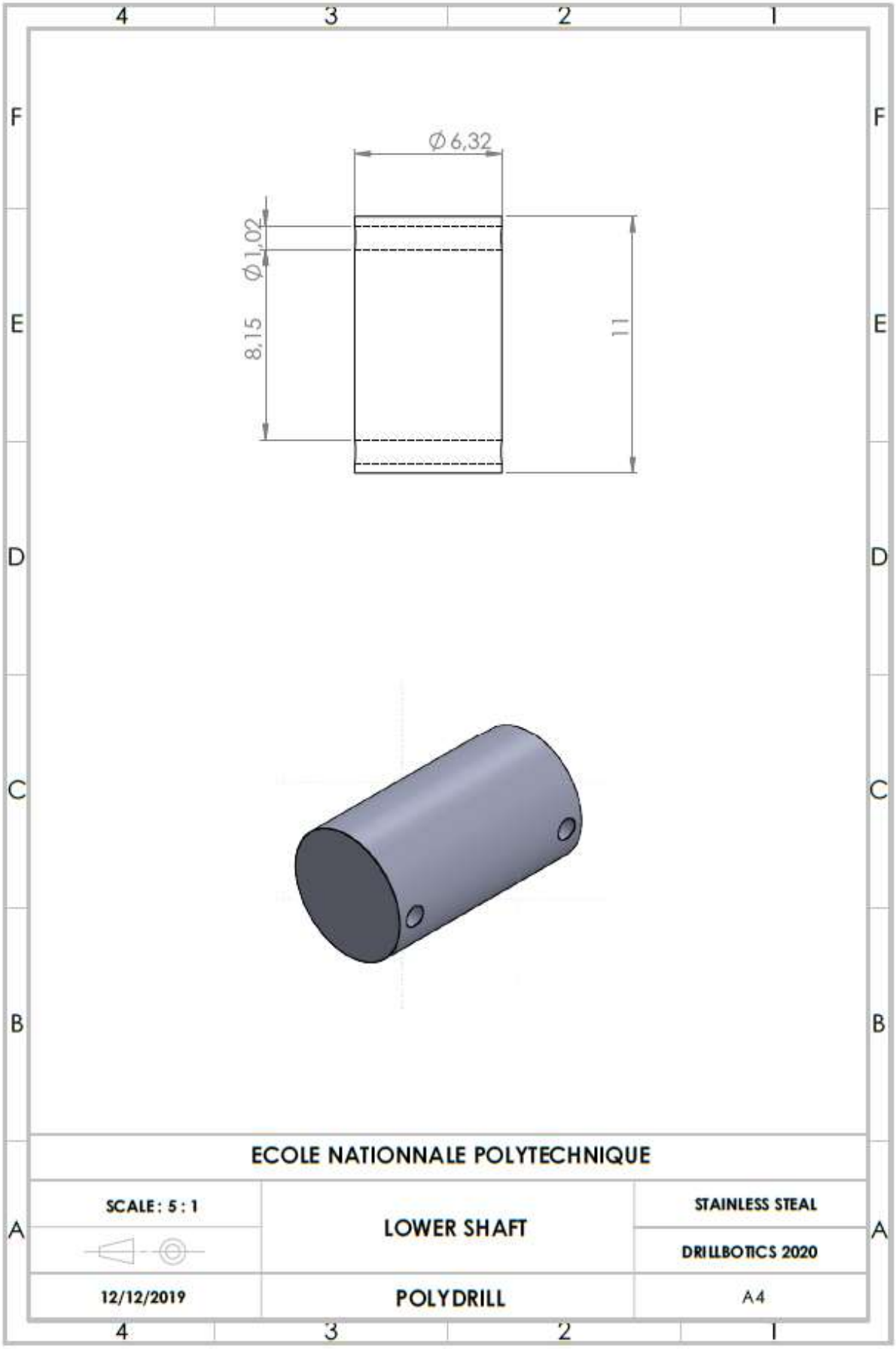

Figure 66: BHA Specifications 10

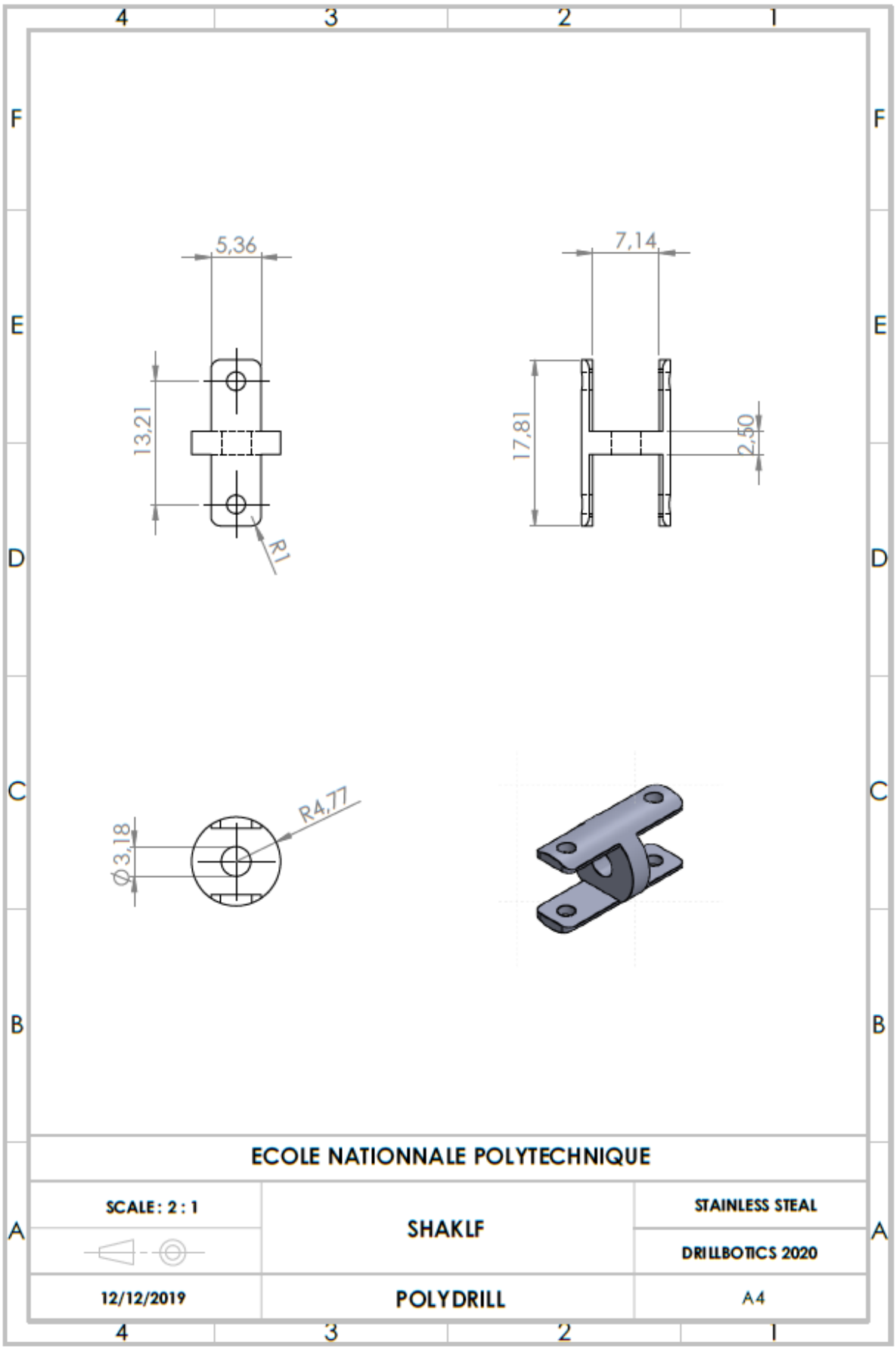

Figure 67: BHA Specifications 11

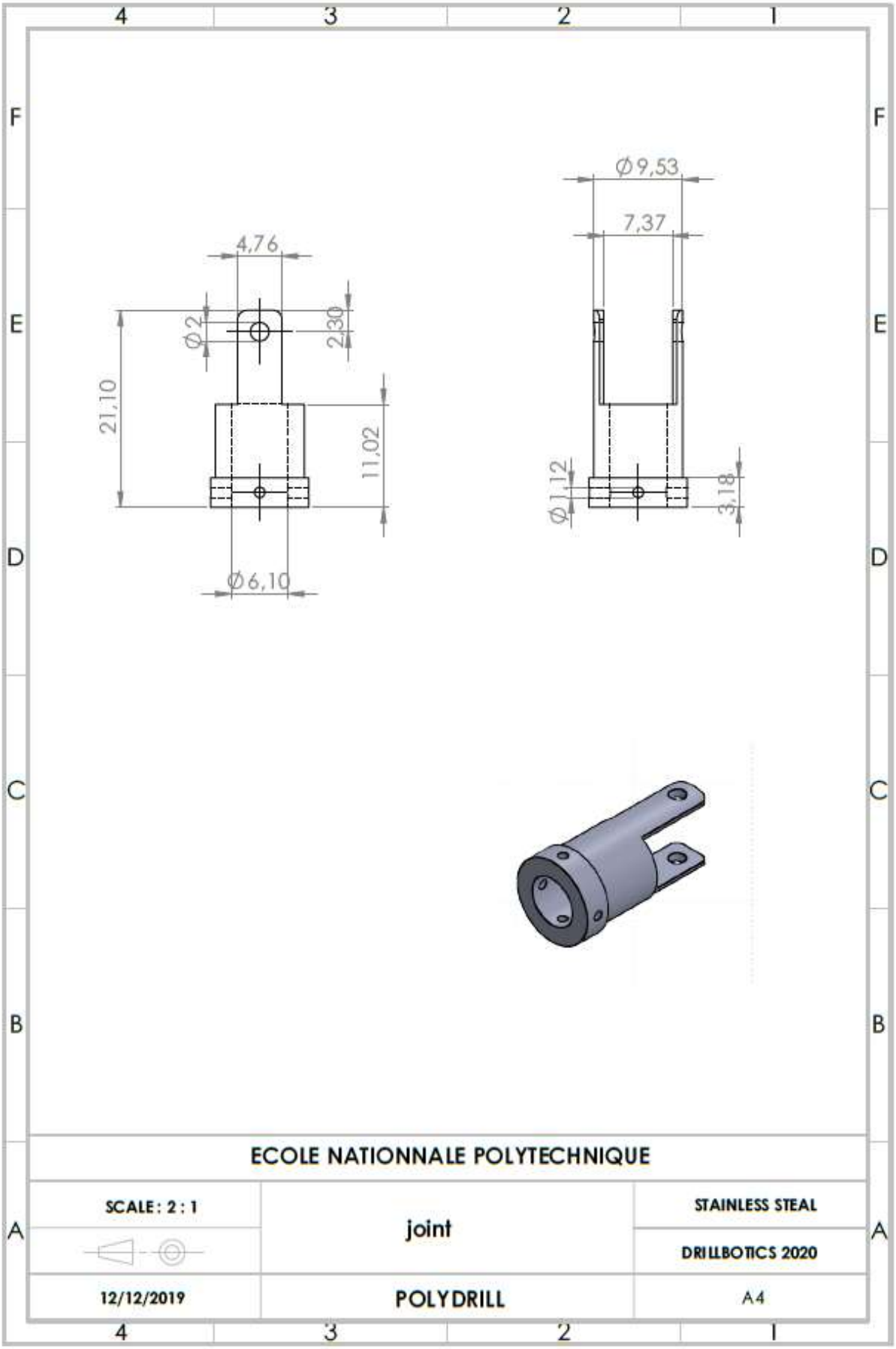

Figure 69: BHA Specifications 12

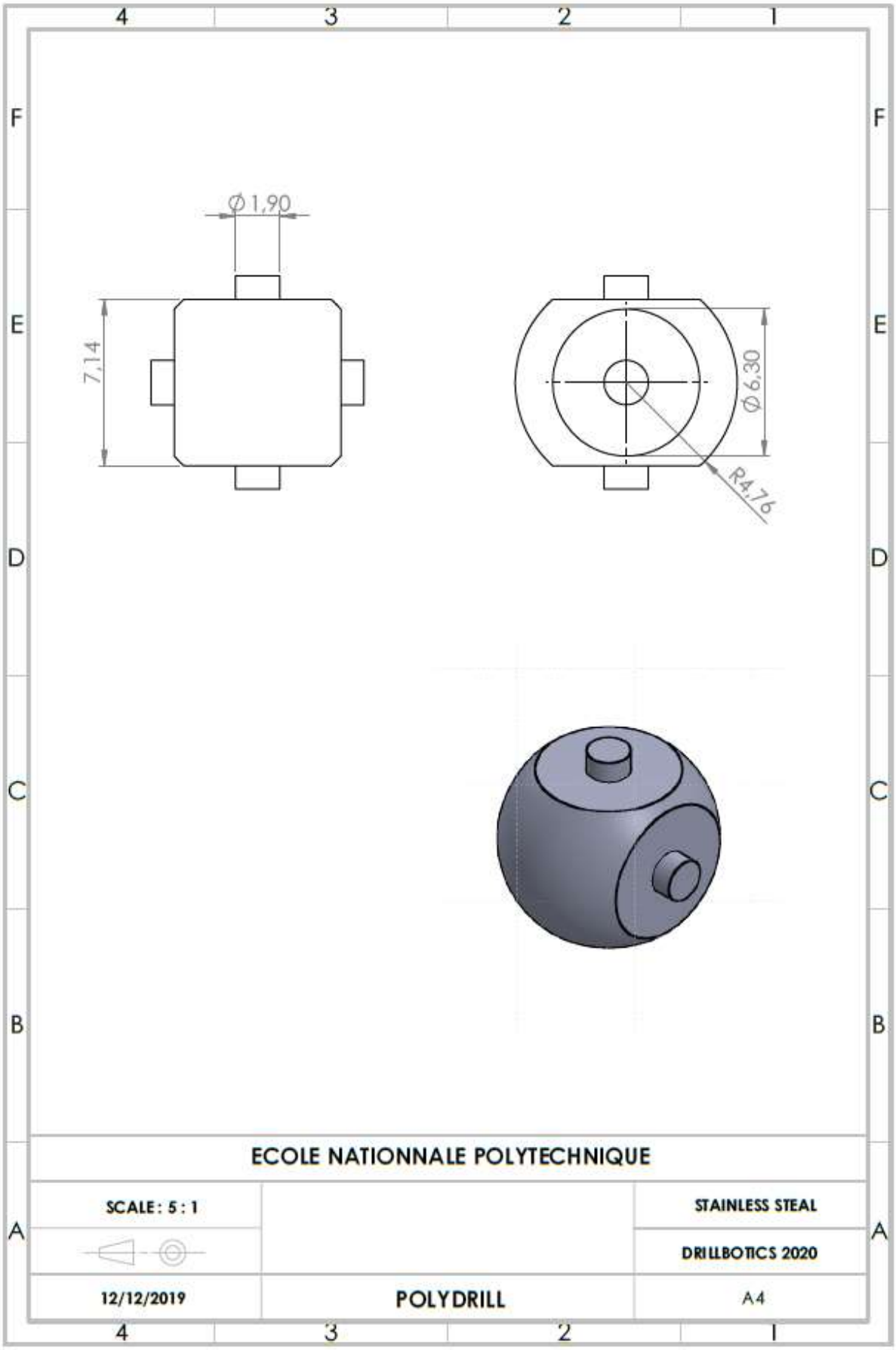

Figure 68: BHA Specifications 13

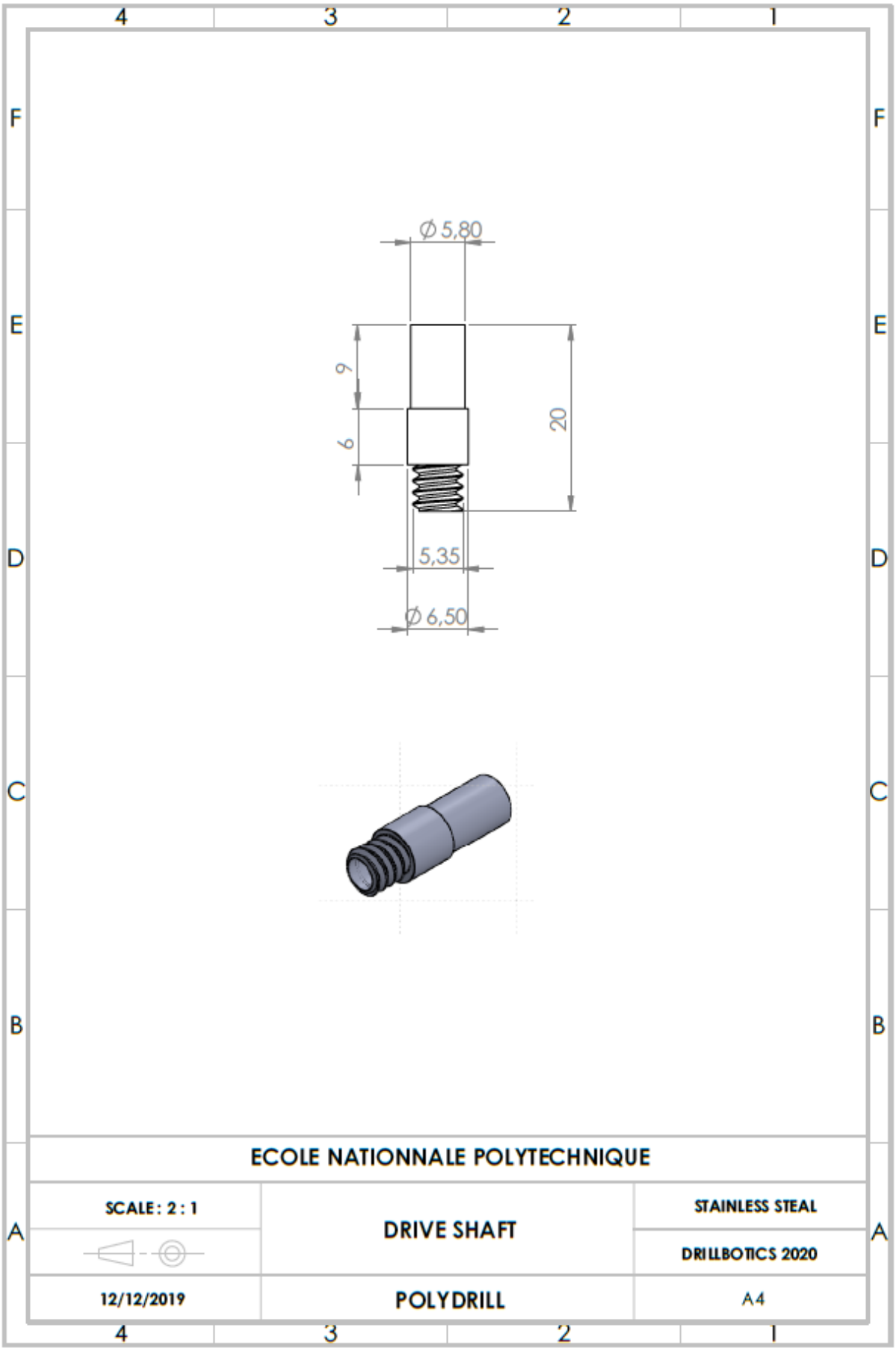

Figure 69: BHA Specifications 14

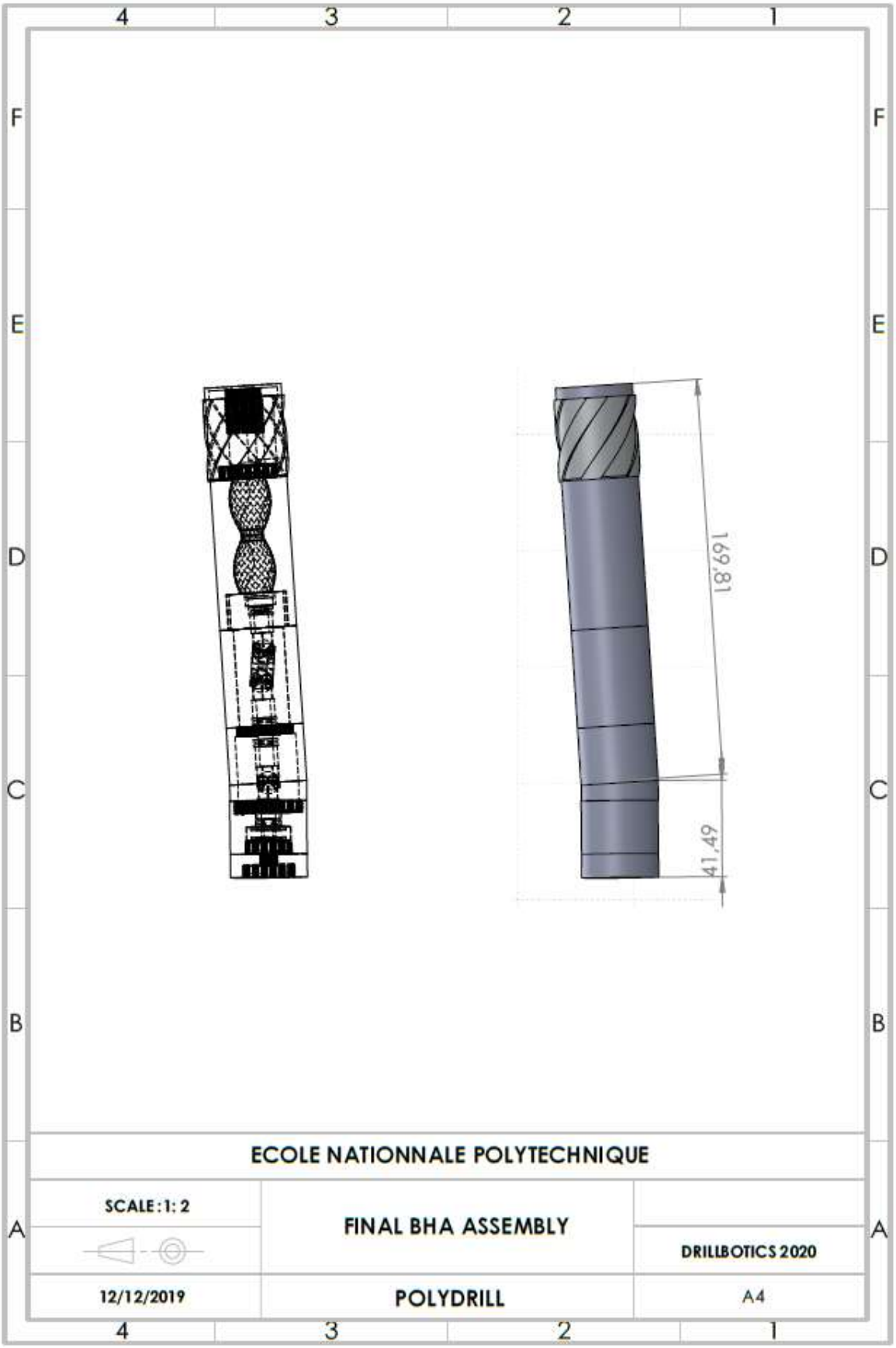

Figure 70: BHA Specifications 15

E Motors Specifications

E.1 Top Drive Motor (Delta ECMA-E1830S Permanent Magnet AC Servo Motor)

ECMA	E△13				E△18			G△13			F△13	F△13	F△18	F113	
	05	10	15	20	20	30	35	03	06	09	05	08	30	13	18
Rated power (kW)	0.5	1.0	1.5	2.0	2.0	3.0	3.5	0.3	0.6	0.9	0.5	0.85	3.0	1.3	1.8
Rated torque (N-m)*1	2.39	4.77	7.16	9.55	9.55	14.32	16.71	2.86	5.73	8.59	3.18	5.41	19.10	8.34	11.48
Max. torque (N-m)	7.16	14.3	21.48	28.65	28.65	42.97	50.13	8.59	17.19	21.48	8.92	13.8	57.29	23.3	28.7
Rated speed (r/min)	2000							1000						1500	
Max. speed (r/min)	3000							2000						3000	
Rated current (A)	2.9	5.6	8.3	11.01	11.22	16.1	19.2	2.5	4.8	7.5	3.9	7.1	19.4	12.6	13
Max. instantaneous current (A)	8.7	16.8	24.9	33.03	33.66	48.3	57.6	7.5	14.4	22.5	12.1	19.4	58.2	38.6	36
Max. power per second (kW/s)	7.0	27.1	45.9	62.5	26.3	37.3	50.8	10.0	39.0	66.0	9.8	21.52	66.4	34.78	52.93
Rotor inertia (x10-4kg-m^2)	8.17	8.41	11.18	14.59	34.68	54.95	54.95	8.17	8.41	11.18	10.3	13.6	54.95	20	24.9
Mechanical constant (ms)	1.91	1.51	1.10	0.96	1.62	1.06	1.08	1.84	1.40	1.06	2.8	2.43	1.28	1.62	1.7
Torque constant-KT(N-m/A)	0.83	0.85	0.87	0.87	0.85	0.89	0.87	1.15	1.19	1.15	0.82	0.76	0.98	0.66	0.88
Voltage constant -KE(mV/(r/min)	30.9	31.9	31.8	31.8	31.4	32.0	32	42.5	43.8	41.6	29.5	29.2	35.0	24.2	32.2
Armature resistance (Ohm)	0.57	0.47	0.26	0.174	0.119	0.052	0.052	1.06	0.82	0.43	0.624	0.38	0.077	0.124	0.185
Armature inductance (mH)	7.39	5.99	4.01	2.76	2.84	1.38	1.38	14.29	11.12	6.97	7	4.77	1.27	1.7	2.6
Electric constant (ms)	12.96	12.88	15.31	15.86	23.87	26.39	26.39	13.5	13.50	16.06	11.22	12.55	16.5	13.71	14.05

Figure 71: Top Drive Motor Specifications 1

Insulation class	A 級（UL），B 級（CE）														
Insulation resistance	100MΩ，DC 500V 以上														
Insulation strength	1.8k Vac,1 sec														
Weight – without brake (kg)	6.8	7.0	7.5	7.8	13.5	18.5	18.5	6.8	7.0	7.5	6.3	8.6	18.5	9.4	10.5
Weight – with brake (kg)	8.2	8.4	8.9	9.2	17.5	22.5	22.5	8.2	8.4	8.9	7.7	10.0	22.5	10.8	11.9
Radial max. loading (N)	490	490	490	490	1176	1470	490	490	490	490	490	490	1470	490	490
Axial max. loading (N)	98	98	98	98	490	490	98	98	98	98	98	98	490	98	98
Max. power per second (kW/s) (with brake)	6.4	24.9	43.1	57.4	24.1	35.9	48.9	9.2	35.9	62.1	8.8	19.78	63.9	32.66	50.3
Rotor inertia (x10-4kg-m^2) (with brake)	8.94	9.14	11.90	15.88	37.86	57.06	57.06	8.94	9.14	11.9	11.5	14.8	57.06	21.3	26.2
Mechanical constant (ms) (with brake)	2.07	1.64	1.19	1.05	1.77	1.10	1.12	2.0	1.51	1.13	3.12	2.65	1.33	1.73	1.79
Brake holding torque [Nt-m (min)]*2	10.0	10.0	10.0	10.0	25.0	25.0	25.0	10.0	10.0	10.0	10	10.0	25.0	10.0	10.0
Brake power consumption (at 20°C)[W]	19.0	19.0	19.0	19.0	20.4	20.4	20.4	19.0	19.0	19.0	19	19.0	20.4	19.0	19.0
Brake release time [ms (Max)]	10	10	10	10	10	10	10	10	10	10	10	10	10	10	10
Brake pull-in time [ms (Max)]	70	70	70	70	70	70	70	70	70	70	70	70	70	70	70
Vibration grade (μm)	15														
Operating temperature (°C)	0°C to 40°C (32°F to 104°F)														
Storage temperature (°C)	-10°C to 80°C (-14°F to 176°F)														
Operating humidity	20 to 90%RH (non-condensing)														
Storage humidity	20 to 90%RH (non-condensing)														
Vibration capacity	2.5G														
IP rating	IP65 (use the waterproof connector and shaft seal installation (or oil seal))														
Certification	CE c UL us														

Figure 72: Top Drive Motor Specifications 2

E.2 Hoisting Motor (Dual Shaft Nema 34 CNC Stepper Motor)

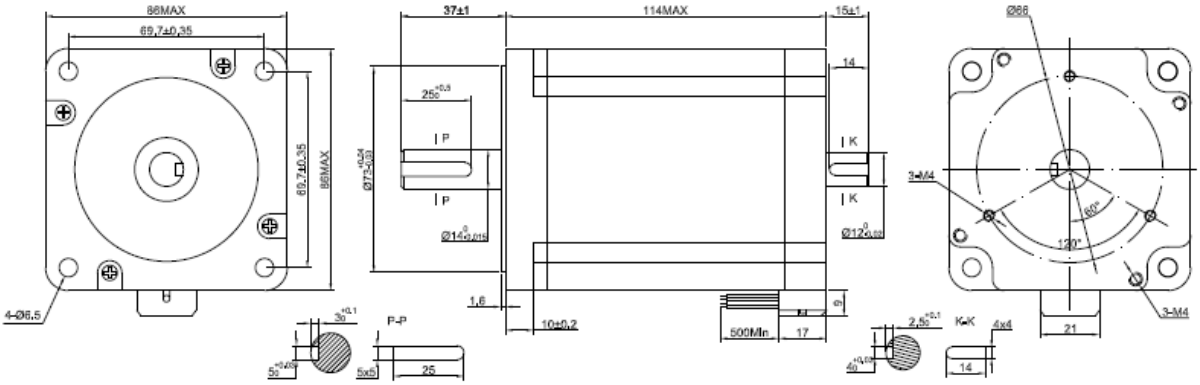

Figure 73: Hoisting Motor Dimensions

Table 7: Hoisting Motor Specifications

SPECIFICATION / CONNECTION	BIPOLAR
AMPS/PHASE	5.00
RESISTANCE/PHASE(Ohms)@25°C	1.00±10%
INDUCTANCE/PHASE(mH)@1KHz	11.00±20%
HOLDING TORQUE(Nm)[lb-in]	8.50[75.23]
STEP ANGLE(°)	1.80
STEP ACCURACY(NON-ACCUM)	±5.00%
LEAD STYLE	FVR 4X0.75mm² CABLE
LIFE(h)	6000
TEMPERATURE RISE;MAX.80°C (MOTOR STANDSTILL;FOR 2PHASE ENERGIZED)	
AMBIENT TEMPERATURE -10°C~50°C[14°F~122°F]	
INSULATION RESISTANCE 100 Mohm (UNDER NORMAL TEMPERATURE AND HUMIDITY)	
INSULATION CLASS B 130°C[266°F]	
DIELECTRIC STRENGTH 500VAC FOR 1MIN (BETWEEN THE MOTOR COILS AND THE MOTOR CASE)	
AMBIENT HUMIDITY MAX.85%(NO CONDENSATION)	

Table 8: Hoisting Motor Step

TYPE OF CONNECTION (EXTERN)		MOTOR	
PIN NO	BIPOLAR	LEADS	WINDING
1	A —	RED	A
2	C —	BLK	C
3	B —	YEL	B
4	D —	BLU	D

FULL STEP 2 PHASE-Ex. ,
WHEN FACING MOUNTING END (X)

STEP	A	B	C	D		CCW
1	+	+	-	-	↓	↑
2	-	+	+	-		
3	-	-	+	+		
4	+	-	-	+	CW	

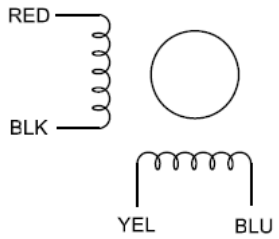

F Pump Specifications (Qingeal ZW50-10-20 Pump)

Brand Name: Qingeal pump
Model Number: ZW50-10-20
Place of Origin: Zhejiang, China
Application: wastewater treatment, sewage, waste water
Structure: Single-stage Pump
Certification: ce
Theory: Centrifugal Pump
Standard or Nonstandard: Standard
Material: cast iron
Flow: 10m3/h
Head: 20m
Voltage: 220v/380v
Outlet dia: 50mm
Power : 2.2kw

G Drive Specifications

G.1 Top Drive Motor Drive (ASDA-A2R-3023-U Servo Motor Drive)

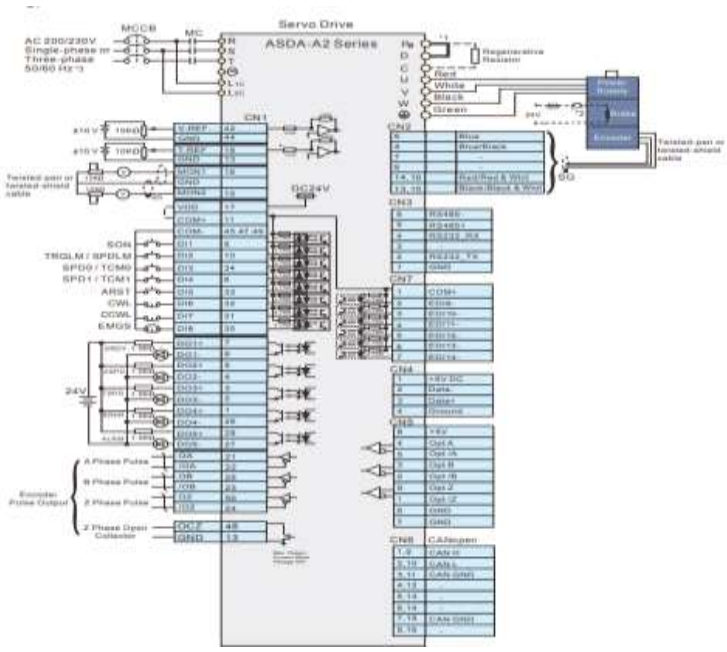

Figure 74: Top Drive Motor Drive Interface

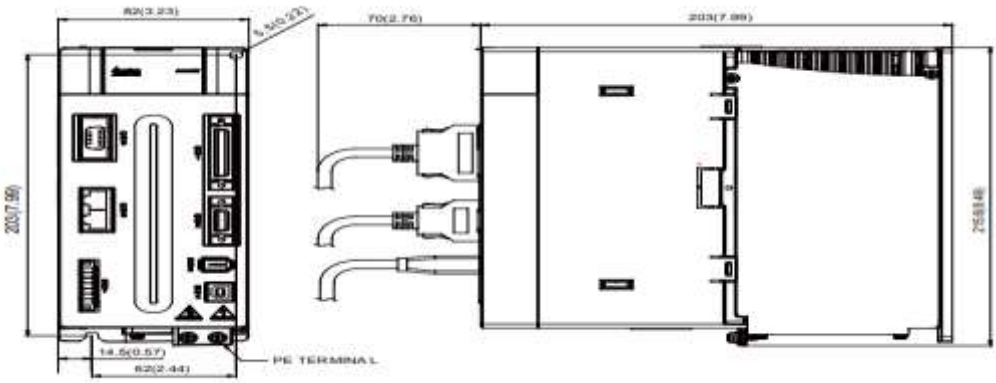

Figure 75: Top Drive Motor Drive Dimensions

G.2 Hoisting Motor Drive (DM556 Stepper Motor Drive)

- Anti-Resonance, provides optimum torque and nulls mid-range instability
- Motor auto-identification and parameter auto-configuration technology, offers optimum responses with different motors
- Multi-Stepping allows a low resolution step input to produce a higher microstep output for smooth system performance
- Microstep resolutions programmable, from full-step to 102,400 steps/rev
- Supply voltage up to 50 VDC, Output current programmable, from 0.4A to 5.6 A
- Pulse input frequency up to 200 kHz
- TTL compatible and optically isolated inputs
- Automatic idle-current reduction and software configured reduction rate
- Suitable for 2-phase and 4-phase motors
- Over-voltage, over-current, phase-error protections
- Support PULSE/DIRECTION and CW/CCW modes

Figure 76: Hoisting Motor Drive Advantages

Table 9: Hoisting Motor Drive Specifications

Output Current:	0.4 to 4.0 A RMS (5.6 A Peak)
Operating Voltage:	20 to 50 V DC
Logic Signal Current:	7 to 16 mA
Pulse Input Frequency:	0 to 200 kHz
Isolation Resistance:	500 MΩ

The drive is suitable for a wide range of stepping motors, from NEMA frame size 17 to 24. It can be used in various kinds of machines including CNC machines, laser cutters, laser markers, high precision X-Y tables and labeling machines. Its unique features make the DM442 an ideal solution for applications that require both low-speed smoothness and high speed performance.

Figure 77: Hoisting Motor Drive Uses

G.3 Pump Motor Drive (Usfull FU9000A Pump Motor Drive)

Place of Origin: Zhejiang, China
Brand Name: Usfull
Model Number: FU9000A
Type: AC inverter
Output Type: Single, TRIPLE
Output Current: 2.7A-605A
Output Frequency: 0-400HZ
Size: 170*125*162--600*800*2000
Weight: 2.16KGS--160KGS
Certificate: ISO9001, CE
Colour: black

	Brand: USFULL
	Power: 0.75kw 1.5kw 2.2kw
	Rated Current: 9.3A 15.7A 24A
	Input Voltage: Single Phase 220V or Dc 200V - 400V
	Output Votage: Three Phase 220v
	Dimensions: 18.5cm*12.5cm*16cm
	Installation Dimensions: 17.5cm*17.5cm
	Weight: 1.8kgs

Figure 78: Pump Drive Specifications

Figure 79: Pump Drive Interface

H Sensor Specifications

H.1 Torque Sensor (Omega TQ513 Torque Sensor)

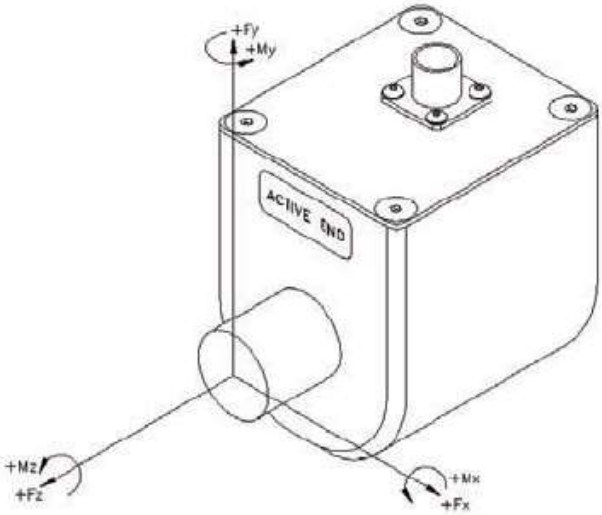

Figure 80: Torque Sensor Technical Drawing

Table 10: Torque Sensor Specifications

Input Resistance	1000 Ω	Maximum Ambient Temperature	121 (C) (250 (F))
Excitation Voltage	20 Vdc maximum	Maximum Compensation Temperature	76 (C) (170 (F))
Minimum Ambient Temperature	-54 (C) (-65 (F))	Output Resistance	1000 ohms
Measurement Units	Aluminum	Minimum Compensation Temperature	21 (C) (70 (F))
Safe Overload	150% of Capacity	Temperature Effects	Zero: ±0.002% FS/°F Span: ±0.002% rdg/°F
Zero Balance	1.0% FS		

Excitation Voltage: 20 Vdc maximum
Bridge Resistance: 1000 ohms
Output at Full Scale: 2.0 mV/V nominal
Linearity: 0.10% FS
Hysteresis: 0.10% FS
Zero Balance: 1.0% FS
Operating Temperature: -54 to 121°C (-65 to 250°F)
Compensated Temperature: 21 to 76°C (70 to 170°F)
Thermal Effects
Zero: 0.0036% FS/°C
Span: 0.0036% FS/°C
Overload Capacity: 150% FS
Material:
<100 in-lb: SS shafts, aluminum sensor
≥100 in-lb: Steel shaft and sensor
Maximum Shaft Speed: 5000 RPM
Electrical Connection: 4-pin twist lock connector (mating connector supplier); 10-pin twist lock connector with optional optical encoder (mating connector supplied)

Figure 81: Torque Sensor Specifications

H.2 Load Cell (Omega Miniature Stud-Mount Load Cell)

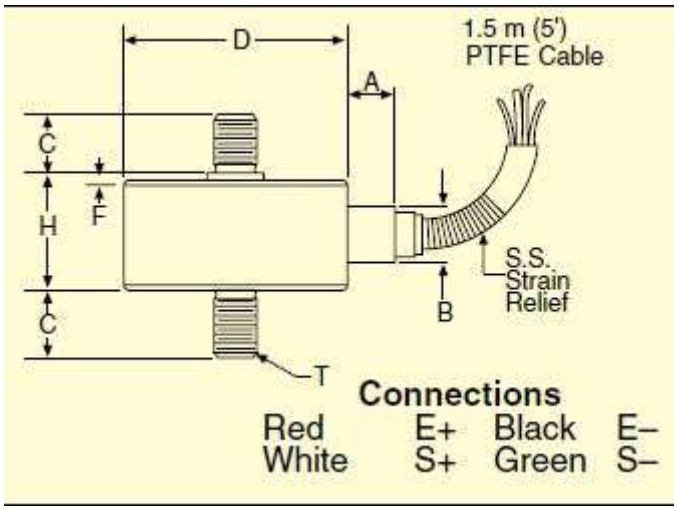

Figure 82: Load Cell Technical Drawing

Table 11: Load Cell Dimensions

Dimensions: mm (inch)

CAPACITY	T, THREAD	F	D DIA.	H	A	B DIA.	C	WEIGHT g (oz)
1 kg to 10 lb	#6 - 32 UNC	1.3 (0.05)	19 (0.75)	12.7 (0.50)	7.9 (0.31)	4.8 (0.19)	6.35 (0.25)	42 (1.48)
10 to 50 N	M5 x 0.8							
25 to 100 lb	#10 - 32 UNF	3 (0.12)	25.4 (1.00)	16.3 (0.64)	12.7 (0.50)	6.35 (0.25)	6.35 (0.25)	56 (1.98)
100 to 500 N	M6 x 1.0							
250 to 1000 lb	¼-28 UNF	0.76 (0.03)	25.4 (1.00)	14.0 (0.55)	12.7 (0.50)	6.35 (0.25)	9.7 (0.38)	68 (2.40)
1 to 5 KN	M6 x 1.00							

SPECIFICATIONS

Excitation:
- **≤10 lb/50 N:** 5 Vdc
- **≥25 lb/100 N:** 10 Vdc

Output:
- **2.2 lb/10 N:** 1.5 mV/V (nom)
- **≥5 lb/20 N:** 2 mV/V (nom)

Accuracy (Linearity and Hysteresis Combined):
- **≤100 lb/500 N:** ±0.15% FSO
- **≥250 lb/1000 N:** ±0.20% FSO

Repeatability:
- **≤2.2 lb:** ± 0.15% FSO
- **≥5 lb/10 N:** 0.20% FSO

5-Point Calibration (in Tension):
0%, 50%, 100%, 50%, 0%

Zero Balance: ±2% FSO

Operating Temp Range:
-54 to 121°C (-65 to 250°F)

Compensated Temp Range:
16 to 71°C (60 to 160°F)

Thermal Effects:
- **Span:** ±0.009% FSO/°C
- **Zero:** ±0.009% FSO/°C

Safe Overload: 150% of capacity

Ultimate Overload: 300% of capacity

Bridge Resistance: 350 Ω minimum

Construction: Stainless steel

Electrical Connection: 1.5 m (5')
4-conductor, shielded cable
- **≤10 lb/50 N:** SS overbraided PTFE with temperature compensation board

Protection Class: IP65

Figure 83: Load Cell Specifications

H.3 6-Axis IMU (GY-521 MPU-6050 6-axis IMU)

Table 12: Gyroscope Specifications

VDD = 2.375V-3.46V, VLOGIC (MPU-6050 only) = 1.8V±5% or VDD, T_A = 25°C

PARAMETER	CONDITIONS	MIN	TYP	MAX	UNITS	NOTES
ACCELEROMETER SENSITIVITY						
Full-Scale Range	AFS_SEL=0		±2		*g*	
	AFS_SEL=1		±4		*g*	
	AFS_SEL=2		±8		*g*	
	AFS_SEL=3		±16		*g*	
ADC Word Length	Output in two's complement format		16		bits	
Sensitivity Scale Factor	AFS_SEL=0		16,384		LSB/*g*	
	AFS_SEL=1		8,192		LSB/*g*	
	AFS_SEL=2		4,096		LSB/*g*	
	AFS_SEL=3		2,048		LSB/*g*	
Initial Calibration Tolerance			±3		%	
Sensitivity Change vs. Temperature	AFS_SEL=0, -40°C to +85°C		±0.02		%/°C	
Nonlinearity	Best Fit Straight Line		0.5		%	
Cross-Axis Sensitivity			±2		%	
ZERO-G OUTPUT						
Initial Calibration Tolerance	X and Y axes		±50		m*g*	1
	Z axis		±80		m*g*	
Zero-G Level Change vs. Temperature	X and Y axes, 0°C to +70°C		±35			
	Z axis, 0°C to +70°C		±60		m*g*	
SELF TEST RESPONSE						
Relative	Change from factory trim	-14		14	%	2
NOISE PERFORMANCE						
Power Spectral Density	@10Hz, AFS_SEL=0 & ODR=1kHz		400		µ*g*/ √Hz	
LOW PASS FILTER RESPONSE						
	Programmable Range	5		260	Hz	
OUTPUT DATA RATE						
	Programmable Range	4		1,000	Hz	
INTELLIGENCE FUNCTION INCREMENT			32		mg/LSB	

Table 13: Accelerometer Specifications

VDD = 2.375V-3.46V, VLOGIC (MPU-6050 only) = 1.8V±5% or VDD, T_A = 25°C

PARAMETER	CONDITIONS	MIN	TYP	MAX	Units	Notes
TEMPERATURE SENSOR						
Range			-40 to +85		°C	
Sensitivity	Untrimmed		340		LSB/°C	
Temperature Offset	35°C		-521		LSB	
Linearity	Best fit straight line (-40°C to +85°C)		±1		°C	
VDD POWER SUPPLY						
Operating Voltages		2.375		3.46	V	
Normal Operating Current	Gyroscope + Accelerometer + DMP		3.9		mA	
	Gyroscope + Accelerometer (DMP disabled)		3.8		mA	
	Gyroscope + DMP (Accelerometer disabled)		3.7		mA	
	Gyroscope only (DMP & Accelerometer disabled)		3.6		mA	
	Accelerometer only (DMP & Gyroscope disabled)		500		µA	
Accelerometer Low Power Mode Current	1.25 Hz update rate		10		µA	
	5 Hz update rate		20		µA	
	20 Hz update rate		70		µA	
	40 Hz update rate		140		µA	
Full-Chip Idle Mode Supply Current			5		µA	
Power Supply Ramp Rate	Monotonic ramp. Ramp rate is 10% to 90% of the final value			100	ms	
VLOGIC REFERENCE VOLTAGE	MPU-6050 only					
Voltage Range	VLOGIC must be ≤VDD at all times	1.71		VDD	V	
Power Supply Ramp Rate	Monotonic ramp. Ramp rate is 10% to 90% of the final value			3	ms	
Normal Operating Current			100		µA	
TEMPERATURE RANGE						
Specified Temperature Range	Performance parameters are not applicable beyond Specified Temperature Range	-40		+85	°C	

Table 14: Other Specifications

VDD = 2.375V-3.46V, VLOGIC (MPU-6050 only) = 1.8V±5% or VDD, T_A = 25°C

PARAMETER	CONDITIONS	MIN	TYP	MAX	UNITS	NOTES
GYROSCOPE SENSITIVITY						
Full-Scale Range	FS_SEL=0		±250		°/s	
	FS_SEL=1		±500		°/s	
	FS_SEL=2		±1000		°/s	
	FS_SEL=3		±2000		°/s	
Gyroscope ADC Word Length			16		bits	
Sensitivity Scale Factor	FS_SEL=0		131		LSB/(°/s)	
	FS_SEL=1		65.5		LSB/(°/s)	
	FS_SEL=2		32.8		LSB/(°/s)	
	FS_SEL=3		16.4		LSB/(°/s)	
Sensitivity Scale Factor Tolerance	25°C	-3		+3	%	
Sensitivity Scale Factor Variation Over Temperature			±2		%	
Nonlinearity	Best fit straight line; 25°C		0.2		%	
Cross-Axis Sensitivity			±2		%	
GYROSCOPE ZERO-RATE OUTPUT (ZRO)						
Initial ZRO Tolerance	25°C		±20		°/s	
ZRO Variation Over Temperature	-40°C to +85°C		±20		°/s	
Power-Supply Sensitivity (1-10Hz)	Sine wave, 100mVpp; VDD=2.5V		0.2		°/s	
Power-Supply Sensitivity (10 - 250Hz)	Sine wave, 100mVpp; VDD=2.5V		0.2		°/s	
Power-Supply Sensitivity (250Hz - 100kHz)	Sine wave, 100mVpp; VDD=2.5V		4		°/s	
Linear Acceleration Sensitivity	Static		0.1		°/s/g	
SELF-TEST RESPONSE						
Relative	Change from factory trim	-14		14	%	1
GYROSCOPE NOISE PERFORMANCE	**FS_SEL=0**					
Total RMS Noise	DLPFCFG=2 (100Hz)		0.05		°/s-rms	
Low-frequency RMS noise	Bandwidth 1Hz to10Hz		0.033		°/s-rms	
Rate Noise Spectral Density	At 10Hz		0.005		°/s/ √ Hz	
GYROSCOPE MECHANICAL FREQUENCIES						
X-Axis		30	33	36	kHz	
Y-Axis		27	30	33	kHz	
Z-Axis		24	27	30	kHz	
LOW PASS FILTER RESPONSE						
	Programmable Range	5		256	Hz	
OUTPUT DATA RATE						
	Programmable	4		8,000	Hz	
GYROSCOPE START-UP TIME	**DLPFCFG=0**					
ZRO Settling (from power-on)	to ±1°/s of Final		30		ms	

H.5 Flow Sensor (YF-S201 Flow Sensor)

No.	Item	Material	Qty.
1	Connection wire		1
2	Bonnet	PA	1
3	Screw		4
4	Valve body	PA	1
5	Leak press valve		1
6	Magnet		1
7	Hall		1
8	Impeller	POM	1
9	Rustless steel axis	SUS304	1
10			
11			

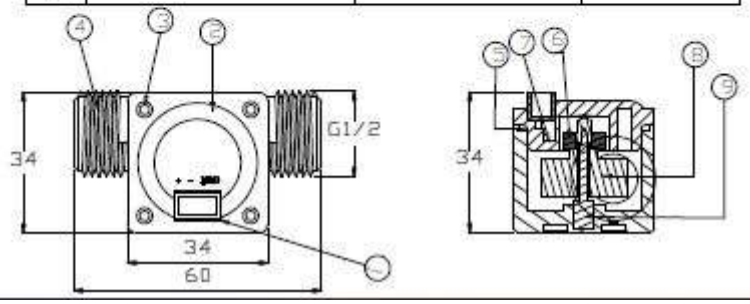

Figure 84: Flow Sensor Technical Drawing

1.Modle:YF-21
2.Product Name:Hall sensor
3.Flow Range: 1-30L/MIN
4.(1)Connection Method

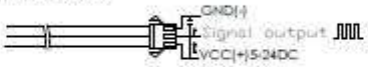

(2)Voltage Range: 3.5-24VDC, Pluse Characteristic:F=7Q(L/MIN
(3)Extent of error:±5%.
(4)Flow-Pulse
2L/MIN=16HZ 4L/MIN=32.5HZ 6L/MIN=49.3HZ
8L/MIN=65.5HZ 10L/MIN=82HZ

Figure 85: Flow Sensor Specifications

一.Flow Range:100L/H-/1800H-L/H

Flow (L/H)	Frezq.(HZ)	Erro range
120L/H	16	±10
240L/H	32.5	
360L/H	49.3	
480L/H	65.5	
600L/H	82	
720L/H	90.2	

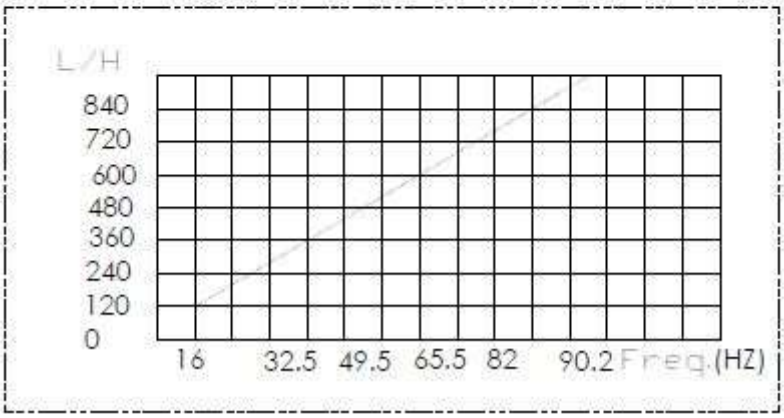

Figure 86: Flow Sensor Flow Range

I Wi-Fi Module Specifications (NodeMCU ESP2866 12E Wi-Fi Module)

Table 15: Wi-Fi Module Specifications

Categories	Items	Values
WiFi Paramters	WiFi Protocles	802.11 b/g/n
	Frequency Range	2.4GHz-2.5GHz (2400M-2483.5M)
Hardware Paramaters	Peripheral Bus	UART/HSPI/I2C/I2S/Ir Remote Contorl
		GPIO/PWM
	Operating Voltage	3.0~3.6V
	Operating Current	Average value: 80mA
	Operating Temperature Range	-40°~125°
	Ambient Temperature Range	Normal temperature
	Package Size	16mm*24mm*3mm
	External Interface	N/A
Software Parameters	Wi-Fi mode	station/softAP/SoftAP+station
	Security	WPA/WPA2
	Encryption	WEP/TKIP/AES
	Firmware Upgrade	UART Download / OTA (via network) / download and write firmware via host
	Ssoftware Development	Supports Cloud Server Development / SDK for custom firmware development
	Network Protocols	IPv4, TCP/UDP/HTTP/FTP
	User Configuration	AT Instruction Set, Cloud Server, Android/iOS App

Table 16: Wi-Fi Module Sensitivity

Parameters	Min	Typical	Max	Unit
Input frequency	2412		2484	MHz
Input impedance		50		Ω
Input reflection			-10	dB
Output power of PA for 72.2Mbps	15.5	16.5	17.5	dBm
Output power of PA for 11b mode	19.5	20.5	21.5	dBm
Sensitivity				
DSSS, 1Mbps		-98		dBm
CCK, 11Mbps		-91		dBm
6Mbps (1/2 BPSK)		-93		dBm
54Mbps (3/4 64-QAM)		-75		dBm
HT20, MCS7 (65Mbps, 72.2Mbps)		-72		dBm
Adjacent Channel Rejection				
OFDM, 6Mbps		37		dB
OFDM, 54Mbps		21		dB
HT20, MCS0		37		dB
HT20, MCS7		20		dB

Table 17: Wi-Fi Module Dimensions

Length	Width	Height	PAD Size(Bottom)	Pin Pitch
16 mm	24mm	3 mm	0.9 mm x 1.7 mm	2mm

J Past Rig Cost Estimations

J.1 2018-2019 Rig Cost Estimation

Table 18: 2018-2019 Rig Cost Estimation

Sl. No.	Description	Unit Cost (USD)	Qty	Total (USD)
1.	SIEMENS SIMATIC S7-1200 PLC - CPU 1214C	380	1	380,00
2.	Dell OptiPlex Desktop Computer (2.1GHz MPU - 4GB RAM - 160GB HDD)	125	1	125,00
3.	BLDC motor 130DK-M10030-24V	300	1	300,00
4.	Stepper motor bipolar with DUAL Shaft + Stepper motor driver, DM860A	165	1	165,00
5.	GY-521 MPU-6050 Module Three-Axis Gyroscope + Accelerometer	6,99	1	6,99
6.	Node MCU ESP 2866 E-12 Wi-Fi Module	3,89	1	3,89
7.	OMEGA Gear-tooth Hall-effect RPM sensor	172	1	172,00
8.	Allegro ACS714 Hall-effect current sensor	8,95	1	8,95
9.	YGX Miniature Load cell strain gauge	108	1	108,00
10.	Hallow shaft rotary encoder (position sensor)	56	1	56,00
11.	UTMOST linear position transmitter (LVDT)	130	1	130,00
12.	FST800-211 piezoelectric pressure transducer	65	1	65,00
13.	DN50 POM Hall-effect Flow sensor	15	1	15,00
14.	Wiring/packaging and Electrical instruments	300	1	300,00
15.	Stainless steel	100	1	100,00
16.	Track roller - guide rails-threaded shaft	186	1	186,00
17.	glass	165	1	165,00
18.	Flexible Shafts Coupling	15	1	15,00
19.	Casters	30	1	30,00
20.	Plywood panels	24	1	24,00
21.	Aluminum for other tools	200	1	200,00
22.	Hypro 6500C Roller Pump w/ 1321-0006 + pump motor + tools	700	1	700,00
23.	220V 4KW Frequency Inverter Variable Frequency Converter for Water Pump Motor	170	1	170,00
24.	Input 110/220VAC Output 24VDC 15A 360W Power Supply	39	1	39,00
25.	Others	270	1	270,00
			Total	3734,83

J.1 2019-2020 Rig Cost Estimation

Table 19: 2019-2020 Rig Cost Estimation

Item Description	Unit Cost (USD)	No. of Units	Total Item Cost (USD)
PDM Printing	300	1	300
Drill Pipes	10	20	200
ATO-SERVO-150S3000 Brushless AC Servo Motor	688	1	688
ATOMG-1000 AC Servo Motor Drive	372	1	372
Omega TQ513 Torque Sensor	200	1	200
Omega Miniature Stud-Mount Load Cell	200	1	200
FST800-211 Silicon Strain Gauge Piezoelectric Pressure Sensor	65	1	65
YF-S201 Flow Sensor	8	1	8
GY-521 MPU-6050 6-axis IMU	7	1	7
NodeMCU ESP2866 12E Wi-Fi Module	4	1	4
Wires and connections	300	1	300
Others	200	1	200
Total Rig Cost (USD)	**2544**		
Total (Plus 20% Contingency Cost) (USD)	**3053**		